



**University of
Zurich**^{UZH}

Uncertainties in Modelling Glacier Lake Outburst Floods: Sensitivity Analyses of Mass Movements in Northern Kyrgyzstan

GEO 511 Master's Thesis

Author

Claudius Brüniger
17-711-771

Supervised by

Dr. Alessandro Cicoira
Dr. Jessica Munch (jessica.munch@slf.ch)

Faculty representative

Prof. Dr. Christian Huggel

31.01.2023

Department of Geography, University of Zurich

Acknowledgements

This thesis would not have been possible without the help and support of a variety of people. Most importantly, I would like to express my gratitude to my supervisor Dr. Alessandro Cicoira who has guided me from start to finish and who always provided valuable feedback and shared his extensive knowledge on the topic with great enthusiasm and passion. Besides, I could greatly benefit from his knowledge of physical processes and geomorphology which was essential to understand GLOFs per se but also how model results should be interpreted. It was always a pleasure to meet and discuss the progress made and the challenges I faced.

Further, I would like to thank:

- Dr. Jessica Munch from the Institute for Snow and Avalanche Research SLF, my Co-Supervisor, who helped me narrow down my research topic. Further, she was always willing to help me with technical problems I encountered and gave great inputs on structuring my thesis. Before submission, she kindly proofread my thesis and provided last suggestions on improvements.
- Prof. Dr. Christian Huggel, who helped me conceptualise my thesis and whom I could always reach out to for questions related to content and structure. He very generously reviewed an initial draft and supported me a lot with finalising my thesis.
- Laura Niggli, who provided valuable feedback when needed and kindly shared her images of the study site.
- Dr. Perry Bartelt, also from SLF, who was a great help when formulating my research problems and from whom I could learn key model features during multiple webinar sessions.
- Marc Christen, also from SLF, for providing clarity on the model setup of RAMMS and for supporting with his technical knowledge.
- Guillaume Meyrat, also from SLF, with whom I had a discussion shortly before submitting my thesis during which he explained the main advantages of the two-phase model, provided more insights into the model setup, and shared valuable inputs on how results should be interpreted.
- Vitalii Zaginaev, from the Research Institute of Water Problems and Hydro-Energy Problems at the Kyrgyz Republic Academy of Sciences, who shared his knowledge about the study site and could provide valuable details on past GLOF events and erosion dynamics within the catchment.
- My brother, Laurin Brüniger, for proofreading parts of my thesis and for always being very supportive.
- My friends and family for constantly encouraging me throughout the development of my thesis and for being a welcome distraction.

Abstract

Glacier lake outburst floods (GLOFs) are considered among the most dangerous glacier hazards worldwide. The variability in flow magnitudes and the ability to transform into powerful debris flows pose challenges to affected regions and have caused fatalities and infrastructural damage in several regions across the globe. In recent years, the efforts in modelling GLOF dynamics have increased and a variety of modelling approaches were used to approximate realistic flow behaviour to estimate possible runout distances and other flow characteristics. This thesis aims to enhance the understanding of the impact different outburst mechanisms and entrainment along the flow trajectory can have on resulting flow parameters by performing sensitivity analyses at a site in Northern Kyrgyzstan. The single-phase numerical modelling tool RAMMS is used to evaluate the uncertainty and variability in flow dynamics. It is shown that the variability in release discharges can lead to very distinct mass movements, which amplifies the challenges for hazard and risk assessment. Further, it is demonstrated how sediment entrainment can reduce travel times by up to 50% while also altering flow magnitudes, which is reflected in heavily increased flow heights and velocities. Although the single-phase version of RAMMS allows modelling the erosive force of mass flow fronts, results are limited when it comes to differentiating between solid and fluid phases, which in turn increases the uncertainty when modelling the flow composition and spatial evolution of the density. The dynamics and impacts of flow type transformations can therefore only be approximated and require certain assumptions. Additionally, most analyses performed in this thesis neglect interactions between different input parameters which might constrain the model results to some extent. Future studies and hazard assessments shall therefore focus on understanding parameter interactions better and on modelling flow type transformations using multi-phase models.

Table of Contents

List of Abbreviations.....	v
1 Introduction	1
1.1 Global Context.....	1
1.2 Situation in Central Asia.....	3
1.3 GLOFCA	3
2 Scientific Background	5
2.1 GLOF Characteristics and Lake Types	5
2.2 Related Mass Movements.....	7
2.2.1 Entrainment of Solid Material.....	8
2.2.2 Transitions to Other Mass Movements	9
2.3 Research on GLOF Modelling	12
2.3.1 Different Model Types	12
2.3.2 Previous GLOF Studies.....	14
2.3.2.1 Research on Boundary Conditions.....	15
2.3.2.2 Research on Erosion	16
2.3.2.3 Research on GLOF Transitions.....	17
3 Research Objectives	19
3.1 Research Gap	19
3.2 Research Questions.....	20
4 Data and Methods.....	22
4.1 Study Site.....	22
4.1.1 Climate	22
4.1.2 Landforms	23
4.2 RAMMS Software.....	28
4.2.1 Underlying Equations and Assumptions	28
4.2.2 Friction	29
4.2.3 Release Settings.....	30
4.2.4 Erosion	30
4.2.5 Additional Simulation Parameters	32
4.3 Data Acquisition	32

4.4	Calibration in RAMMS	32
4.4.1	Definition of a Hydrograph	33
4.4.2	Basis Simulation.....	35
4.5	Sensitivity Analyses	36
4.5.1	Boundary Conditions.....	37
4.5.2	Erosion Dynamics	39
4.5.3	Variability in Travel Times	42
4.5.4	Scenario-based Modelling.....	42
4.5.5	Monitored Variables.....	44
5	Results	46
5.1	Boundary Conditions	46
5.1.1	Release Velocity	46
5.1.2	Peak Discharge	46
5.1.3	Release Volumes	48
5.1.4	Time of Arrival.....	49
5.2	Erosion Dynamics.....	50
5.2.1	Erosion Depths	50
5.2.2	Limits to Erosion.....	54
5.2.3	Impact on Temporal Aspects.....	55
5.3	Variability in Travel Times	57
5.4	Scenario-based Modelling	58
6	Discussion	62
6.1	Boundary Conditions	62
6.2	Erosive Processes	64
6.3	Transitional Behaviour	68
6.4	Further Limitations	69
7	Conclusion & Future Work	71
8	References	73
9	Appendix	80
	Personal Declaration	90

List of Abbreviations

AD	anno Domini
ALOS	Advanced Land Observation Satellite
ASF DAAC	Alaska Satellite Facility Distributed Active Archive Center
BASEMENT	Basic Simulation Environment
DEM	Digital Elevation Model
ESA	European Space Agency
GIS	Geographic Information System
GLOF	Glacial Lake Outburst Flood
GLOFCA	Glacial Lake Outburst Floods in Central Asia
HEC-RAS	Hydrologic Engineering Center's River Analysis System
LIA	Little Ice Age
NASA	National Aeronautics and Space Administration
QGIS	Quantum GIS = Quantum Geographic Information System
RAMMS	Rapid Mass Movements Simulation
SLF	Institute for Snow and Avalanche Research
UNEP	United Nations Environment Programme
UNESCO	United Nations Educational, Scientific and Cultural Organization
WSL	Swiss Federal Institute for Forest, Snow and Landscape Research
1/2/3-D	One/two/three-dimensional

1 Introduction

1.1 Global Context

Across the world, global warming has led to the retreat of glaciers and will continue to contribute to substantial glacier ice loss in the future (Zemp et al., 2015). Global glacier shrinkage is considered one of the most obvious signs of climate change (Huggel et al., 2020). Climate change and the resulting glacier retreat have significant implications for high-mountain hazards. Glacier retreat is causing glacial lakes to form behind moraine or ice dams and in glacially formed depressions (Frey et al., 2018; Harrison et al., 2018). In 2018, drainage of the entire volume contained in glacial lakes would have led to a sea level rise of 0.43 mm sea level rise (Shugar et al., 2020). The existence of lakes adjacent to a glacier can further increase glacier recession (Shugar et al., 2020), often leading to the destabilization of rock faces which in turn might promote slope failure, a process referred to as ‘debuttressing’ (Cossart et al., 2008; Worni et al., 2014). Additionally, the destabilisation of rock faces due to increasing temperatures and resulting permafrost degradation has been shown to further exacerbate slope instability (Muccione and Fiddes, 2019). As a result, moraine failures or rockfalls are likely to occur more frequently, and, if released in close proximity to a glacial lake, they could generate massive flood waves causing a GLOF (Harrison et al., 2018). Apart from moraine and slope failures, increased water input through heavy precipitation or glacier meltwater can lead to the release of large water volumes (Richardson and Reynolds, 2000). Depending on the geomorphological setting, the outburst occurs as a pure overflow, a dam breach or drains through subglacial channels (Harrison et al., 2018). As GLOFs normally consist of both water and solid material, the large volumes and discharges usually lead to a far-reaching mass movement that often happens very abruptly (Worni et al., 2014). GLOFs are considered one of the most dangerous natural hazards when it comes to glacier changes (Huggel et al., 2020). The United Nations Environment Programme (UNEP) stresses that GLOFs can be considered as the largest glacial hazard due to their high damage potential (GLOFCA, 2023).

In addition to high water discharges, GLOFs are often the cause of debris and mudflows due to either material from the moraine dam being swept away or sediment deposits along the flow path being entrained in the large water volumes (Bolch et al., 2012). The entrained material causes higher flow volumes and discharges, resulting in transitions to other types of mass flows (Shugar et al., 2020). In the past century, outburst floods together with entrained solid material have been the cause of thousands of fatalities and large infrastructural damage across the world (Harrison et al., 2018; Mergili et al., 2011). Alone in Peru, GLOF events were responsible for the deaths of 32'000 people during the twentieth century (Richardson and Reynolds, 2000).

Nevertheless, since GLOF hazard is comprised of multiple and partly independent factors, GLOF dynamics cannot solely be attributed to changes in global climate patterns, as topography, geology, and further components also have an impact on GLOF hazard (Haeberli et al., 2017). Hence, it has been pointed out that the observed increase in the number of glacial

lakes in the past decades does not necessarily result in higher GLOF hazard since the majority of glacial lakes drain slowly (Shugar et al., 2020). Yet, provided that dam geometry, triggering mechanism and other local characteristics favour a GLOF to occur, these mass movements might pose extreme risks, particularly if settlements and critical infrastructure are situated along the path without the necessary adaptation measures in place (Harrison et al., 2018; Shugar et al., 2020). Figure 1 illustrates a possible setting of a GLOF released at a lake fed by glacial melt water, whereby the trajectory can be characterized by three typical processes. Firstly, the outburst processes shaped by trigger mechanism and lake type determine how water drains from the lake. Along the valley, the flow propagation is shaped by topography, geomorphic features, and the entrainment of sediments. Further below where the slope decreases, deposition of solid material sets in and results in a phase transformation to a less solid-laden mass movement and might in some regional settings affect people and infrastructure. The GLOF simulations performed for this thesis address such a setting based on different scenarios.

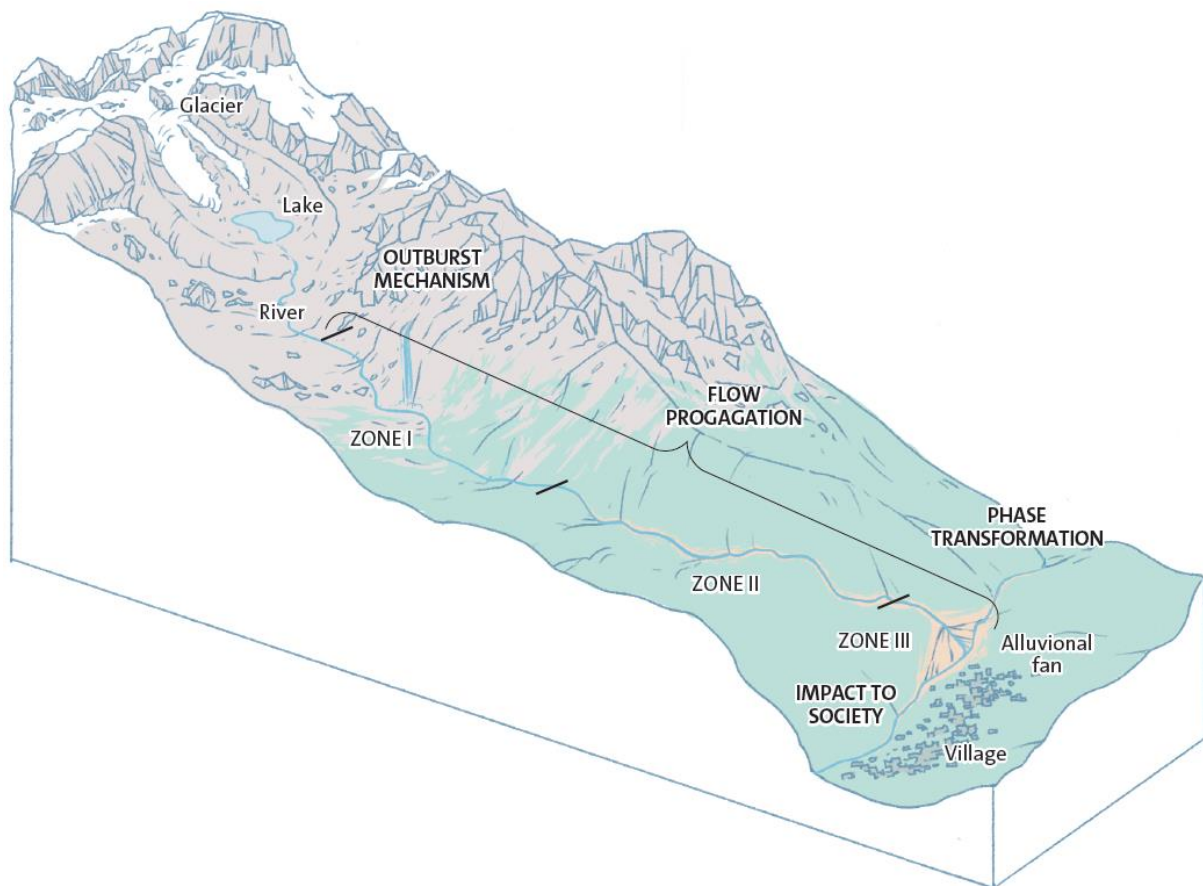


Figure 1: Schematic of dominant processes during a GLOF event whereby the flow trajectory is divided into three zones affected by the outburst mechanism, flow propagation, and phase transformation. Graphic designed by Tara von Grebel, University of Zurich, Information Technology, MELS/SIVIC.

Although there has been a decline in the number of reported GLOF events since the late twentieth century, rising temperatures are expected to result in more frequent GLOFs, partly due to a greater number of glacial lakes being projected in regions where ground instability might enhance the likelihood of mass movements (Harrison et al., 2018; Zheng et al., 2021). It is assumed by Haeberli et al. (2017) that GLOF frequency shows a lagged response to glacial

changes since a decline in the number of GLOFs has been observed while glaciers were retreating faster. Prior to the decline in GLOF events, Harrison et al. (2018) reported a period of increased GLOF frequency, which they suggest to attribute to the Little Ice Age (LIA, AD 1303 – 1850) glacier retreat.

1.2 Situation in Central Asia

For Central Asia, Muccione and Fiddes (2019) highlight that future projections show higher warming rates than the global average. This would presumably be accompanied by a faster recession of Central Asian glaciers. Whilst on a global level, the number of glacial lakes grew by 53% between 1990 and 1999 (Shugar et al., 2020), Zheng et al. (2021) state that in the period between 1990 and 2015, the number of lakes in the ‘Third Pole’, which includes the Hindu Kush-Himalaya, Tibetan Plateau and other surrounding areas such as the Tian Shan Mountains, has risen by 5.9%. Thereby, the Western and Eastern Tian Shan region show a surge in lake number of 28.5% (Zheng et al., 2021). Furthermore, the changes across this region are mainly driven by an increase in moraine-dammed lakes while for other dam types, the number remained relatively constant (Zheng et al., 2021).

Lake management, early warning systems, and the implementation of other adaptation measures can certainly reduce the number of GLOF events and their impacts on society (Kapitsa et al., 2017). However, in some regions, glacier retreat and the simultaneous formation of glacial lakes have shown strong deviations from the global average. In the Tian Shan Mountains in Central Asia for instance, glacier retreat is found to be four times faster than the global average and is becoming more heterogeneous in terms of glacier mass balance variability (Farinotti et al., 2015; Barandun et al., 2021). Zheng et al. (2021) assume that the subsequent lake area expansion will continue at high rates in Central Asian mountain ranges for multiple decades. In addition to the rising number and area of glacial lakes, Central Asia has experienced GLOF events more frequently than the region of Hindukush-Karakoram-Himalaya (Petrakov et al., 2020). Contrasting to global trends, a high number of GLOF events was reported for the Pamir and Tian Shan throughout the 1970s until they faced a decline in the mid-1980s as well (Harrison et al., 2018). Since countries in Central Asia such as Kyrgyzstan can be characterized by high exposure to GLOF and debris flow hazard, the threat for local inhabitants is substantially high unless adaptation and mitigation strategies are undertaken (Thurman, 2011).

1.3 GLOFCA

The thesis is embedded in a project called ‘Glacial Lake Outburst Floods in Central Asia’ (GLOFCA) which was initiated in response to a regionally rising threat of GLOFs and related natural hazards. Glacier recession and the resulting increase in glacial lake area and volume endanger populations in different regions, especially where exposure is coupled with vulnerability. The lack of adaptive capacity and loss prevention in Central Asian countries has led to the creation of the project guided by the United Nations Educational, Scientific and Cultural Organization (UNESCO) and financed through the Adaptation Fund. The overarching

mission of the project is to reduce vulnerabilities and enhance resilience to climate change by strengthening monitoring and response capacities in the four Central Asian countries Kazakhstan, Kyrgyzstan, Tajikistan, and Uzbekistan. These countries have been affected by multiple GLOF events that caused fatalities and severe damage in the last decades. In many mountainous regions, the required knowledge and infrastructure to prevent future damage from natural hazards is scarce. In the past, response capacities following natural disasters in those countries have generally been greater than preventive measures. Hence, UNESCO intends to contribute to disaster risk reduction by promoting pre-disaster management. The collaboration of the UNESCO Cluster Office in Almaty, governmental bodies, and regional institutions as well as scientific experts from the University of Zurich aims to optimise the knowledge base for decision-making regarding climate change adaptation, especially when it comes to the installation of early warning systems and monitoring strategies. In the past, the lack of cooperation between local and national authorities prevented the implementation of effective adaptation measures. Especially when GLOFs and related natural hazards are of transboundary character, necessary institutions did not exist and hence, knowledge and experience in the field of hazard management could not be shared across the border. By bringing together local knowledge holders, scientific experts, and regional and national authorities, the GLOFCA project aims to eradicate these barriers. For each country, scientific reports have been compiled focusing on the current knowledge about GLOFs in Central Asian countries. In each of the four regions, a selection of pilot sites was defined where initial studies and hazard assessments will be carried out. (GLOFCA, 2023)

Since the thesis focuses on one of the pilot sites in Northern Kyrgyzstan specifically, the gained insights into GLOF dynamics shall further the existing knowledge base and could help in decision-making regarding climate change adaptation and disaster risk reduction. The thesis aims to identify sources of uncertainty in GLOF modelling and how different outburst mechanisms and erosive behaviour affect flow dynamics downstream of glacial lakes which eventually shall provide knowledge on how GLOF hazard is influenced by the lake and channel characteristics in different regional settings.

2 Scientific Background

2.1 GLOF Characteristics and Lake Types

Glacial lake outburst floods are mass movements that occur when, often suddenly, water is released from a glacial lake (Mergili et al., 2011; Worni et al., 2014). Due to their potential to erode vast amounts of material along the way, their flow behaviour is considered very unsteady and changes as the mass travels downstream (Somos-Valenzuela et al., 2016). Depending on the outburst process and the amount of entrained sediment, these mass movements can travel further than most mountainous hazards and reach settlements located tens of kilometres downstream of the lake (Richardson and Reynolds, 2000). The powerful nature of GLOFs coupled with high peak discharges and their ability to travel large distances makes them a considerable threat in glaciated regions since they usually flow along existing river channel beds where people and infrastructure are concentrated (Worni et al., 2014; Frey et al., 2018). GLOFs are often regarded as a process chain consisting of cascading events, whereby trigger mechanisms, outburst processes, and flood propagation determine the eventual flow dynamics (Worni et al., 2014; Frey et al., 2018). The resulting flow magnitude can vary and depends on multiple factors including the lake volume, outburst mechanism and erosive processes (Kattel et al., 2020; Liu et al., 2020a). Similar factors govern how long the GLOF event will last. Significant differences arise when it comes to the temporal aspect of an outburst flood. While in some cases, the outburst requires only a very short time, other events have shown that the lake drainage can last multiple hours or even days, partly driven by the lake and drainage characteristics (Richardson and Reynolds, 2000; Mergili et al., 2011). Besides the outflow duration, knowledge about the time required by the mass flow to arrive at specific locations with high exposure and increased vulnerability is essential for evacuation and real-time disaster response (Melo et al., 2020).

Current literature distinguishes mainly between three different glacial lake types, namely moraine-, ice-, and bedrock-dammed lakes (Huggel et al., 2004). Wang et al. (2013) additionally account for glacial lakes that form in flat glacier forefields. Based on the type of lake, the possible trigger and outburst mechanisms as well as magnitudes of discharge can vary, which often adds substantial uncertainty to flow dynamics (Huggel et al., 2004). Thereby, bedrock-dammed lakes are the most stable, while moraine- and ice-dammed lakes are considered rather prone to failure (Huggel et al., 2004).

Moraine-dammed lakes exist in many high-mountain ranges whereas most of the moraines that act as natural dams formed during the LIA (Westoby et al., 2014). Provided there are no existing outflow channels and the moraine dam is mostly impermeable, glacial meltwater will accumulate in the depression formed by the glacier in earlier times (Richardson and Reynolds, 2000; Westoby et al., 2014). Theoretically, the lake can increase in volume until the height of the moraine dam is reached and overtopping is initiated, however, small pores and channels

within the moraine generally result in a natural regulation of the water level (Westoby et al., 2014).

In current literature, several processes are identified as possible triggers for the release of water from moraine-dammed lakes. On the one hand, mass movements that originate upslope of the lake and reach the water can cause impact waves which eventually lead to overtopping of the dam or dam failure through erosion (Richardson and Reynolds, 2000; Huggel et al., 2004). Additionally, in cases where the glacier is connected to the lake, calving and collapsing ice floes are further triggers with the ability to generate massive flood waves (Mergili et al., 2011).

On the other hand, the melting of ice cores and thawing of permafrost within the moraine can directly cause the collapse of the dam, whereby the released water can further widen and deepen the outflow channel (Bolch et al., 2012; Harrison et al., 2018).

Furthermore, higher water input resulting in an increasing hydrostatic pressure can cause an outburst, usually washing away large amounts of morainic material (Richardson and Reynolds, 2000). Additionally, increased water volumes can promote retrogressive erosion of the dam (Mergili et al., 2011). In some cases, seismic activity has also been found to cause the degradation and collapse of a moraine dam (Bolch et al., 2012). Westoby et al. (2014) list up to seven common triggers with the ability to cause an outburst flood at a moraine-dammed lake (Figure 2).

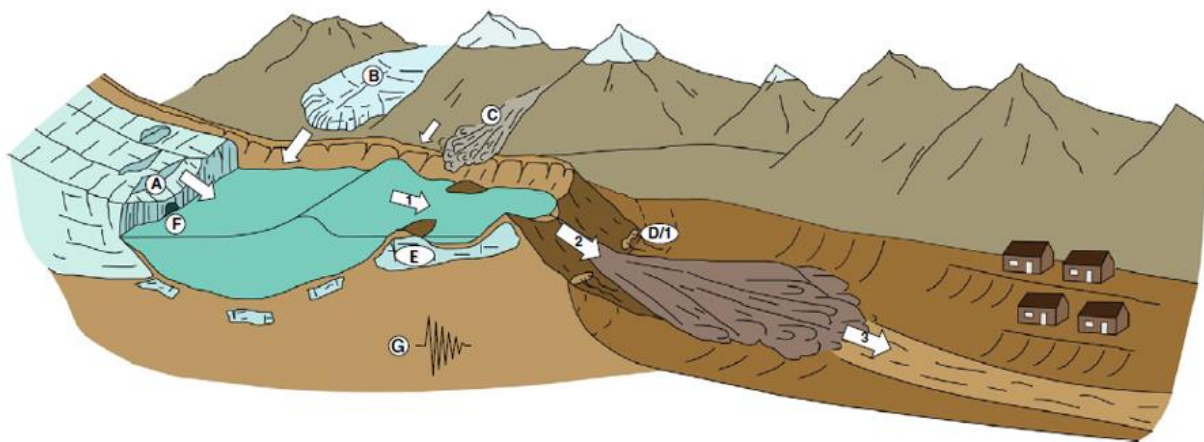


Figure 2: Illustration of potential triggers and key components of a GLOF event at a moraine-dammed lake. Key components consist of 1) flood wave propagation; 2) dam breach & outburst; 3) mass movement downstream of the dam. Processes that potentially lead to the outburst flood include A) glacial calving; B) ice fall from near-by glaciers; C) rock or snow avalanches; D) dam subsidence or piping; E) melting of buried ice cores within the moraine; F) rapidly rising water volume; G) seismic activity. (Adopted from Westoby et al., 2014)

Apart from moraine-dammed lakes, water can accumulate in sub-, supra- or englacial pockets, and even glacier tongues can act as a dam and form a glacial lake (Walder and Costa, 1996). Similar to moraine-dammed lakes, the failure of ice dams can also lead to catastrophic outbursts (Huggel et al., 2004). Furthermore, a rising lake volume and, resultingly, growing water pressures can cause the enlargement of subglacial channels and enhance drainage from the lake (Richardson and Reynolds, 2000). Once the channels close due to the cryostatic pressure exceeding the water pressure, the outflow is reduced again (Richardson and Reynolds, 2000).

However, flow volumes during drainage through subglacial channels are substantially smaller than for dam breaches (Huggel et al., 2004; Walder and Costa, 1996). Although the water often drains through englacial channel systems, impact waves and overtopping can be triggered by mass movements or glacier calving as well (Mergili et al., 2011; Worni et al., 2014).

What distinguishes ice-dammed lakes from moraine-dammed lakes is that often, ice-dammed lakes are characterized by a certain degree of seasonality. Subglacial channels allow lakes to drain until they get blocked due to ice deformation and freezing, only before the melt season leads to the opening and growing of the channels again. Hence, ice-dammed glacial lakes often exist for shorter periods as seasonal drainage is common, which also explains why lakes frequently form in the same depressions. (Narama et al., 2018)

GLOF events can additionally originate at bedrock-dammed lakes where the water is kept above an impermeable bedrock layer. Although bedrock-dammed lakes are not prone to failure, which is a reason why they are considered the most stable among the different lake types, GLOFs can still be triggered by mass movements entering the lake (Huggel et al., 2004). Nevertheless, according to Vilímek et al. (2014), only a small number of reported GLOFs have been observed at bedrock-dammed lakes.

In Central Asia, and specifically in Kyrgyzstan, the highest threat is expected from moraine-dammed lakes (Janský et al., 2010). Nonetheless, GLOF events originating from moraine-dammed lakes through dam failure are observed more frequently in the Himalayas, whereas in Central Asia, floods from short-lived ice-dammed lakes are more common (Narama et al., 2018; Zheng et al., 2021). Although surface flows are generally producing higher discharge, outbursts through subsurface channels are considered dangerous as well since the temporal aspect of subsurface flow is understood only poorly (Zaginaev et al., 2019).

When it comes to lake size and volume, recent developments at glacial lakes in Central Asia follow a similar pattern as it is observed on a global level. Although many studies point out that lakes in Central Asia are comparably small in size, lakes have grown rapidly during the last decades, and the lake number in some subregions has grown at even higher rates than the global mean (Narama et al., 2018; Shugar et al., 2020; Zheng et al., 2021).

In regard to trigger mechanisms, GLOFs reported in the Himalayas are typically triggered by mass movements entering the lake, which subsequently leads to dam failure (Lala et al., 2018; Liu et al., 2020a). In contrast, despite a lack of literature on typical triggers for Central Asia, the fact that the majority of GLOFs in Central Asia are initiated through subsurface drainage suggests that increased water pressures and other mechanisms leading to channel opening are processes representative for this region (Narama et al., 2018).

2.2 Related Mass Movements

After a GLOF has been triggered, the flow behaviour of the mass movement can vary significantly, also depending on the outburst mechanism. On the one hand, solid material can

be entrained during the outburst in the event of a moraine-dam breach. Thereby, the outburst itself can result in vast amounts of moraine material being entrained in the outflow as a consequence of dam erosion (Westoby et al., 2014). On the other hand, unconsolidated sediments and deposits from former mass movements along the trajectory can be eroded by the mass flow (Richardson and Reynolds, 2000; Breien et al., 2008). The collapse of lateral moraines caused by a passing flood can additionally lead to the uptake of solid material (Liu et al., 2020a). As a consequence, although floods are released from glacial lakes, entrainment can result in a transition to debris flow-like mass movements (Richardson and Reynolds, 2000). Bolch et al. (2012) state that in the Northern Tian Shan, GLOFs were responsible for the occurrence of mudflows in 11% of the reported severe events. In Breien et al. (2008), it is discussed that typical triggers of debris flows are characterised by surface water flow eroding sediments found at the channel bed. Ranging from pure floods with low viscosity to more sediment-laden mass flows, the entrainment of solids and the subsequent transition to various forms of mass movements usually increases the flow volume manyfold (Westoby et al., 2014; Frank et al., 2017). As the amount of solid material entrained is highly variable, further uncertainties related to GLOF dynamics arise in addition to the varying release conditions.

2.2.1 Entrainment of Solid Material

Provided that unconsolidated sediments are available in the channel bed, a certain velocity of the mass flow is required to transport the solids, which is mainly driven by the slope of the channel (Bolch et al., 2012). Unless the average channel slope is between 10-15°, mass movements with high solid fractions tend to come to a halt or at least get only seldom triggered (Huggel et al., 2002b; Westoby et al., 2014). Hence, the solid fraction of GLOF-induced mass movements does not necessarily stem from moraine dams, but also floods originating from subsurface drainage can transform into debris flows provided that sufficient erodible material is available in the channel bed or deposits are found on the lateral sides of the flow path (Narama et al., 2018). Although the temporal evolution of the initial discharge, what typically is referred to as a hydrograph, is governed by the trigger and lake or drainage characteristics, flow dynamics further downstream are controlled by topographic factors and sediment availability shortly after the release zone (Westoby et al., 2014).

Although the front of the mass flow usually has the largest flow height, flow characteristics vary owing to changing solid volumes (McArdell et al., 2007). Schürch et al. (2011) found that flow height to a large extent governs erosive processes, which explains why sediments are eroded mainly while the flow front passes by (Berger et al., 2011). Three processes through which the flow height promotes erosion at the flow front are discussed in Schürch et al. (2011): On the one hand, basal shear stress rises with increasing flow depth. On the other hand, larger particles and boulders moving within the flow snout generate further stresses on the channel bed (Stock and Dietrich, 2006). Moreover, the flow front's hydraulic pressure acting on the channel bed can cause the liquefaction thereof (Sassa and Wang, 2005).

Despite flow heights being coupled with discharge, channel gradient and geometry can alter the flow dynamics which subsequently can lead to the deposition of solids once the terrain becomes flatter or flow momentum is reduced (Schürch et al., 2011). Additionally, the solid-liquid ratio and viscosity of the mass do have a substantial influence on flow behaviour (Worni et al., 2014). Due to entrainment in areas downstream of the lake, even initially low-volume floods can evolve into massive debris flows, which resultingly increases the peak flow volume and discharge by factors of 3 and higher (Huggel et al., 2003; Mergili et al., 2011). This is in line with other studies (Cenderelli and Wohl, 2003; Westoby et al., 2014) where the impacts of entrainment regarding discharge variations compared to initial breach hydrographs are discussed. Breien et al. (2008) claim that a positive feedback effect could be the reason why mass movements' flow volumes increase as observed since erosion is promoted with higher solid fractions.

When it comes to the effects of increased volumes on flow mobility, Breien et al. (2008) generally claim that flow velocities rise in response to the addition of debris. As a result, not only does flow momentum increase but the runout distance reached is affected as well (Westoby et al., 2014). Nevertheless, a growing solid fraction will alter viscosity and cohesion within the flowing mass which in turn might have a reverse effect and lead to a decrease in mobility (Breien et al., 2008). According to Iverson et al. (2011), the effect on flow mobility additionally depends on the terrain properties as wet terrain generally promotes mobility and momentum whereas dry terrain usually tends to impede further momentum growth. Resulting from changes in flow momentum, entrainment can quickly evolve into deposition, often leading to alternating areas in which either entrainment or deposition dominates, a process that Carrivick et al. (2010) mainly attribute to frictional forces and geomorphic landforms.

2.2.2 Transitions to Other Mass Movements

Resulting of the entrainment of solid material as well as potential fluid sources apart from lake water, GLOFs can take on various characteristics and evolve into different mass movements. Since definitions of mass movements do depend on various factors including their composition, solid-liquid ratio, trigger, velocity, and other flow characteristics, distinguishing between types of movements has proven difficult (Coussot and Meunier, 1996). Furthermore, the fact that some criteria change during the same event adds to the difficulties and uncertainties in classifying the type of event (Coussot and Meunier, 1996). Consequently, transitions between mass movement types can be fluent and blurry, which is why several studies have tried illustrating the transitions between multiple phenomena (Figure 3).

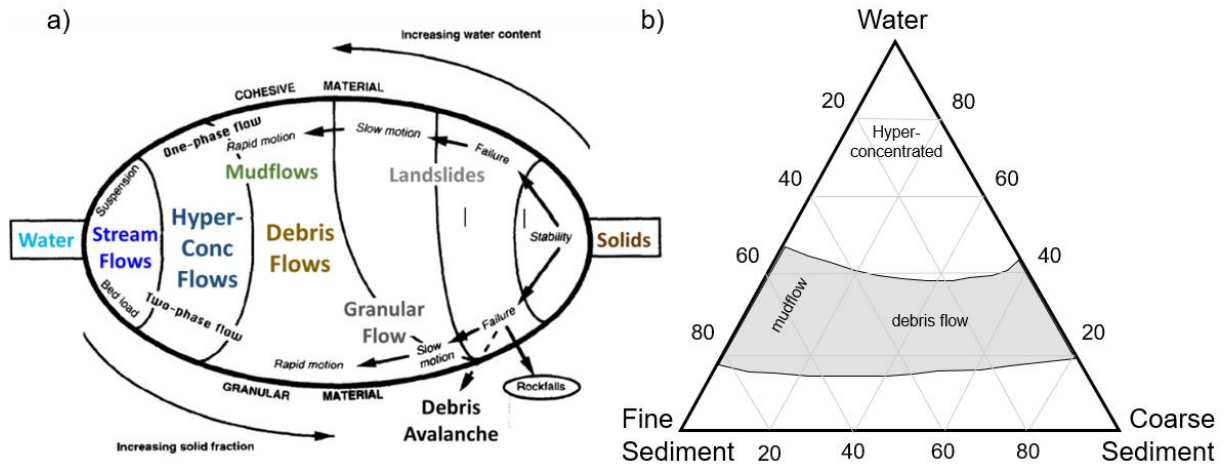


Figure 3: a) Taxonomy of mass movements after Coussot & Meunier (1996); b) Classification of geophysical flows after Phillips & Davies (1991) (adopted from Gibson et al., 2020).

When it comes to the transition from GLOFs to debris flows, it is pointed out that the availability of sediments does determine how fast the mass movement evolves into a debris flow. Apart from the outburst process, the amount of debris in proximity to the release zone controls how fast the composition of the flow changes and how fast sediment concentrations can increase. Hence, the mass flow sequentially turns into different types of geophysical flows, while sediment concentrations normally increase continuously provided that enough debris and deposits are available. (Cui et al., 2010)

The transition from pure water to debris flow passes the stage of hyperconcentrated flows (Figure 4). Although sediment has been entrained in hyperconcentrated flows, they can be distinguished from debris flows based on the solid fraction. While hyperconcentrated flows usually are characterised by a solid fraction lower than 25% of the total volume, debris flows normally exhibit solid fractions of more than 50% and up to 90% of the flow volume (Coussot and Meunier, 1996). However, it is stressed in Coussot and Meunier (1996) that the solid-liquid ratio can vary substantially within a mass movement as well. Thus, debris flow fronts can show a far greater fraction of solid material than the more liquid tail of the mass flow (Coussot and Meunier, 1996). Pierson (1986) agrees by claiming that debris flows tend to have multiple sections with different characteristics and solid-liquid ratios (Figure 4).

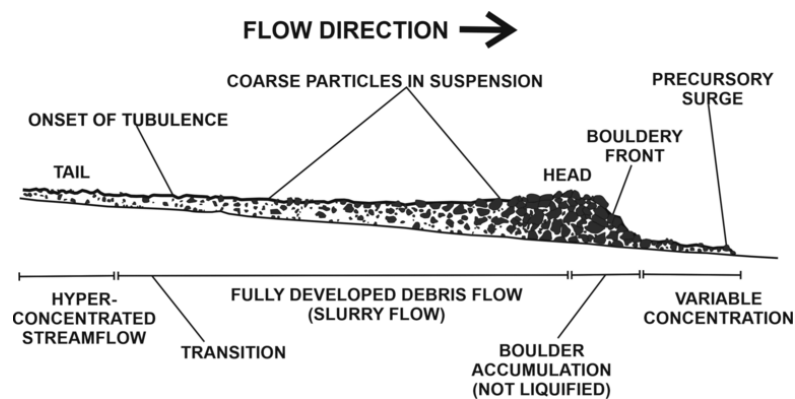


Figure 4: Illustration of a debris flow showing different sections and flow compositions (adopted from Pierson, 1986).

Pierson (1986) shows that the flow front is both characterised by the largest flow depths and the highest number of boulders, whereas particles behind the front continuously decrease in size while the liquid fraction increases towards the back of the mass. The mass flow type is additionally determined to a great extent by the sediment size (Cui et al., 2010) (Figure 3b). While the incorporation of fine particles leads to transitions to mudflow-like movements, the entrainment of larger debris and boulders results in debris flows. Additionally, mass movements with similar solid-liquid ratios can be distinguished by flow velocity, however, thresholds between mass flows do vary among available studies (Pierson and Costa, 1987).

Transformations to other mass movement types are hence characterized by a great amount of uncertainty. On the one hand, the classification remains difficult mainly owing to multiple factors driving the amount of entrained sediment in the flow, and secondly due to inconsistencies in defining the types and transitions of geophysical flows. On the other hand, the consequences resulting from transformations can increase uncertainties related to disaster response and evacuation measures.

Compared to GLOFs, which can last several hours depending on the outburst mechanism, the duration of debris flows usually is shorter (Coussot and Meunier, 1996). Thereby, by referring to the study by Pierson (1986), Coussot and Meunier (1996) stress that, on the one hand, the relative flow velocity of the solid and liquid particles is rather low, and, on the other hand, the entire mass experiences similar deformations, which is why debris flows can be considered as single-phase flows in simplified models. Nevertheless, the different characteristics between a debris flow's front and its tail make it difficult to account for varying solid-liquid ratios, especially when describing the processes and flow behaviour during transitions from GLOFs to other types of mass movement.

Irrespective of the solid-liquid ratio, the entrainment of solids increases the damage potential of GLOFs (Baggio et al., 2021; Liu et al., 2020b). According to Petrakov et al. (2020), this is the reason why Central Asia has experienced more disasters caused by GLOFs than in the Hindukush-Karakoram-Himalaya region, although glacial lakes tend to be comparably smaller in Central Asia. Peak discharges are estimated to have reached up to $12'000 \text{ m}^3 \text{ s}^{-1}$ while entrained sediment volumes are said to have amounted up to a few million cubic meters in past events (Petrakov et al., 2020). When it comes to the runout distance, Richardson and Reynolds (2000) stress that although glacial lakes are usually located in remote regions, they can reach settlements and cities lying dozens of kilometres downstream, in one case even exceeding a distance of 200 km.

Nonetheless, Harrison et al. (2018) point out that both in Central Asia and in the Hindukush-Karakoram-Himalaya, GLOF frequency has declined in the past decades, which is in line with developments on a global scale. In Harrison et al. (2018), GLOF frequency is compared with temperature records from the last century, and they observe a relatively strong correlation. However, the attribution of GLOF frequency and risk to climate change is still questioned by contemporary scholars since the occurrence of GLOFs to a wide extent also depends on other

factors mentioned earlier in this chapter (Huggel et al., 2020). While climate change has direct impacts on certain factors such as glacier retreat and lake expansion, others are either independent or only driven indirectly by global warming.

2.3 Research on GLOF Modelling

In recent years, there has been a growing interest and effort in modelling glacier lake outburst floods and related processes. A substantial fraction of studies have examined GLOFs within the scope of hazard assessments (Frey et al., 2018; Sattar et al., 2020), while others have focused more on modelling entire process chains, where the GLOF itself only constitutes one process within a cascade of events (Lala et al., 2018; Somos-Valenzuela et al., 2016; Worni et al., 2014). Since transformations into more sediment-laden flows increase the potential impact pressure of mass movements, scholars have increasingly been interested in analysing erosive processes during an event (Frank et al., 2015, 2017). Furthermore, glacial lake volumes and outburst mechanisms determine to a great extent how much water is released during a certain timeframe. Therefore, peak discharge and the shape of hydrographs have also increasingly been experimented upon in recent literature (Anaconda et al., 2015; Paixão et al., 2021; Sattar et al., 2020). Although numerous studies share similar research topics, different findings result since their modelling approaches vary.

2.3.1 Different Model Types

As pointed out by Mergili et al. (2011), GLOF modelling has proven complicated since the flow behaviour of GLOFs resembles both, debris flows and floods. However, existing models are only designed for simulations of one or the other without considering their transitional character between the separate types of movement. Despite most models applying to only one type of mass movement in theory, GLOF modelling approaches have used such models by adjusting certain parameters to reflect the behaviour of GLOFs more accurately (Mergili et al., 2011). Although physical models exist and are often used for simulating GLOFs, simple empirical models have been applied mainly because input data requirements are less demanding and nevertheless produce useful results (Anaconda et al., 2018; Westoby et al., 2014).

Their dynamic counterparts, physically based models, consider GLOF flow behaviour in much more detail and take into account complex behaviour such as flow momentum, particle interactions, frictional resistance, and other flow dynamics (Worni et al., 2014). Since multiple physical characteristics are considered, such flow models are regarded as essential for understanding GLOF dynamics and hazard (Anaconda et al., 2018). On the contrary, Westoby et al. (2015) stress that physically based models are not used as often as one might expect because the amount of data requirements constrain the use of such detailed models. To reconstruct past events, knowledge of discharge, particle sizes, or the solid-liquid ratio are required, which cannot be obtained in all regions (Westoby et al., 2015). As precise field data would be required for accurate simulations, uncertainty in the results usually increases with a rising level of detail in such models (Frey et al., 2016).

A further distinction between the models applied in GLOF-related studies refers to the number of spatial dimensions used. While one-dimensional models have also successfully been applied for GLOF simulations (Somos-Valenzuela et al., 2016), Westoby et al. (2014) claim that multiple flow dynamics and channel characteristics such as the flow's momentum loss through boundary friction are not accounted for in one-dimensional (1-D) models and only have an impact on the results in 2-D and 3-D models. Modelling non-Newtonian flow behaviour, meaning that the fluid's viscosity can change in response to changing shear stress, which is observed in GLOFs and debris flows therefore is not possible in many 1-D models (Westoby et al., 2014). Anacona et al. (2018) emphasise that in particular the variations between Newtonian and non-Newtonian flow behaviour cannot be modelled precisely. However, the amount of knowledge and input data required in 2-D and 3-D models might constrain their application and promote the use of models with fewer requirements (Anacona et al., 2018).

The variety of models applied for simulating GLOFs can additionally be divided into models that consider the moving mass as single- or multi-phase flow. Coussot and Meunier (1996) have discussed that in simplified models, debris flow-like mass movements can be considered as single-phase flows, which is why several models exist which treat debris flows as having only one rheology and behave as a bulk flow (Mitchell et al., 2022). Nevertheless, since the incorporation of solid material at the start of the mass flow as well as entrainment during the event significantly impact the dynamics of GLOFs, some scholars emphasise the importance of two-phase flow models for more realistic simulations (Worni et al., 2014; Mergili et al., 2018a). Not only do multi-phase models distinguish between solid and fluid fractions, but they also consider how solid and fluid particles interact within the moving mass (Mergili et al., 2018a). Despite their level of detail and their improved representation of reality, multi-phase models often require information on input parameters which is difficult to obtain (Mitchell et al., 2022). Thus, in areas such as engineering, single-phase models are commonly preferred over multi-phase versions (Mitchell et al., 2022).

Simulations for this thesis are carried out using the Rapid Mass Movements Simulation (RAMMS) software, which is a single-phase numerical and physically-based model with a debris flow module that has been applied in multiple GLOF-related studies (Anacona et al., 2018; Frey et al., 2018). Although there exist models such as the extended version of RAMMS as well as *r.avaflo*¹ (described in detail in Mergili et al., 2017), which consider the two-phase characteristic of geophysical flows and account for erosion as well as deposition of material along the channel, less data-heavy models such as the single-phase version of RAMMS or FLO-2D² (Cesca and D'Agostino, 2008) are often preferred. A significant advantage of RAMMS is that the entrainment of additional material can be accounted for, which makes it applicable for studies focusing on transitions from GLOFs to debris flows where the flow volume changes during the event (Mergili et al., 2011; Worni et al., 2014).

¹ Two-phase mass flow simulation tool: <https://www.landslidemodels.org/r.avaflo/>

² 2D flood routing model: <https://flo-2d.com/>

2.3.2 Previous GLOF Studies

Before RAMMS can be applied properly in a catchment, parameters need to be adjusted for the given location. In general, reconstructions of past GLOF events are a common way how to calibrate a model in a specific region where hazard assessments and other analyses are carried out (Frey et al., 2018; Worni et al., 2014). To recreate the flow dynamics of past events, studies usually focus on geomorphic features and deposition characteristics that are available in the field (Anaconda et al., 2018). Surveys at the field site can additionally help determine indicators for flow heights, widths, or other flow parameters that can be used to finetune the model parameters (Klimeš et al., 2014; Zaginaev et al., 2016). Others have used knowledge of local inhabitants to get an understanding of flow characteristics (Anaconda et al., 2015). Usually, reconstructions of events help calibrate the model to enable further analyses in the catchment (Worni et al., 2014). In cases where data is scarce, sensitivity analyses are performed so that, on the one hand, the remaining parameters can be adjusted for calibration, and, on the other hand, the variability of model results in response to parameter changes is determined (Worni et al., 2014).

Several previous studies have analysed the impacts of different input parameters on model results either in RAMMS or other models. Many scholars that used RAMMS for their GLOF and debris flow simulations have evaluated the impact of two friction parameters on flow dynamics (Anaconda et al., 2018; Frank et al., 2015; Schraml et al., 2015). Frey et al. (2016) have analysed the impact of RAMMS' turbulent friction parameter ζ on multiple flow characteristics and have found that in their catchment, the height and velocity of the mass as well as the distance reached by the flow barely vary with a change in ζ . It was found by Anaconda et al. (2018) that runout distance is more strongly governed by μ , which is the second friction coefficient in RAMMS. Changing frictional behaviour based on the type of mass movement, ranging between hyperconcentrated flows and viscous debris flows, allowed to approximate the behaviour of different mass flow types (Frey et al., 2018).

Anaconda et al. (2018) have additionally investigated how different sizes of mass movements behave along the flow trajectory by mainly changing flow density and release volume. Although such sensitivity analyses can provide valuable information about a possible range of scenarios originating at the lake, there has been a growing interest in determining the release volume based on the processes that triggered the eventual GLOF event. Another area where GLOF and debris flow modelling are applied therefore deals with the cascade of processes that often occurs in mountainous regions. Usually, those process chains are divided into three main components representing the lake impact, dam breach or outburst mechanism, and the flood propagation downstream of the lake (Westoby et al., 2014; Worni et al., 2014). As there exists no single model with the ability to combine the different components, usually multiple models are used for the subsequent processes (Frey et al., 2018). Thereby, the results of earlier steps are used to define initial conditions for the following model (Frey et al., 2018). Somos-Valenzuela et al. (2016) and others (Frey et al., 2018) have used the RAMMS Avalanche module to simulate the

first component of the process chain and to analyse the generation of an impact wave at a glacial lake caused by avalanches of different sizes. Flood wave propagation can then be carried out in models such as FLOW-3D³, where lake bathymetry and impact volume are the main drivers (Frey et al., 2018; Somos-Valenzuela et al., 2016). In the case of moraine-dammed lakes, the subsequent processes that are usually considered in process chain modelling are mechanisms related to overtopping or dam breaching. For simulating a dam breach, again multiple models exist, whereby BASEMENT⁴ or HEC-RAS⁵ are reported in recent studies (Somos-Valenzuela et al., 2016). Frey et al. (2018) stress that except for the susceptibility of the moraine dam, most processes are governed directly by the avalanche dynamics and their impact at the lake. The fact that models designed for the different components of a GLOF have not been developed explicitly for simulating a cascade of processes is a limitation to process chain modelling as outputs of one model need to be coupled with the subsequent model (Worni et al., 2014). Resultingly, uncertainties stemming from prior processes can be carried along the cascade which additionally constrains the result (Westoby et al., 2015). Nevertheless, combining the initial trigger, wave propagation and outburst mechanisms can provide valuable information on the outflow hydrograph which in turn determines the initial conditions for the flood propagation downstream of the lake and, hence, influences the eventual GLOF behaviour. In addition to defining the breach hydrograph, such modelling strategies can support the determination of the solid volume incorporated in the flow at the time of an outburst.

2.3.2.1 Research on Boundary Conditions

Not only are outburst hydrographs exposed to uncertainties in process chain modelling, but also if the model is used to simulate the flood propagation of a GLOF separately, the choice of the hydrograph's shape has significant impacts on flow dynamics. Sattar et al. (2020) have analysed how the inundation depth and velocity of the mass movement vary in response to altered outflow volumes. By varying breach width and depth of the moraine dam, they controlled the volume of water released by the lake. While breach depth determines largely how much water drains from the lake, the temporal aspect of the dam failure governs how much water is released in a certain time period. Sattar et al. (2020) found that the temporal aspect of the dam breach has a greater impact on the hydrograph than the breach depth. Although the results are based on simulations at a moraine-dammed lake in Central Himalaya, they are applicable also in similar settings since both lake volume, as well as breach depth, are not necessarily site-specific. In contrast, Zaginaev et al. (2019), who investigated GLOF dynamics in the Ala Archa National Park in Kyrgyzstan, used a different approach where they focused on peak discharge rather than on the temporal dimension of a hydrograph. To determine possible inundation depths in the valley below, they modelled lake outbursts using a scenario-based approach, where historical data of different discharge observations were implemented. If there is a lack of historical data, uncertainty in defining the initial conditions increases, which is why Frey et al. (2018) have

³ Computational fluid dynamics software: <https://www.flow3d.com/>

⁴ Basic Simulation Environment: <https://basement.ethz.ch/>

⁵ Hydrologic Engineering Center's River Analysis System: <https://www.hec.usace.army.mil/software/hec-ras/>

used empirical equations presented in Heller et al. (2009) to derive possible release volumes. Another approach to cope with uncertainty arising from natural variability, which is similar to the study by Sattar et al. (2020), is discussed in Mitchell et al. (2022) who have analysed debris flow events in Canada by evaluating the impacts of varying input hydrographs on flow heights and velocities. Mitchell et al. (2022) found that observed discharge values in certain channel sections cannot be related to specific input hydrographs since topography significantly alters the flow magnitude which highlights the importance of evaluating the variability of outcomes in response to altered release hydrographs.

Apart from release volumes and peak discharges, the initial velocity also contributes to the boundary conditions at the initiation of the mass movement. Sattar et al. (2020) have investigated how the flow velocity changes along the channel and found a relatively strong sensitivity to slope meaning that channel characteristics have a strong impact on the velocity of the mass. Furthermore, Westoby et al. (2014) argue that geomorphic features, sediment availability, and other channel properties can result in significant changes to the mass movement in a comparably short time. In Rosli et al. (2021), the importance of flow velocity, which is driven to some degree by the composition of the mass, is discussed by considering the direct impact on evacuation time for settlements downstream of the release area. Depending on the distance to the settlements and on the flow velocity, evacuation times vary considerably. In Melo et al. (2020), it is discussed that depending on the initial conditions, the time available to people in exposed regions to evacuate themselves varies substantially.

2.3.2.2 Research on Erosion

Despite the importance of entrainment in GLOF and debris flow dynamics, several models are used in GLOF studies where entrainment is not taken into account. Provided that one aims to simulate the total flow volume nonetheless, the initial volume should therefore already include all the solid material that would have been entrained during the flow (Frank et al., 2015). A limitation of this approach is described by Frank et al. (2015) who claim that due to geomorphic characteristics, flow behaviour likely deviates from expected mechanisms also because discharge values in the early stages of the flow certainly exceed the expected flow magnitude. As the deposition of solid material might occur earlier since channel capacity is reached due to a high initial discharge, a substantial amount of material might be lost along the trajectory, and the runout distance and area might even be underpredicted (Frank et al., 2015). Despite two sources of uncertainty arising from the neglect of entrainment in flow models, the incorporation of such behaviour also results in increased uncertainty as additional information on erosion parameters is required, which in many cases involves taking assumptions (Luna et al., 2012). Additionally, the variability in the amount of erodible material and the timing of entrainment add to the uncertainty (Frank et al., 2015; Somos-Valenzuela et al., 2016). Furthermore, Somos-Valenzuela et al. (2016) stress that the physical properties of the mass flow especially regarding the entrained sediments and the resulting solid-liquid ratio further amplify the uncertainty in model results. Nonetheless, Frank et al. (2017) argue that adding

mass during the flood propagation will provide more realistic results and improves the prediction of flow dynamics and runout areas.

While outburst floods originating at moraine-dammed lakes usually are characterized by large volumes of sediments being incorporated during the dam breach due to dam erosion, other scenarios at different lake types will mainly obtain their solid fraction from channel erosion (Frey et al., 2018). In RAMMS and other software, areas within the catchment can be defined to allow the mass flow to erode additional material, an approach that has been used in multiple studies (Frey et al., 2018; Mergili et al., 2018). Frey et al. (2018) have enabled erosion in various areas using available field data to simulate transformations from GLOFs to other types of mass movements whereby entrainment was considered in regions with slopes greater than 5.71° (10%).

Since the incorporation of solids is widely considered an essential factor controlling the area affected by an event, various studies have used dynamic models to enhance the understanding of the main drivers of erosion during a mass movement. Frank et al. (2017) have investigated how changes in several erosion parameters affect the total eroded volume during debris flows. Similarly, Vicari et al. (2021) have evaluated how varying friction parameters influence the eroded volume. It is suggested that the two friction coefficients in RAMMS affect the flow height which in turn drives the shear stress acting on the channel bed responsible for the onset of erosion (Vicari et al., 2021). Schürch et al. (2011) agree by pointing out that the timing and amount of erosion are controlled to a large extent by flow height, which explains why debris flow fronts can erode much more material than the rather flood-like tail. Resultingly, the fact that substantial erosion takes place at the time the flow front reaches a location supports the statement that flow height is a strong driver of erosion as it increases shear stress on the channel surface, a factor that must be considered more carefully in debris flow and GLOF models (Berger et al., 2011; Schürch et al., 2011). Nevertheless, the temporal aspect of erosion has not been explored as much as the drivers of entrainment. In Cuomo et al. (2016), variations in the timing of erosion are investigated, however, only a debris flow-like mass movement with a short travel distance is considered.

2.3.2.3 Research on GLOF Transitions

Many studies focus on the interplay of slope and flow velocity and their influence on entrainment and deposition (Luna et al., 2012). In Westoby et al. (2014), it is discussed that the uptake of sediments and the resulting volume increase will lead to rising flow velocities. Although higher flow volumes at the beginning will increase flow mobility, mechanisms induced by cohesion and viscosity could force the flow to slow down again (Westoby et al., 2014). These feedback effects do also depend on the initial conditions that prevail at the channel topography, as wet terrain normally promotes flow velocities and mobility to increase whereas dry terrain tends to have a decelerating effect (Iverson et al., 2011). As found by Huggel et al. (2002), the critical slope angle below which debris flows begin to decelerate and deposition starts approximately lies between 10 and 11° . Topographic and geomorphic features are capable

of forcing the deposition of solids as well, however, in general, for a continued mass flow, the critical slope angle must be sustained. If a GLOF has not fully transformed into a debris flow, the critical slope angle is reduced, as pure floods are sustained even at slopes of 2° , which would theoretically differentiate debris flow models from GLOF simulations (Huggel et al., 2002a). Mergili et al. (2011) emphasise the importance of modelling different rheologies of GLOFs since results ranging between pure floods and debris flows provide higher robustness and allow findings to cover various types of mass movements. One method is presented by Frey et al. (2018) who attempt to approximate the dynamics of multi-phase flows and to simulate the transitions to other types of mass movements with the single-phase model RAMMS, an approach that has been applied only infrequently. Since the vast majority of models are designed for one mass flow type specifically, modelling of flow type transitions is associated with considerable uncertainties, as input and flow parameters need to be adjusted to account for changing compositions of the mass (Mergili et al., 2011). Meyrat et al. (2021) have modelled debris flow dynamics using a multi-phase model whereby the spatial evolution of flow composition and density within the same mass flow could successfully be simulated. A main advantage of such models is that frictional behaviour is controlled as a function of flow composition, leading to much higher variability in friction compared to the approach discussed in Frey et al. (2018). While in the single-phase version, the entrainment of sediments does not alter the density and viscosity of the flowing mass, the addition of solid material automatically affects the flow composition of the interplay of solid and liquid fractions in enhanced models and enables the modelling of dilatancy (Meyrat et al., 2021).

3 Research Objectives

3.1 Research Gap

Although numerous studies on modelling GLOF dynamics exist, some mechanisms are still poorly understood. In recent literature on GLOF modelling, the majority of studies relate to the analysis of entrainment and deposition as well as to different flow magnitudes. Experiments involving the release mechanisms and initial conditions of GLOFs mainly investigate process chains where the hydrograph of a GLOF is determined based on processes occurring before the lake outburst. A few studies have evaluated how different release volumes affect downstream regions, however, especially the temporal variations between different scenarios have only seldom been discussed. Despite findings in Westoby et al. (2014), which show that the first wave released from a moraine-dammed lake reached the valley in the order of minutes, there is a lack of knowledge when it comes to travel times in different scenarios although evacuation plans and other disaster responses could greatly benefit from such studies. Only Melo et al. (2020) and Rosli et al. (2021) have touched upon estimating the time available to people to evacuate depending on initial conditions set at the release of the mass movement. Additionally, while the boundary conditions define the characteristics at the beginning of mass movements, there remains substantial uncertainty regarding how long those boundary conditions have an impact on the flow. As pointed out by Sattar et al. (2020), initial flow velocities might change rapidly after the outburst. Similarly, Westoby et al. (2014) stressed that mainly because solid material is entrained during the flow, discharge measurements further downstream strongly deviate from initial discharge values. Hence, Paixão et al. (2021) suggest examining the sensitivity of various flow dynamics, especially regarding the defined boundary conditions.

Regarding erosive processes and entrainment during GLOFs and debris flows, a vast amount of literature exists. In recent studies, sensitivity analyses on friction and erosion parameters as well as experiments regarding the spatial variability of erosion and deposition have been used to analyse erosive patterns during mass movements. Nevertheless, Schürch et al. (2011) emphasise that the flow behaviour of debris flows still is associated with a substantial amount of uncertainty, partly due to the complexity of sediment transport and deposition. Especially the quantification of entrainment is so far not covered and understood sufficiently to improve dynamic modelling of such mass movements (Luna et al., 2012; Worni et al., 2014). The lack of knowledge could partly be explained by the limited availability of relevant data (Breien et al., 2008).

It is suggested by Anaconda et al. (2018) that analyses of erosion rates could enhance the understanding of erosive processes. In turn, Frank et al. (2015) propose to focus on the solid volume eroded by mass movements since the area inundated by an event strongly depends on how much material is added to the flow. Particularly for Central Asia, there is a lack of research dedicated to GLOF processes also because other regions such as the Himalayas have shown larger GLOF-related disasters (Narama et al., 2010). Erokhin et al. (2018) do confirm that the

small number of GLOF-related literature does not reflect the large number of potentially dangerous glacial lakes in Central Asian countries.

What is more, literature dealing with flow type transitions is scarce since modelling the flow dynamics of distinct types of movements is constraint by the model set up. Nevertheless, the entrainment of solid material significantly alters flow behaviour and needs to be accounted for in realistic simulations which is why analyses focusing on these flow transformations should be carried out more often as they can enhance the knowledge about relevant processes despite the substantial amount of uncertainty that results from such modelling approaches.

Since the vast majority of models are designed for one mass flow type specifically, modelling of flow type transitions is associated with considerable uncertainties, as input and flow parameters need to be adjusted to account for changing compositions of the mass (Mergili et al., 2011).

3.2 Research Questions

Based on the available literature discussed above, three areas have been identified where this thesis aims to improve the knowledge of GLOF processes.

As boundary conditions and parameter values at the initiation of the mass movement are often associated with epistemic uncertainties, simulations with varying outburst scenarios should provide more insights into how different release conditions affect the downstream regions and how the variability of results can be quantified. Epistemic uncertainties are described in Beven et al. (2015) and include the lack of knowledge about parameter ranges and initial conditions. In GLOF and debris flow modelling, epistemic uncertainties above all relate to defining input hydrographs whereby potential peak discharges and temporal aspects of lake drainage pose challenges to modellers (Westoby et al., 2015). Resultingly, variations in flow depth and flow velocities are observed downstream of the release zone owing to different hydrograph scenarios. Furthermore, changes in peak discharge and flow volumes lead to varying flow durations, which have direct impacts on people living in areas in proximity to the channel. The time until the mass flow arrives at certain locations is assumably driven largely by boundary conditions; an aspect which, to the authors' knowledge, has not been examined in detail so far. Furthermore, depending on the scenario, release conditions might influence the mass flow only in the early stages of the event, whereas in lower sections, the flow behaviour could be subject to change either due to geomorphic features or gained momentum of the mass but also owing to sediment entrainment during the flow.

When it comes to entrainment modelling, many studies have pointed out that processes involving erosion and deposition are understood only poorly. Although multiple studies have investigated the sensitivity of the runout area to erosion and friction parameters, there is a lack of literature regarding the spatial and temporal variability of erosion. Using the erosion parameters available in the RAMMS debris flow module, processes and mechanisms within different regions of the catchment will be analysed to improve the understanding of how GLOF

behaviour is affected by entrained material and how flow dynamics change in response to varying sediment inputs. Besides spatial variability, the temporal aspect will be investigated so that findings from other literature can be supported or questioned since studies on the timing of erosion are still scarce. Since the impact on people and infrastructure is heavily dependent on the flow behaviour shaped by boundary conditions and entrainment along the channel, the variability in travel times will be analysed since there is a lack of literature dealing with the influence of varying flow and channel properties on the time available for evacuation.

Additional uncertainties arise owing to the model used since the RAMMS version where all simulations are performed in only allows to model single-phase mass flows. Nevertheless, as knowledge of local parameters and field data about the catchment is limited, the lower number of input data needed in the single-phase model is beneficial. Contrary to other existing models, the entrainment module incorporated in RAMMS allows modelling of transitions to other flow types to a certain degree. Since GLOFs can transition to various types of mass movements depending, amongst other factors, on the amount of sediment available, initially defined boundary conditions do not always result in the same outcome. As suggested by Mergili et al. (2011), simulating a variety of flow rheologies can provide details on how pure liquid, as well as more solid-laden mass movements, would behave, despite the constraints of a single-phase model. Changes in liquid and solid volumes can thus be used to interpret how possible events in the catchment could behave and how they could impact the downstream regions. The approach discussed in Frey et al. (2018) will be partly adapted to enable analyses of the transitional behaviour of GLOFs and similar mass movements.

Different sources of uncertainty and variability in scenarios originating at a glacial lake shall be investigated using the following research questions:

How do uncertainties in release conditions and channel characteristics affect the flow behaviour of GLOFs and similar mass movements?

- 1) How do different outburst mechanisms and hydrograph shapes affect flow dynamics?
- 2) How large is the variability in flow duration in response to different boundary conditions?
- 3) How are the amount and the timing of erosion governed by channel properties and flow dynamics?
- 4) How do erosive processes affect uncertainties in model results?
- 5) To what extent can different mass movement types be simulated with single-phase models?

Guided by those questions, the simulations performed will allow analyses of the impacts caused by different outburst mechanisms and compositions of the mass on flow dynamics. Furthermore, the findings shall improve the knowledge about the variability of outcomes that can help design adaptation strategies to protect local people and infrastructure in downstream regions.

4 Data and Methods

4.1 Study Site

The scenarios modelled in RAMMS simulate mass movements originating at a glacial lake situated in Northern Kyrgyzstan. The study site lies in the Ala Archa National Park about 35 kilometres south of Bishkek, the capital city of Kyrgyzstan. The Ala Archa catchment is located in the Kyrgyz Ala-Too Range which forms part of the Northern Tian Shan Mountains and stretches from west to east for almost 400 km (Kattel et al., 2020) (Figure 5). Its water feeds the Chui River, which is utilized for water supply and irrigational purposes in the border region between Kazakhstan and Kyrgyzstan (Erokhin et al., 2018).

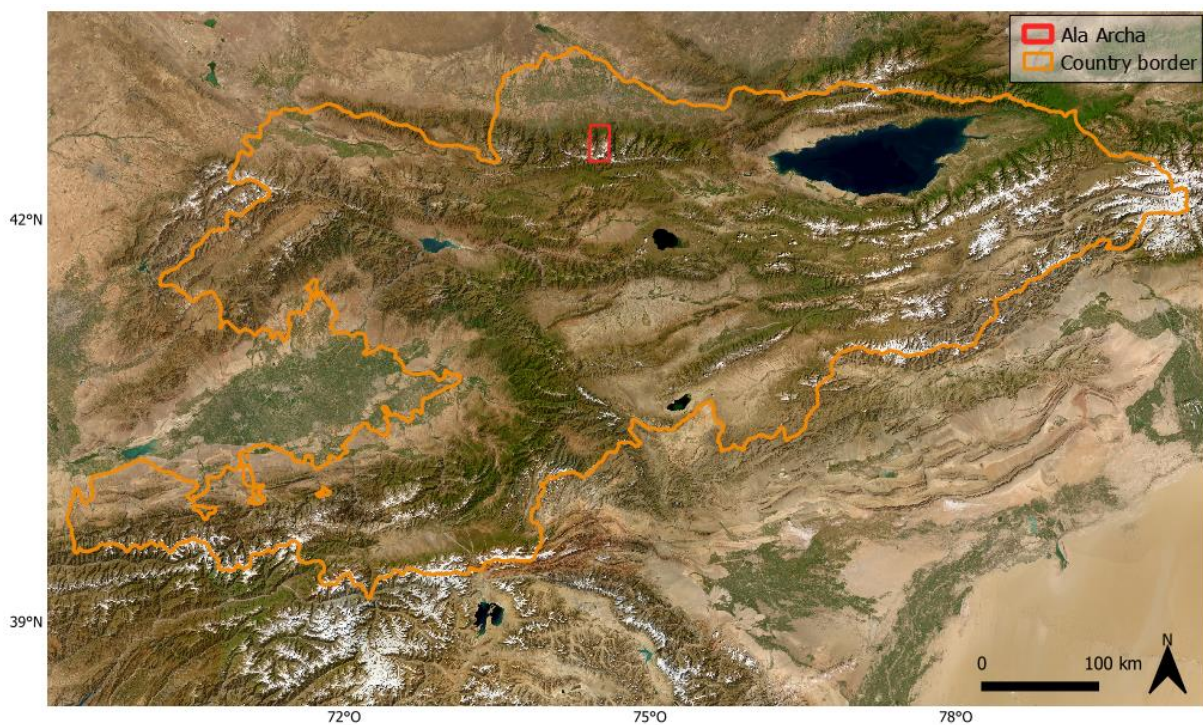


Figure 5: Location of the Ala Archa catchment (red) within the country of Kyrgyzstan (orange).

To the east of the main valley, the Aksay stream acts as a tributary to the Ala Archa River. The Aksay catchment has a size of 28.3 km² and its elevation ranges from 2250 m.a.s.l. at the confluence with Ala Archa to 4895 m.a.s.l. at Semenov-Tian-Shansky Peak (Zaginaev et al., 2016).

4.1.1 Climate

Mean annual precipitation data from the hydrometeorological station at Alplager (74.482926 °N, 42.561901 °E), which lies ca. 1 km downstream of the confluence of Aksay and Ala Archa, has shown a declining trend since 1975 and ranges from 350 to 850 mm per year (Zaginaev et al., 2019). The highest precipitation records are observed in spring and early summer when the weather comes from north-western and western directions (Erokhin et al., 2018). Temperature records from the station at Alplager covering the same time span show that mean maximum

values in summer can amount up to 27 °C while in winter they reach -22 °C (Zaginaev et al., 2019). Mean annual air temperature varies between 1.7 °C and 3.8 °C and has risen by ca. 0.5 °C since 1975 (Zaginaev et al., 2019). Resultingly, relatively low mean annual temperature lead to extensive permafrost areas in high altitude regions (Erokhin et al., 2018).

4.1.2 Landforms

The Aksay valley is mainly influenced by two glaciers that lie in the eastern (Uchitel glacier) and south-eastern (Aksay glacier) part of the catchment (Figure 6a). With a glaciated area of 8.5 km² in 2017, almost a third of the total catchment area was covered by glaciers (Zaginaev et al., 2019). The tongues of both glaciers are partly covered by debris and lie at altitudes between 3300 and 3700 m.a.s.l. (Zaginaev et al., 2016). According to Solomina et al. (1994), the tongues of the two glaciers have been connected in the past. This is in line with results from Narama et al. (2010) who found that during the LIA, two moraines formed downstream of where their tongues are located today.

At an elevation of 3617 m.a.s.l., close to the tongue of Uchitel glacier, a small pro-glacial lake (Uchitel lake) formed around the year 1990 as meltwater started filling a depression (Zaginaev et al., 2019) (Figure 6b). The glacial lake is one of several pilot sites in the GLOFCA project and has produced several outbursts in the past. The analyses carried out in this thesis are based on simulations originating at Uchitel lake. (Zaginaev et al., 2019)

The continued retreat of Uchitel glacier led to the expansion of the intra-moraine depression. The eastern to south-eastern side of the lake is marked by steep ice cliffs with heights of 15 to 25 m. While there is no regular drainage on the surface, the water leaves the lake via subsurface drainage channels that re-appear on the surface about 500 m downslope of the lake (Figure 7). The capacity of the subsurface drainage channels determines how fast the lake can drain which can lead to an unsteady amount of water exiting the depression. (Zaginaev et al., 2019)

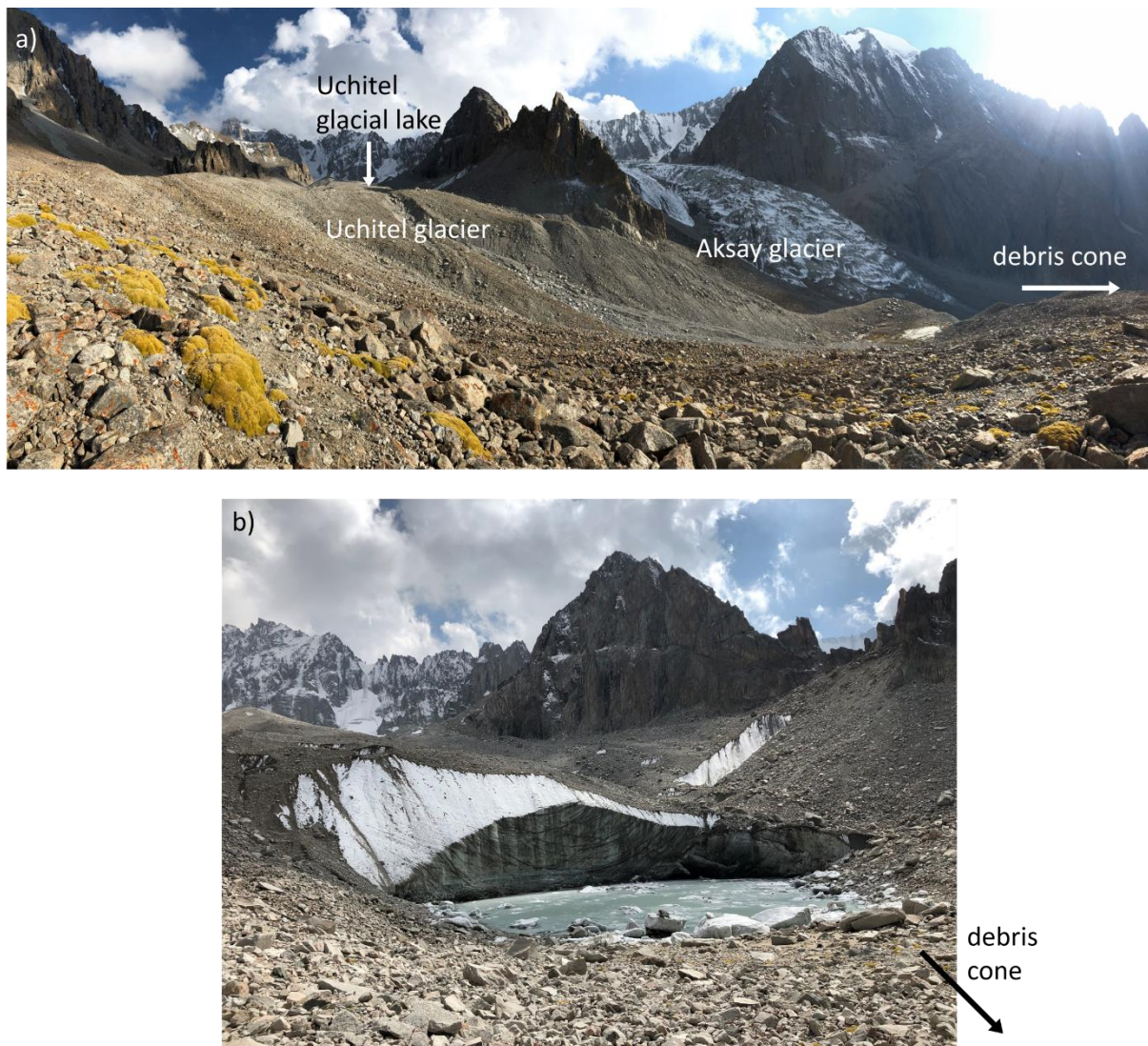


Figure 6: a) Uchitel and Aksay glacier used to be connected before reaching the Aksay canyon upstream of the debris cone. b) Uchitel lake in September 2022. (Pictures: Laura Niggli, September 2022)

The evolution of the lake area between May 2012 and August 2018 is given below (Table 1). Between August 2014 and October 2015, almost all lake water had drained, before the lake grew in size once more.

Table 1: Lake area change between 27.05.2012 and 01.08.2018 (Zaginaev et al., 2019).

Date	Lake Area [m ²]
27.05.2012	6733
12.07.2012	3760
22.04.2013	6597
01.10.2013	6559
30.08.2014	3716
06.10.2015	1603
08.06.2017	3347
13.08.2017	4180
01.08.2018	4870

While in 2012, the average lake depth was found to be 7.1 m, the melting of ice at the bottom led to subsidence of the lake and resultingly to a lake depth increase. In 2016, the volume amounted to ca. 27'000 m³. Besides an increase in depth, the subsidence is also assumed to have led to a change in the runoff system. While in previous years, the lake emptied at the surface, the subsidence resulted in a change to subsurface drainage via channels below the lake. The lake is dammed by a mixture of moraine deposits and buried ice on top of a rock ledge. However, as long as the drainage occurs mainly via subsurface channels, erosion and breach of the dam as well as a superficial outburst are not likely. Nevertheless, an increase in the water table might lead to a pressure increase and eventually to the opening or widening of the channels. Hence, the speed and variability of the lake drainage depend to a great extent on the size of the channels. (Zaginaev et al., 2019)

According to Zaginaev et al. (2019), the average annual discharge of the Aksay stream is 0.5 m³ s⁻¹. Downstream of the lake, after the drainage channel re-appears on the surface (74.534412 °N, 42.529288 °E), the stream traverses a glacier forefield which is characterised by a cover of glacial till that was deposited during the retreat of Uchitel and Aksay glacier. Erosive forces might as well lead to the entrainment of bedrock material and deposits of previous landslides or rockfalls. The amount of loose material available makes the valley prone to GLOF-induced mass movements. Subsequently, the Aksay stream enters a narrow canyon (Figure 7) where the maximum slope amounts up to 50°. After passing the canyon with an approximate length of 1100 m, the terrain becomes increasingly flat and reaches a slope of 21° near the confluence with the main Ala Archa river (Figure 8a). Deposition of entrained material occurs in the section following the canyon and at the confluence with the Ala Archa river where a wide and massive debris cone formed during past GLOF and debris flow events (Isaev et al., 2022; Zaginaev et al., 2019) (Figure 8b). The debris cone lies within the Ala Archa National Park and is often visited by tourists and hikers (Zaginaev et al., 2016).



Figure 7: Extent of the Aksay catchment (red) and the most prominent landforms.

The debris cone covers altitudes of 2200 to 2350 m.a.s.l. and has an approximate volume of more than $10'000 \text{ m}^3$ (Zaginaev et al., 2019). On the debris cone, several channels can be identified that stem from past debris flow events (Zaginaev et al., 2016). Among the deposited material found in the central part of the cone are large boulders which were transported by events that happened in the 1960s, whereas in the currently active channel on the southern side of the cone, the size of boulders is much smaller (Zaginaev et al., 2016, 2019). In 2016, a dam with an average height of 0.8 m was constructed manually to deflect future mass movements to the southern part of the debris cone (Zaginaev et al., 2019). Zaginaev et al. (2019) claim that debris flow events require discharges of $300 \text{ m}^3 \text{ s}^{-1}$ to be able to destroy the dam.

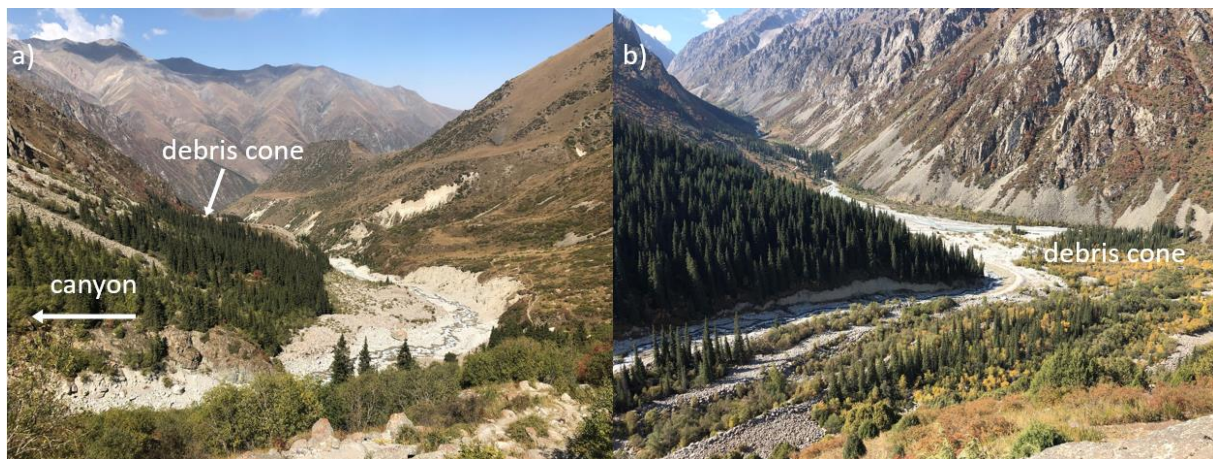


Figure 8: a) Channel section right below the canyon and upstream of the debris cone. b) Lowest section of the Aksay valley where the Aksay river reaches the debris cone. (Pictures: Laura Niggli, September 2022)

In recent decades, additional material deposited on the debris cone has resulted in the Ala Archa river being forced increasingly westwards (Zaginaev et al., 2019). Either heavy rainfall, the sudden release of large amounts of water during GLOFs, or other forms of meltwater release were cited as triggers for these debris flows (Zaginaev et al., 2019). Not only the Aksay valley but the entire Ala Archa basin has been affected by multiple GLOFs and similar mass movements in the past decades. Kattel et al. (2020) show that between 1950 and 2013, most GLOFs reported in different basins on the northern slopes of the Kyrgyz range have been reported in the Ala Archa valley (Figure 9).

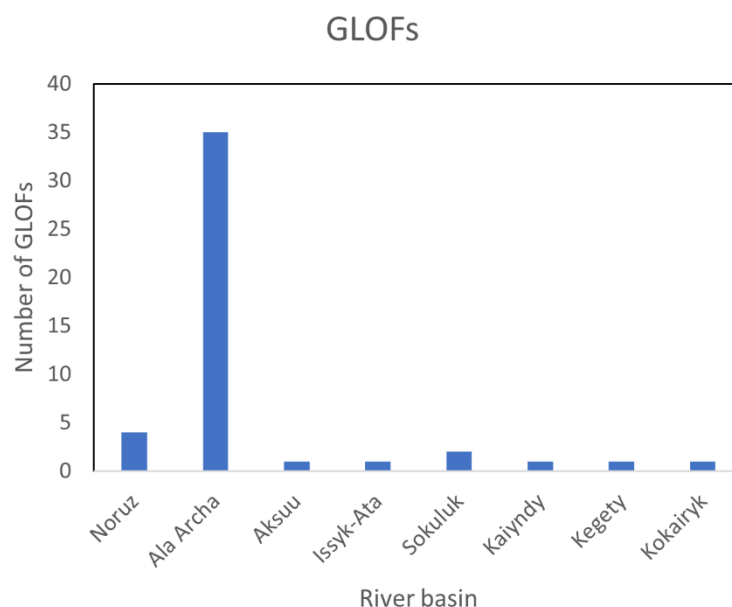


Figure 9: Number of GLOFs in multiple basins on the northern slopes of the Kyrgyz range between 1950 and 2013 (adapted from Kattel et al., 2020).

For the Aksay valley, an analysis based on tree disturbances on the debris cone suggests that there have been 11 to 14 debris flow events potentially triggered by GLOFs in the same period (Zaginaev et al., 2016). For the largest events amongst those (1968 and 1969), it is confirmed

that a sudden drainage of an englacial water pocket has caused the mass movement (Zaginaev et al., 2016). Today's circumstances with subsurface drainage of the pro-glacial lake make it very unlikely that similar discharge values in the order of several hundred cubic meters per second occur (Zaginaev et al., 2016).

4.2 RAMMS Software

RAMMS is a numerical modelling tool developed by the Institute for Snow and Avalanche Research (SLF) and the Swiss Federal Institute for Forest, Snow and Landscape Research (WSL). Being composed of an avalanche, a debris flow, and a rockfall module, the main application areas of RAMMS include the simulation of mass movements, hazard mapping and safety assessments, and research on natural processes.

The RAMMS debris flow module has been successfully applied in different regions of the world and it has also been used for GLOF modelling. The movement of mass between the release and deposition area is computed in three-dimensional terrain, all being based on numerical depth-averaged equations of motion (Bartelt et al., 2017; Christen et al., 2010). Frictional behaviour is governed by the Voellmy-fluid approach which divides frictional resistance into a turbulent friction parameter ζ [m s^{-2}] and a Coulomb parameter μ [-] (Salm et al., 1990; Salm, 1993). While the turbulent friction parameter ζ is velocity-dependent and controls frictional resistance when the mass moves with high velocity, the mass movement is dominated by the velocity-independent coefficient μ when the motion is slow (Frank et al., 2015).

In addition, erosive processes can be modelled using the built-in entrainment model, which is essential during the transition of a GLOF to a debris flow when mass is added to the system. Erosion is controlled by the shear stress and the erosion rate (Bartelt et al., 2017). Regarding the discharge of the mass movement, RAMMS enables the user to either initiate the simulation using a block release or by defining an input hydrograph whereby the discharge over time can be regulated (Bartelt et al., 2017).

4.2.1 Underlying Equations and Assumptions

The basis for simulations in RAMMS is formed by the depth-averaged shallow water equations within a Cartesian coordinate system with coordinates x , y , and z , where x and y reflect the horizontal coordinates and z represents the vertical component perpendicular to the flow direction. Additional independent variables include g denoting the vector of gravitational acceleration as a function of (x, y, z) and t indicating time (Christen et al., 2010).

The incorporation of shallow-water equations into the model requires the assumption of small flow heights compared to the length scale and can be derived by vertically integrating the Navier-Stokes equations (Bao et al., 2019). Additionally, the Voellmy-Salm model supposes constant density and incompressibility of the flowing mass (Christen et al., 2010).

Furthermore, since a single-phase debris flow module is used for GLOF modelling, phase interactions of fluid and solid components cannot be modelled realistically as the underlying

Voellmy model considers the relative fractions as being constant in space and time (Bartelt et al., 2017).

Based on the above assumptions, the mass balance equations can be derived by combining the field variable flow height $H(x, y, t)$ together with the flow velocity $U(x, y, t)$ (Christen et al., 2010; Frank et al., 2017):

$$\dot{Q}(x, y, t) = \partial_t H + \partial_x(HU_x) + \partial_y(HU_y), \quad (\text{eq. 1})$$

where $\dot{Q}(x, y, t)$ stands for the mass production source term, meaning the rate of entrainment or deposition over time t . The depth-averaged flow velocities are described by U_x and U_y (Christen et al., 2010).

When adding S_g , the effective gravitational acceleration, and S_f , the frictional deceleration, the equation accounts for the conservation of momentum in both horizontal directions:

$$S_{g_x} - S_{f_x} = \partial_t(HU_x) + \partial_y(HU_xU_y) + \partial_x(c_xHU_x^2 + g_xk_{a/p}\frac{H^2}{2}), \quad (\text{eq. 2})$$

$$S_{g_y} - S_{f_y} = \partial_t(HU_y) + \partial_x(HU_xU_y) + \partial_y(c_yHU_y^2 + g_yk_{a/p}\frac{H^2}{2}), \quad (\text{eq. 3})$$

where c_x and c_y describe topographical coefficients, $k_{a/p}$ represents the earth pressure coefficient which is proportional to the normal stresses in vertical and horizontal directions (Christen et al., 2010; Frank et al., 2017).

4.2.2 Friction

The behaviour of the mass movement is driven by the two friction coefficients. Since the RAMMS debris flow module uses a single-phase model, fluid and solid phases cannot be distinguished and the flowing material is modelled as bulk flow. The Voellmy-Salm friction approach allows one to differentiate between high and low-velocity regions by dividing frictional resistance into a friction coefficient that relates to the normal stress (coefficient μ) and one that is associated with the velocity squared (coefficient ζ) (Bartelt et al., 2017; Christen et al., 2010). Frictional resistance can then be described by:

$$S_f = \mu\rho Hg \cos(\Phi) + \frac{\rho g u^2}{\xi}, \quad (\text{eq. 4})$$

where ρ is the density, and u stands for the flow velocity vector in x - and y -direction. The term $\rho H g \cos(\Phi)$ indicates that μ is independent of flow velocity and can be represented by the single quantity N denoting the normal stress on the surface (Christen et al., 2010). Hence, coefficient μ becomes dominant when the mass is flowing slowly (Bartelt et al., 2017). On the contrary, the second term including ξ increases with higher flow velocities and reflects the frictional resistance of the turbulent fluid phase (Christen et al., 2010).

As additional factors influencing the deceleration of the flow, the impact of yield stress and terrain curvature was incorporated into RAMMS' frictional resistance equation. For the debris flow module to account for the internal resistance of particles within the mixture of the material,

the parameter N_0 , representing the yield stress, has been included in eq. 5 since cohesion for muddy materials is not characterised by a linear relation (Bartelt et al., 2017).

$$S = \mu N + \frac{\rho g u^2}{\xi} + (1 - \mu)N_0 - (1 - \mu)N_0 e^{\frac{N}{N_0}} \quad (\text{eq. 5})$$

Together with μ , which acts as a hardening parameter, the plastic nature of the flow can be represented. In this way, eq. 5 results in the frictional resistance approaching zero when both the normal stress N and the velocity u get closer to zero, leading to an increase in shear stress which in turn causes the mass movement to stop earlier (Bartelt et al. 2017).

Regarding the curvature, RAMMS accounts for the impact of twists in the flow trajectory on the normal force N by incorporating centrifugal forces that are dependent on the flow velocity and terrain curvature. The centrifugal force F is derived from:

$$F = \rho h f \quad , \quad (\text{eq. 6})$$

whereby the centrifugal acceleration is given by:

$$f = u K u^T \quad , \quad (\text{eq. 7})$$

with K being a matrix reflecting the terrain curvature in all directions. Incorporating curvature will normally lead to an increase in friction and a decrease in flow velocity where the flow direction changes (Bartelt et al., 2017).

4.2.3 Release Settings

For simulating the release process, the RAMMS debris flow module offers two initiation mechanisms. By deploying a *block release*, the mass is released from a manually defined area with an adjustable initial depth. In that case, all the material is released at the same time and accelerated by gravity which would be the preferred option for landslide failures (Bartelt et al., 2017). For simulating debris flows or GLOFs flowing through channelized topographies, the second release option of a *hydrograph* is usually preferred (Bartelt et al., 2017).

To deploy a hydrograph in RAMMS, the discharge at different times must be defined at the release location. Thereby, the hydrograph must be described in at least three time steps. For a so-called triangular hydrograph, the total release volume, release velocity, time to peak discharge, and peak discharge need to be defined. If only the total volume is known, empirical relationships help to derive possible ranges for the maximum discharge and the time to peak discharge (Bartelt et al., 2017). If in addition to the total volume, more field data is available, the user can define discharge values at up to 10 different points in time.

4.2.4 Erosion

As the entrainment of solid material can significantly change the composition of the mass flow which in turn might result in higher flow speeds and volumes, incorporating erosion in GLOF modelling is considered essential (Narama et al., 2018). To account for erosive processes

occurring during a debris flow or a GLOF event, the RAMMS debris flow version contains an erosion module that is based on empirical data obtained from the debris flow observation station in Illgraben, Switzerland (Bartelt et al., 2017; Schürch et al., 2011). Thereby, the mass entrained in the process is controlled by a rate-based method. Using the erosion module, RAMMS calculates the eroded volume determined from the shear stress of the mass movement on the channel bed (Frank et al., 2015). The shear stress τ exerted by the mass movement on any point at the channel base is described by:

$$\tau = \rho ghS , \quad (\text{eq. 8})$$

where ρ describes the bulk mass density of the material, h is the flow height and S represents the channel slope (Frank et al., 2015). While normally, higher shear stresses on the channel bed will lead to an increase in erosion depth, observations have shown that the shear stress needs to exceed a critical value τ_c before erosion occurs (Bartelt et al., 2017; Schürch et al., 2011).

Using the basal shear stress τ , the critical shear stress τ_c , and an average potential erosion depth $\frac{dz}{d\tau}$, the erosion algorithm derives the maximum potential depth of erosion e_m (Frank et al., 2015):

$$e_m = \begin{cases} 0 & \text{for } \tau < \tau_c \\ \frac{dz}{d\tau}(\tau - \tau_c) & \text{for } \tau \geq \tau_c \end{cases} \quad (\text{eq. 9})$$

This method allows erosion to occur until the maximum erosion depth is reached. To prevent all erodible material from being entrained during one single time step, the entrainment rate $\frac{dz}{d\tau}$ is included and describes the change in elevation for each grid point during time step t (Frank et al., 2015).

Although erosion in RAMMS is considered as the decrease in elevation in each grid cell, the digital elevation model (DEM) is not adjusted during a simulation. However, the user is allowed to modify the DEM between two model runs which could be essential for modelling successive events in the same catchment (Bartelt et al., 2017; Frank et al., 2015). Further, it should be noted that RAMMS does not account for lateral erosion since only the change in the vertical coordinate z is considered (Frank et al., 2015).

If field data or knowledge on the in-situ geology is available, RAMMS enables the definition of erosion zones to account for different geological properties so that one can distinguish between areas where increased erosion can be expected and regions with less erodible material (Bartelt et al., 2017).

To include erosion in the simulations, users must define at least one area in the catchment either directly within RAMMS or using a geographic information system (GIS) software. For each polygon, the density of the erodible material [kg m^{-3}], the erosion rate [m s^{-1}], the potential erosion depth in dependence on the maximum shear stress [m kPa^{-1}], the critical shear stress [kPa], and the maximum erosion depth [m] need to be specified (Bartelt et al., 2017).

4.2.5 Additional Simulation Parameters

Apart from the above-mentioned parameters, running a simulation in RAMMS requires a DEM as input topography. While the simulation results improve with an increased resolution of the DEM, the computing time is extended as well. A reduction of the computing time might be achieved by defining a calculation domain within the tool which at the same time demarcates the project boundary. For visualization purposes, optical imagery or a map of the study region can be added (Bartelt et al. 2017).

Additionally, RAMMS entails a stopping criterion controlled by the flow momentum which in classical mechanics is defined as the product of mass and velocity. For every manually specified time step during the simulation, the momenta in all grid cells are computed and summed up before being divided by the maximum momentum sum. The flow momentum of the mass is considered too small and the mass flow stops if the obtained percentage is below a chosen threshold (Bartelt et al., 2017). Hence, low threshold values prevent the mass movement from becoming too slow and from stopping the simulation earlier compared to high thresholds.

4.3 Data Acquisition

The DEM used as topographical input data for RAMMS was obtained from the radiometrically terrain corrected products issued by the Alaska Satellite Facility Distributed Active Archive Center (ASF DAAC) under the National Aeronautics and Space Administration (NASA) (url: <https://asf.alaska.edu/data-sets/derived-data-sets/alos-palsar-rtc/alos-palsar-radiometric-terrain-correction/>; last access: 31.05.2022). The data has been captured by the Advanced Land Observation Satellite (ALOS) with a spatial resolution of 12.5 meters. Optical imagery used for visualization was downloaded from Copernicus Open Access Hub maintained by the European Space Agency (ESA) (url: <https://scihub.copernicus.eu/dhus/#/home>; last access: 11.08.2022).

4.4 Calibration in RAMMS

Since data on past events in the Aksay catchment is scarce, input parameters had to be calibrated based on both the available information about the catchment and on literature about GLOF modelling in general. Limited information on event dates as well as discharge estimations and observations are available, although some discharge observations were reported by alpinists that might not have the experience of realistically estimating discharge of a passing GLOF or debris flow in the channel (Zaginaev et al., 2016; Zaginaev et al., 2019). Furthermore, besides information on peak discharge, a good reconstruction of a past event with RAMMS requires additional knowledge of various input parameters. As a basis for subsequent analyses, the input and output parameters should be reflecting the properties and dynamics in the Aksay catchment. Since the model was used to simulate GLOF dynamics, the default values in RAMMS' debris flow module designed for debris flow simulations had to be partly adapted so they reflect the dynamical properties of a flood movement better. Although the aim is rather to improve the general understanding of different processes during a GLOF event instead of a detailed hazard

assessment within the Aksay catchment, a calibration for the area of interest was required to account for local characteristics and physical variables within the flow channel.

Literature on GLOF modelling as well as studies dealing with the RAMMS debris flow module were used to define plausible ranges for several input parameters. The two friction parameters have been set to $\mu = 0.04$ and $\xi = 500 \text{ m s}^{-2}$ for the basis simulation. Multiple scholars show that a ξ value of 500 m s^{-2} reflects the turbulent friction during debris flow events accurately (Anaconda et al., 2018; Stricker, 2010). Regarding the dry-Coulomb parameter μ , a value of 0.04 was chosen since it reflects a mass movement with a substantial amount of liquid water, which holds true for the Aksay catchment at least in the first section of the flow channel (Frey et al., 2018). Stricker (2010) agrees that a μ value of 0.04 is reasonable for hyperconcentrated flows.

The stop parameter [%] that controls the distance reached by mass movements was set to the default value of 5%.

The density of the moving mass was set to 1100 kg m^{-3} to account for a relatively small amount of solid material in addition to the otherwise almost purely liquid outflow. Since currently, drainage from Uchitel lake occurs via subsurface drainage channels, one can expect less eroded sediment in the beginning compared to mass movements initiated by dam breaches where a lot of solid material is entrained right from the start (Richardson and Reynolds, 2000; Westoby et al., 2014).

Erosional processes were not considered in the basis simulation since information on the availability of sediments and other deposits in the channel was lacking. The effect of entrainment on flow dynamics was evaluated in later analyses.

4.4.1 Definition of a Hydrograph

Although RAMMS allows the user to start a simulation with a block release, whereby all mass is released at the time of initiation, the release characteristics of GLOFs are better approximated by deploying a hydrograph (Bartelt et al., 2017). Hydrographs define the amount of water that enters the system as a function of time. In RAMMS, the user can specify the discharge from the release area for multiple time steps.

In 2016, bathymetry results in the Aksay catchment showed that the volume of the pro-glacial lake amounted to $27'100 \text{ m}^3$ (Zaginaev et al., 2019). In 2018, the lake area was found to have increased to almost $5'000 \text{ m}^2$, meaning that the volume must have increased as well, provided that the average lake depth has not decreased significantly. Hence, the different simulations were carried out using a release volume of $35'000 \text{ m}^3$, assuming an average lake depth of 7 m as it is noted by Zaginaev et al. (2019).

The hydrograph settings require the definition of the discharge as well as the velocity at each time step. The simplest hydrograph type is a triangular hydrograph, meaning that the outflow of water from the release area is controlled by three points in time. The first time step represents the initial conditions, where discharge [$\text{m}^3 \text{ s}^{-1}$] and velocity [m s^{-1}] were both set to zero. The

second time step marks the time when discharge values peak. Eventually, when the release of water has decreased again, the third time step corresponds to the end of the inflow duration when discharge and velocity reach zero again. The integral of the hydrograph shape then coincides with the release volume. The basis simulation for the Aksay catchment was defined by a peak discharge of $20 \text{ m}^3 \text{ s}^{-1}$ (Figure 10).

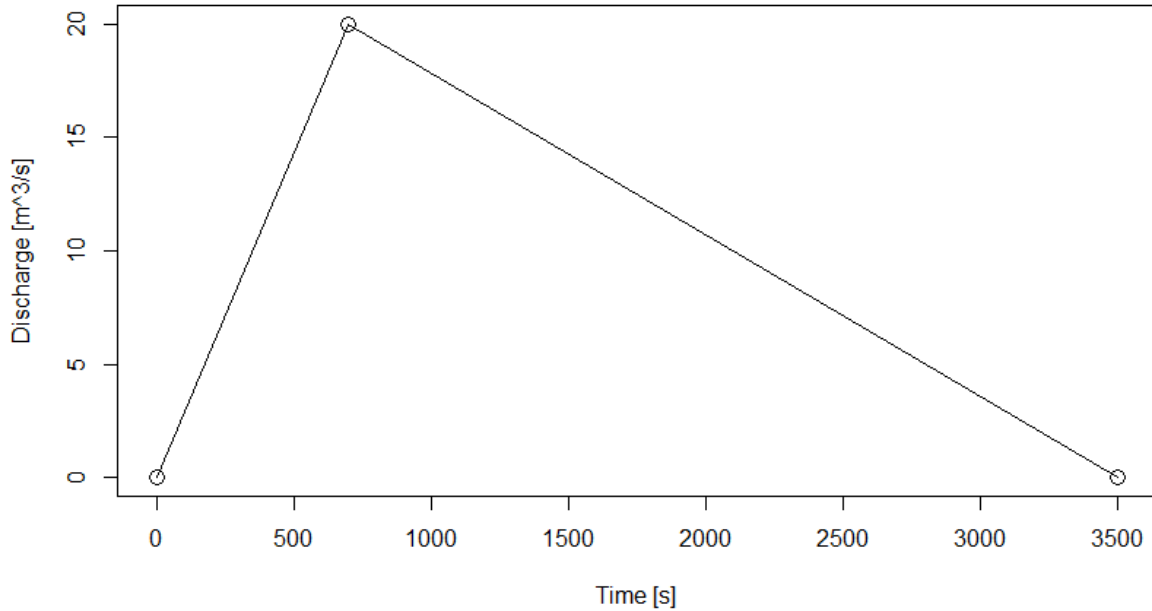


Figure 10: Triangular hydrograph characterised by three points in time. Point 1 at time = 0 s with discharge = $0 \text{ m}^3 \text{ s}^{-1}$; point 2 at time = 700 s and discharge = $20 \text{ m}^3 \text{ s}^{-1}$; and point 3 at time = 3500 s and discharge $Q = 0 \text{ m}^3 \text{ s}^{-1}$. The release volume is set to $35'000 \text{ m}^3$.

The velocity at the time of maximum discharge was calculated using eq. 10, elaborated in Rickenmann (1999), which describes a simplified equation for flow velocities of debris flows in dependence of discharge and slope:

$$v = 2.1Q^{0.33}S^{0.33}, \quad (\text{eq. 10})$$

where v represents the flow velocity at the relevant time step, Q stands for the discharge, and S describes the slope at the location where the subsurface drainage channel appears on the surface. For minimum expected discharges of $5 \text{ m}^3 \text{ s}^{-1}$ and a slope of 2.22 (24.7°), flow velocity varies amount to approximately 4 m s^{-1} or higher which is why for the basis simulation, an initial flow velocity of 4 m s^{-1} was chosen.

Given the subsurface drainage from the glacial lake, maximum discharges are unlikely to reach the flow magnitudes of GLOFs following a dam breach (Westoby et al., 2014). As the capacity of englacial or subglacial channels can vary, a reasonable value had to be chosen. Stuart et al. (2003) have analysed the characteristics of englacial channels on the Austre Brøggerbreen glacier located on Svalbard and claim that the channel size varies substantially and can reach cross-sectional areas of approximately 7 to 20 m^2 (Figure 11).

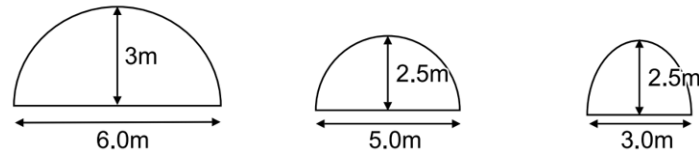


Figure 11: Possible dimensions of englacial channels (Stuart et al., 2013).

To obtain possible discharge values, flow velocities need to be considered in addition to the cross-sectional area. Many studies on glacial drainage systems indicate that flow velocities in subsurface channels are below 1 m s^{-1} (Hooke, 1989; Nienow et al., 1996; Stuart et al., 2003). Due to the lack of information about the drainage system in the Aksay catchment and comparable settings, a range of discharge values has been considered and tested. On the one hand, scenarios with low discharges have been stopped automatically by RAMMS due to a lack of momentum. On the other hand, discharge values exceeding a certain magnitude would be unrealistic under the current circumstances. However, sensitivity analyses carried out in a later step would include simulations with rather unrealistic parameters to account for scenarios more likely to occur in other regions of the world. For the calibration scenario, the peak initial discharge was set to $20 \text{ m}^3 \text{ s}^{-1}$ which produced a reasonable result on top of which the detailed analyses could be carried out.

The last input required for a triangular hydrograph is the duration until the maximum discharge is reached. In Marchi et al. (2021) it is discussed that during high-severity events, peak discharge is reached relatively quickly, whereas for low severities, the relative duration until peak discharge increases. For the basis simulation, peak discharge was set to a fifth of the total inflow duration, which is in line with other studies (Marchi et al., 2021; Mitchell et al., 2022). The total inflow duration is derived automatically from the shape of the triangular hydrograph.

4.4.2 Basis Simulation

Although past mass movements in the Aksay catchment led to erosion along the trajectory, erosional processes were neglected intentionally for the basis simulation. On the one hand, information on sediment availability and type of material was scarce, and, on the other hand, the aim is to analyse how different entrainment scenarios change flow dynamics compared to the basis simulation.

Table 2 shows a summary of all input parameters used for the basis simulation, on top of which later analyses were performed.

Table 2: Parameter values used for the basis simulation.

Parameter	Value
Stop Parameter	5 %
End Time	7500 s
Dump Step	15 s
Density	1100 kg m ⁻³
Lambda ⁶	1
μ	0.04
ξ	500 m s ⁻²
Inflow Direction ⁷	155°
Time to Peak Discharge	700 s
Peak Discharge	20 m ³ s ⁻¹
Flow Velocity at Peak Discharge	4 m s ⁻¹
Total Inflow Duration	3500 s
Release Volume	35'000 m ³

The input parameters presented in Table 2 partly had to be obtained using empirical equations. Others have been adopted from similar studies on modelling mass movements with RAMMS. As the runout area, flow heights, and flow velocities of past events in the Aksay catchment are mostly described insufficiently and are partly based on observations of hikers and not on hydrological and geomorphological measurements, the correctness of the model inputs had to be evaluated qualitatively. However, for the purpose of this thesis, a solid basis simulation on top of which sensitivity analyses can deliver the desired insights and findings is of higher importance than a perfectly accurate reconstruction of a past event.

4.5 Sensitivity Analyses

To provide findings that are applicable also in other regions of the world, sensitivity analyses were carried out to evaluate the impacts of different release mechanisms and entrainment of sediment on flow dynamics. In addition to quantitative results that might only be valid for the Aksay catchment, the outputs and especially the interdependencies between input and output parameters shall represent processes found on a global scale as well.

Multiple scholars have carried out sensitivity analyses in RAMMS to evaluate the impacts of parameter changes on selected variables (Anaconda et al., 2018; Frank et al., 2017; Frey et al., 2016; Sattar et al., 2020). In contrast to so-called global sensitivity analyses, where several input parameters within a parameter space are changed to assess their impact on the output values,

⁶ Lambda is the earth-pressure coefficient which modifies the longitudinal pressure gradients driving the flow (Bartelt et al., 2017: 48).

⁷ The inflow direction describes the angle in which the mass is released in counter-clockwise direction from the x-coordinate of the topographic data (Bartelt et al., 2017: 39)

this study mainly uses local sensitivity analyses, which focus on the importance one factor has on the results (Rakovec et al., 2014).

4.5.1 Boundary Conditions

As the volume of glacial lakes can vary and different lake types exist, outburst mechanisms differ consequently. Despite a variety of other parameters in RAMMS, the release volume determines to a great extent the flow dynamics in downstream areas. While parameters governing frictional behaviour or erosive processes do influence the flow behaviour along the trajectory, the initial conditions during the release process regulate how much mass enters the system in a given period and could be used to approximately simulate different release mechanisms.

Although RAMMS allows the user to describe the release of water at up to ten points in time, the analyses were carried out using triangular hydrographs for two reasons. On the one hand, more complex hydrographs would require additional knowledge of past events to ensure that the scenario still reflects a probable outcome to some degree. On the other hand, the use of more detailed hydrograph shapes would constrain the results to only hold true for a certain release process with a specific hydrograph shape. However, the goal of this analysis is to demonstrate various outburst mechanisms which can be distinguished partly by the peak discharge reached, the total volume released, and the temporal characteristics of the outburst. The usage of a simplified triangular hydrograph, therefore, makes it possible to evaluate the impacts on flow dynamics resulting from several distinct release processes to some extent.

In the first step, peak discharge during the outburst was varied to analyse how flow height and flow velocity along the channel profile change in response to altered release conditions. A series of simulations were run whereby the peak discharge values amounted to 5, 10, 15, 20, 25, 30, 35, 40, 45, and 50 m³ s⁻¹. Although mass movements with higher initial discharge are considered unlikely with today's circumstances at Uchitel lake, three additional scenarios with peak values of 60, 70, and 100 m³ s⁻¹ were simulated to increase the understanding of events that could happen in another setting. Since the temporal characteristics of the hydrographs change owing to the varying peak discharge value and the constant release volume of 35'000 m³, the shapes vary substantially between the different hydrographs (Figure 12). Apart from parameters related to the hydrograph, all other input variables were kept constant were unchanged compared to the basis simulation (Table 4, Appx.).

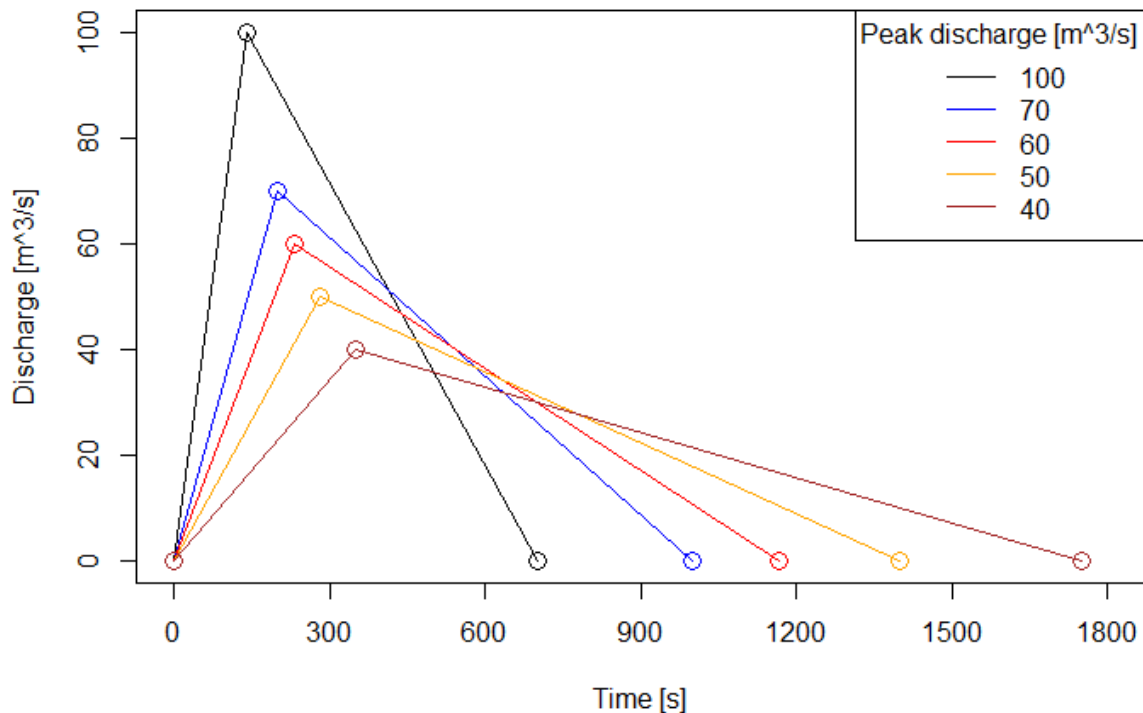


Figure 12: Selected hydrographs with different peak discharge values and total inflow durations. The integral of all curves equals the release volume of 35'000 m³.

Considering that the interval of the curves equals the release volume of 35'000 m³ for each scenario, the inflow duration is reduced with increasing peak discharge values. It was assumed that in all simulations the entire lake would drain.

In a subsequent analysis, the aim was to assess the sensitivity of flow dynamics to varying release volumes. Based on the data found by Zaginaev et al. (2019), the lake volume at the study site likely did not exceed 40'000 to 45'000 m³ in the past decade. The goal to apply the findings in other regions implies that effects on flow dynamics induced by higher release volumes must be understood in addition to impacts caused by different peak discharges. Hence, the same output variables were evaluated based on three different lake volumes. Along with the volume of 35'000 m³, a lake volume of 50'000 m³ was chosen since continued glacial melting in the Aksay catchment might increase the volume of the existing lake under some assumptions. On top of that, a lake volume of 300'000 m³ was evaluated which might provide useful insights applicable in other areas. Both for the 50'000 m³ and the 300'000 m³ scenario, peak discharge values of 50, 60, 70, and 100 m³ s⁻¹ were modelled to compare the results to the smaller scenario with a release volume of 35'000 m³.

The remaining parameters (Table 5, Appx.) were not altered to ensure that observed changes in flow dynamics could be attributed to the increasing lake volume. Owing to the increase of the lake volume and the consistency in discharge values, the inflow duration and, hence, also the time until peak discharge is reached are inevitably prolonged. Nevertheless, this should not have any consequences on maximum flow heights and velocities but only on the time until those variables reach their peaks. Analyses regarding the temporal dimension of flow dynamics might be constraint by the altered inflow duration and time to peak due to changed release

volumes. Furthermore, the influence of the initial conditions was evaluated using the flow velocity at the drainage channel exit. Although the flow velocity for the input hydrograph can be calculated using the empirical equations discussed in section 4.4.1, a sensitivity analysis was carried out to evaluate how the flow velocities downstream of the release area behave depending on varying initial velocities. Since no field data on drainage velocities for the Aksay catchment is available, it was analysed how the velocities change after the release at the appearance of the drainage channels. To reflect a range of probable flow velocities and to enhance the understanding of how topography and the channel bed affect flow dynamics, the initial velocities were fixed between 2 and 20 m s⁻¹ in steps of 3 m s⁻¹. All remaining simulation parameters (Table 6, Appx.) were adopted from the basis simulation. The resulting flow velocities were analysed along the flow channel on the glacier forefield to evaluate the influence of topography and other factors.

4.5.2 Erosion Dynamics

Besides the release conditions, the entrainment of eroded sediment can alter the flow behaviour significantly. Sediment entrainment along the flow channel can lead to the transition of a GLOF into a mud or a debris flow whereby the total volume of the mass movement is likely to increase manifold (Breien et al., 2008; Liu et al., 2020b; Worni et al., 2014).

Apart from input variables such as the initial density and the release volume, which have at least an indirect control on erosion by governing shear strength, RAMMS has enabled the manual definition of multiple input parameters that directly regulate how much entrainment can occur. Within the scope of this thesis, the sensitivity of several flow characteristics to selected erosion parameters was analysed in multiple experiments.

Similar to previous studies (Frey et al., 2018), the catchment was divided into several zones where sediment entrainment can occur (Figure 13). The flow trajectory between the glacial lake and the debris cone in the north-western part of the catchment was divided into three zones, separating the canyon from the glacier forefield and the rest of the flow channel. Four measurement locations were used to derive data from multiple scenarios (Figure 13).

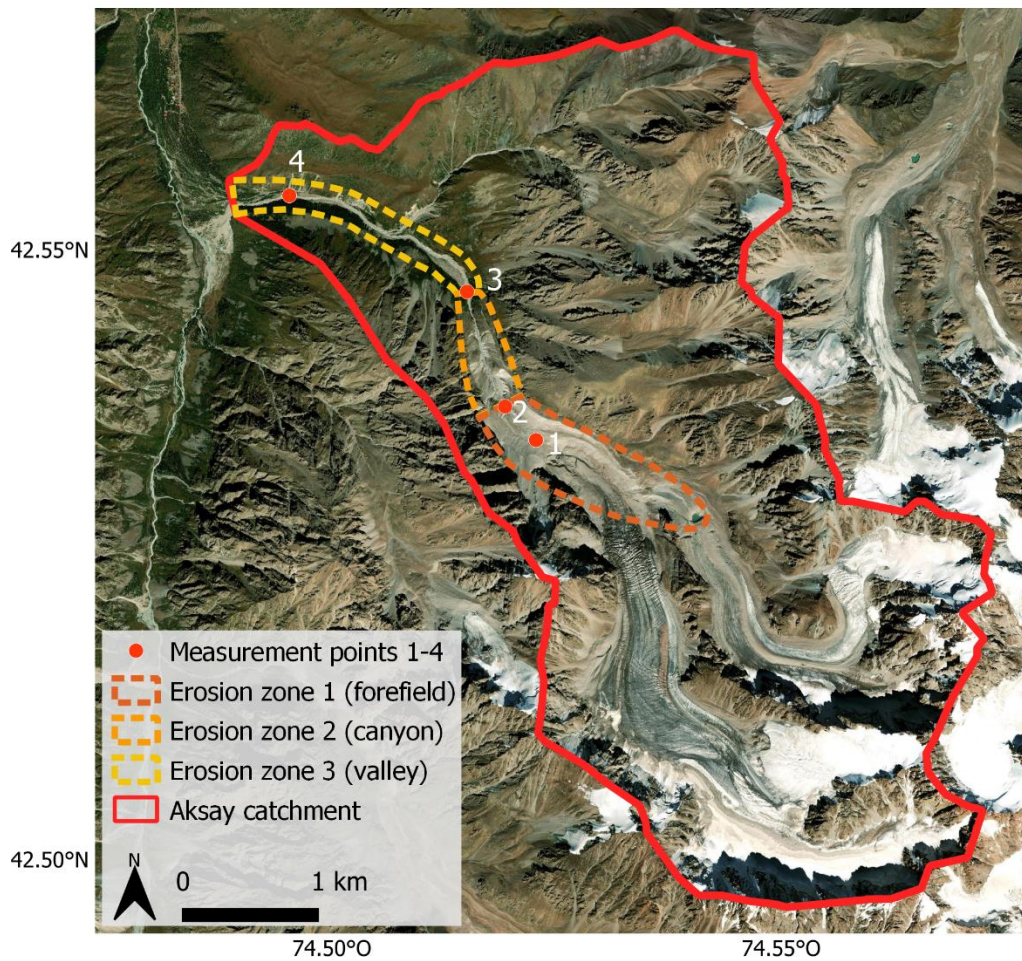


Figure 13: Location of manually defined erosion zones and measurement points within the Aksay catchment.

To evaluate the sensitivity of the model outputs to varying erosion parameters, most input variables including the hydrograph settings were kept constant. Due to the incorporation of erosion and the fact that a transition to a more solid-laden mass movement is likely to result from entrained material, it becomes necessary to adapt frictional behaviour since the flow resistance of a rising solid fraction is altered with increasing erosion (Bartelt et al., 2017). For this reason, the friction parameters were fixed at $\mu = 0.08$ and $\xi = 500 \text{ m s}^{-2}$. According to Frey et al. (2018) and Anaconda et al. (2018), these are typical values for viscous debris flows and have been previously used in debris flow modelling.

In the first analysis, the impact of erosion depth on the flow dynamics was evaluated. In RAMMS, the maximum erosion depth describes the depth of the sediment layer which can be eroded in each cell (Bartelt et al., 2017). For the Aksay catchment, limited information on sediment availability was provided by local knowledge holders. However, as the analyses shall provide insights into how erosion affects flow dynamics in general without being constrained to the study catchment, erosion was considered in all three predefined erosion zones accordingly. This allows a broader application of the findings as other catchments will be characterized by different depths of erodible sediments.

Simulations were run for maximum erosion depths of 0.25, 0.5, 0.75, 1, 1.5, 2, 2.5, and 3 m. The density of erodible was fixed at 1800 kg m^{-3} which is a common density for deposits of morainic and landslide deposits (Gan et al., 2018; Liu et al., 2020a). To promote erosion along the channel, the remaining variables were fixed at the highest selectable values in RAMMS. Resultingly, the erosion rate, which describes how fast the mass can take up sediment from the channel bed, was set to 0.05 m s^{-1} . The potential erosion depth, which relates to the shear stress in each cell and controls the erodible depth per kPa, was fixed at 0.2 m kPa^{-1} . As a last variable, the critical shear stress marks the threshold above which erosion can start to occur. The critical shear stress was set to 0.5 kPa, meaning that material can be entrained once the shear stress in a cell exceeds 0.5 kPa (Bartelt et al., 2017; Frank et al., 2015).

To facilitate additional interpretations, the erosion zones were ‘activated’ separately, so that the mass movement could entrain material within only one of the predefined areas for each simulation. Hence, in each of the three erosion zones, eight erosion depths were applied, resulting in 24 simulations (Table 7, Appx.).

Based on the chosen parameters, one would expect that the eroded volume increases with higher erosion depths since the mass movement can entrain more material if the depth of the sediment layers available in the channel bed increases. Since the three erosion zones have different characteristics in terms of slope, width, and length, results might show slightly different outcomes. Nevertheless, as the erosion depths were set to the same values for the glacier forefield, the canyon, and the valley downstream of the canyon, the outcomes should show similar tendencies.

Secondly, the same experiment was repeated with a lower critical shear stress by reducing the threshold from 0.5 to 0.25 kPa to further promote erosion (Table 8, Appx.). When a high critical shear stress is chosen, it prevents small mass movements from entraining any material since the shear stress they exert on the channel bed is too low to trigger erosion. Hence, and as this study focuses on analysing the impacts caused by erosion, settings were amended in a way that favours additional sediment uptake. By applying not only different erosion depths but also two different values for critical shear stress, the sensitivity of the flow characteristics to the critical shear stress can be evaluated. Therefore, varying a second parameter certainly adds complexity, however, at the same time, it might increase the understanding of how the amount of entrainment occurring during the mass flow is governed by different physical variables.

Thirdly, the dynamics of entrainment during mass movements were examined by inspecting the sensitivity of the flow parameters to varying erosion rates. The erosion rate typically determines the speed at which material is eroded from the channel bed, provided that the critical shear stress at the given location is exceeded. Anaconda et al. (2018) have stressed the importance of analysing the impact of varying erosion rates on flow dynamics. However, according to Bartelt et al. (2017), only a limited amount of field data is available when it comes to erosion rates. Hence, the RAMMS settings allow the user to choose between erosion rates of 0.0125, 0.025, and 0.05 m s^{-1} . Therefore, high erosion rates are expected to result in large debris flow fronts

whereas low erosion rates assumably lead to a more balanced uptake of sediment over time. Once more, entrainment was considered in all three predefined areas separately. While the erosion rate was varied between the three suggested values, potential erosion depth was set to 0.2 m kPa^{-1} , critical shear stress was fixed at 0.25 kPa and the erosion depth was limited to 1 m . The same experiment was repeated with an erosion depth of 0.75 m (Table 10, Appx.). Independent of the speed at which material is entrained in the flow, one would expect that significantly less erosion occurs since the erosion rate per cell only drives entrainment until the erosion depth is reached.

4.5.3 Variability in Travel Times

To enhance the understanding of how strong the variations in the evacuation time could be, multiple simulations have been analysed and compared based on the time needed by the mass movement to reach the debris cone since the impact on people and infrastructure upstream of the debris cone might not be as important. In any case, the aim is to have a quantification of the variability in flow duration in response to changes in selected input parameters. Thereby, the temporal variability caused by varying initial conditions was evaluated once by neglecting erosion and once by assuming an erodible sediment layer with varying depths in the canyon. Additionally, outflow velocities, which can change owing to different lake and dam types as well as trigger mechanisms, are expected to influence the time required to reach a critical point in the channel as well. The analysis on initial flow velocities outlined in section 4.5.1 was extended to incorporate temporal aspects as well so that the dependence of travel times on initial flow velocities could be quantified.

Furthermore, as the critical shear stress is assumed to have a significant impact on erosion which in turn affects flow velocities and travel times, a fourth variable was added to investigate the variability in the time of arrival at the debris cone (Table 9, Appx.). The four selected variables should allow conclusions for both the impact on the time of arrival caused by changed initial conditions as well as by variable entrainment characteristics.

4.5.4 Scenario-based Modelling

Depending on the lake type, the outburst process, and the characteristics of the flow channel, different kinds of mass movements can originate at a glacial lake. With the help of the entrainment module provided in RAMMS, some of the effects a transition to another type of mass movement can have on downstream regions were investigated.

Since the Uchitel lake is not dammed by a moraine and drains via subsurface channels, the released mass likely has a comparably high fluid ratio. As for this thesis, the single-phase version of RAMMS was used, it cannot be distinguished between solid and fluid phases directly. Nevertheless, to account for the solid fraction to increase after the initial release, one can either consider adjusting the release conditions or enabling the entrainment along the trajectory.

To evaluate the impact of different outburst mechanisms on downstream regions, three distinct events were modelled (Table 3). The first scenario simulated a pure flood originating from the lake, meaning that the density of the released mass was set to 1000 kg m^{-3} . As frictional resistance is lower for hyperconcentrated flows and floods than for debris flows, μ was adjusted to 0.02, as suggested by Stricker (2010). The second scenario models a rather granular debris flow originating at the same location with equal hydrograph settings. The initial density for the debris flow was set to 1800 kg m^{-3} since the density of the flowing mass remains unchanged during the simulation despite the entrainment of additional material. As frictional resistance is affected by having a higher solid-liquid ratio in debris flows, μ was increased to 0.2, which is among the typical values discussed in Anaconda et al. (2018). The second friction parameter ζ was left unchanged at 500 m s^{-2} , similar to Frey et al. (2018).

The third simulation represents a mass movement between the two extreme events and aims to reflect a stage during the transition from a flood to a granular debris flow. While density was fixed at 1400 kg m^{-3} to account for a lower solid fraction, μ was set to 0.01 which would characterise a rather viscous debris flow. Compared to the second scenario which might be an approximation to a mass flow that could occur at moraine-dammed lakes where huge amounts of solid material are washed away during the release process, the third scenario is similar to outbursts where solid fractions at the beginning are lower.

The aim of this scenario-based approach is not only to visualize different types of mass movements and compare typical flow variables but also to investigate how the timing and amount of erosion in the channel change depending on the type of event. For each scenario, erosion was enabled in all three erosion zones to stimulate erosion. Erosion depth in the glacier forefield was fixed at a lower value as the solid material is assumed to be mostly comprised of a thin debris cover. In the canyon and the valley further downstream, more erosion can be expected. Hence, erosion depths were fixed at 0.5 m for the glacier forefield and 1 m for the canyon and the valley zone respectively. Erosion density was fixed at 1800 kg m^{-3} , the erosion rate was set to 0.025 m kPa^{-1} , potential erosion depth amounted to 0.1 m kPa^{-1} and the critical shear stress was defined at 0.5 kPa.

Owing to the single-phase nature of the RAMMS version used, transformations to other flow types can only be simulated under certain assumptions. While for the three scenarios outlined above, mainly release properties were adjusted to approximate different outburst processes, realistic transformations and phase changes would occur while the mass flow moves along the trajectory. Similarly, phase changes could only roughly be simulated by varying frictional behaviour during a flow, as was done by Frey et al. (2018). For this purpose, the simulations representing the viscous and granular debris flows were repeated whereby friction was lowered at the debris cone to account for the anticipated deposition of solid material which expectedly results in reduced frictional resistance and a transition to a rather hyperconcentrated flood (Table 3). Consequently, the viscous and granular debris flows were once simulated with

constant friction and once with a reduction in friction parameter μ , whereby μ was lowered to 0.02 downstream of measurement point 4 where the mass reaches the debris cone.

4.5.5 Monitored Variables

Considering that in previous literature covering GLOF and debris flow modelling, a variety of sensitivity analyses on input and output parameters has already been conducted, a subset of the resulting values was selected in order not to exceed the scope of this thesis. The impacts of friction parameters on flow dynamics have been studied extensively and were not repeated in this thesis, except for the approximations to multi-phase flows.

The goal of the sensitivity analyses was to evaluate how flow height, velocity, discharge, and erosion vary as a result of changing initial conditions and the availability of erodible material. To facilitate the analyses, a line profile was drawn manually along the flow channel using the open-source software *QGIS*, which provided further insights in addition to the data derived at the four measurement points. Resulting data containing the variable of interest could then be inspected along the same profile for multiple simulations which ensured that the flow parameters could be compared.

In addition to evaluating flow parameters along the profile, times series at specific locations helped to investigate how the flow dynamics at a certain point in the channel change over time. This has helped especially to emphasise how different types of mass movements and events behave in selected sections in the catchment.

When it comes to measuring discharge values, RAMMS currently has no functionality that allows one to derive the maximum discharge values at each cell automatically. However, the user can extract the values at the relevant cross-sections manually. Although this approach is somewhat inaccurate since the cross sections are not always exactly overlapping, the output obtained nonetheless provides valuable insights about the order of magnitude that can be expected. Data on the amount of erosion could be extracted for each cell of the catchment. Inspecting the erosion values at different points in time allowed for gaining knowledge of how fast erosion occurs in different scenarios.

Table 3: Simulation parameters used for the analyses of three flow type scenarios and for approximations of flow type transformations. Parameters changed in comparison to the basis simulation (Table 2) are marked in italics.

Parameter	Flood	Viscous debris flow	Granular debris flow	Viscous debris flow (reduced friction)	Granular debris flow (reduced friction)
Stop Parameter [%]	5	5	5	5	5
End Time [s]	7500	7500	7500	7500	7500
Dump Step [s]	15	15	15	15	15
Density [kg m⁻³]	<i>1000</i>	<i>1400</i>	<i>1800</i>	<i>1400</i>	<i>1800</i>
Lambda	1	1	1	1	1
μ (from the cone)	<i>0.02</i>	<i>0.1</i>	<i>0.2</i>	<i>0.1 (0.02)</i>	<i>0.2 (0.02)</i>
ξ [m s⁻²]	500	500	500	500	500
Inflow Direction [°]	155	155	155	155	155
Time to Peak Discharge [s]	700	700	700	700	700
Peak Discharge [m³ s⁻¹]	20	20	20	20	20
Release Velocity [m s⁻¹]	4	4	4	4	4
Inflow Duration [s]	3500	3500	3500	3500	3500
Release Volume [m³]	35000	35000	35000	35000	35000
Erosion applied in Zone	<i>1+2+3</i>	<i>1+2+3</i>	<i>1+2+3</i>	<i>1+2+3</i>	<i>1+2+3</i>
Erosion Density [kg m⁻³]	<i>1800</i>	<i>1800</i>	<i>1800</i>	<i>1800</i>	<i>1800</i>
Erosion Rate [m s⁻¹]	<i>0.025</i>	<i>0.025</i>	<i>0.025</i>	<i>0.025</i>	<i>0.025</i>
Potential Erosion Depth [m kPa⁻¹]	<i>0.1</i>	<i>0.1</i>	<i>0.1</i>	<i>0.1</i>	<i>0.1</i>
Critical Shear Stress [kPa]	<i>0.5</i>	<i>0.5</i>	<i>0.5</i>	<i>0.5</i>	<i>0.5</i>
Maximum Erosion Depth [m]	<i>0.5+1</i>	<i>0.5+1</i>	<i>0.5+1</i>	<i>0.5+1</i>	<i>0.5+1</i>

5 Results

5.1 Boundary Conditions

Release conditions which are mainly shaped by lake type, drainage system, and trigger mechanism naturally lead to a variety of hydrographs. As the settings in RAMMS allow the user to manually define the starting velocity, peak discharge, the time until the peak is reached, and the total inflow duration, the variability and uncertainty related to the conditions that define the initial GLOF behaviour were evaluated.

5.1.1 Release Velocity

The impact of the starting velocity was analysed in a series of simulations (Table 6, Appx.) between the release area and measurement point 1 in the glacier forefield (74.522704 °N, 42.534370 °E) whereby the change in flow velocity along the flow channel as well as the variability over time between the seven simulations were evaluated (Figure 14).

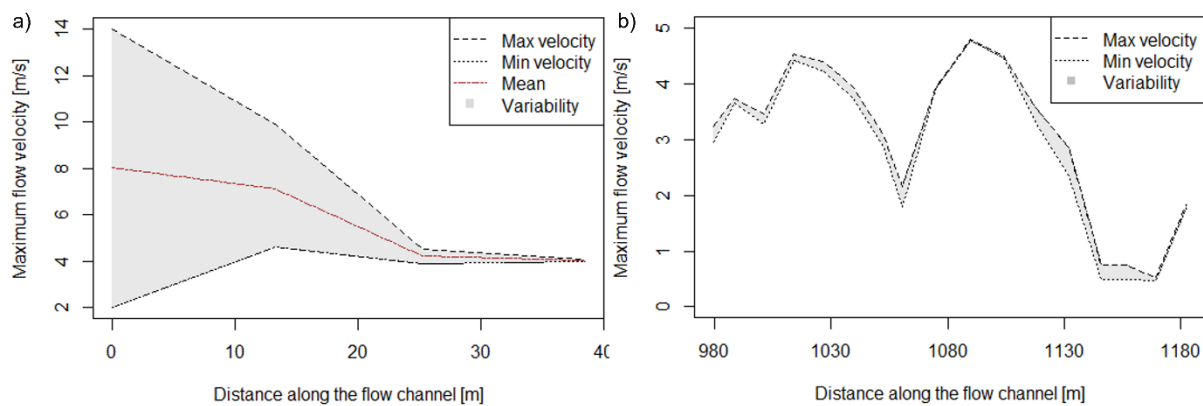


Figure 14: a) Evolution of maximum flow velocities from seven simulations along the flow channel a) within the first 40 m downstream of the release area, and b) within the last 200 m before measurement point 1. Initial velocities were set to 2, 5, 8, 11, 14, 17, and 20 m s^{-1} . The grey area illustrates the variability in maximum flow velocities of all seven simulations and lies between the highest and the lowest observed maximum flow velocity. The red line marks the mean maximum velocity of the seven simulations.

The flow velocity curves for all simulation outputs are relatively similar and show almost indistinguishable patterns. While in the first 25 m, flow velocities of all simulations converge quickly and reach very similar values within the first 40 m downstream of the release area (Figure 14a), variations between the maximum velocities further downstream are comparably low and the highest and lowest maximum flow velocities are closer together than in the first section of the flow channel (Figure 14b). Except for the first 25 m, the initial flow velocity does not have a clear impact on flow velocities further downstream.

5.1.2 Peak Discharge

Peak discharge to a large extent depends on the release process. To account for different outburst mechanisms and natural variability in discharge volumes, a series of scenarios (Table 4, Appx.) has been simulated, whereby peak discharge values were set to 5, 20, 25, 30, 35, 40, 45, 50, 60, 70 and 100 $\text{m}^3 \text{s}^{-1}$ (Figure 15).

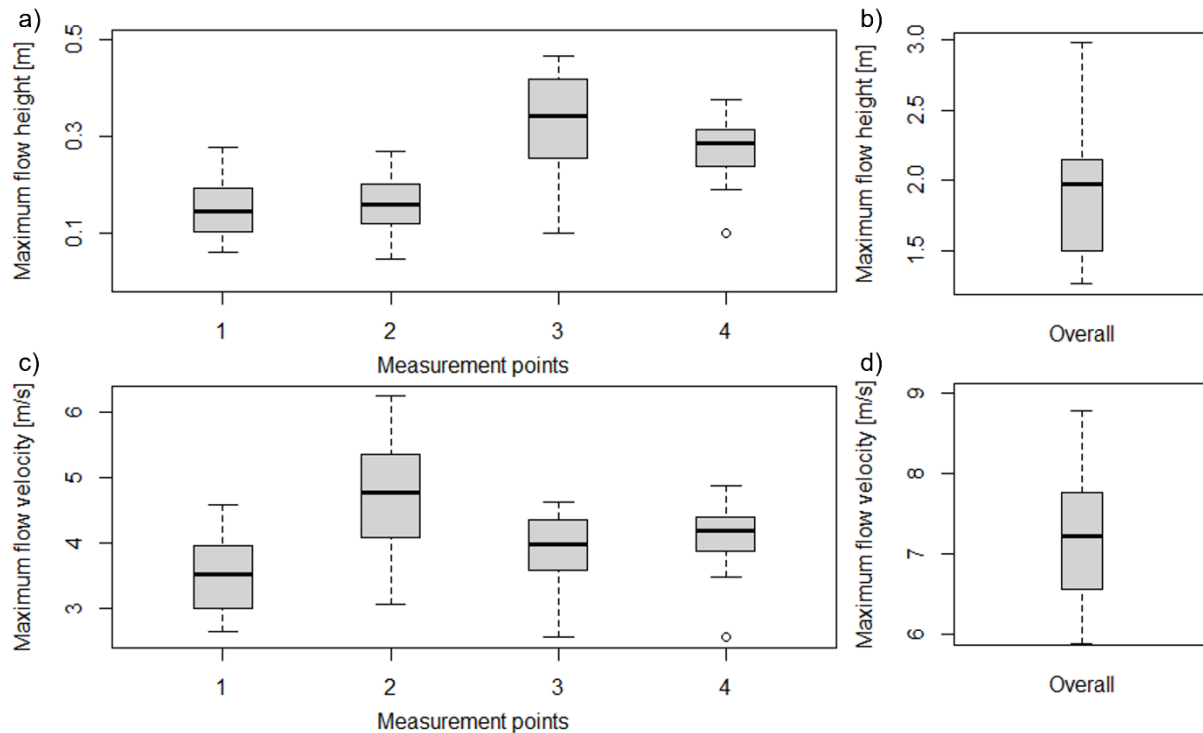


Figure 15: The variability in maximum flow heights (a&b) and flow velocities (c&d) during 11 simulations observed at four measurement points (a&c) and across the entire flow channel (b&d) are plotted as boxplots.

At all four measurement points, maximum flow heights vary between different simulations whereby the variability at point 3 is the highest (Figure 15a). Maximum flow heights across the entire flow channel vary between 1.3 and 3 m in response to different release conditions. Measurements at point 2 show relatively high variability in flow velocities, whereas at point 4, the flow velocities observed in the 11 simulations are rather similar (Figure 15c). Maximum flow velocities observed in the Aksay catchment do vary between 6 and almost 9 m s⁻¹ as a response to changed peak discharges (Figure 15d).

When it comes to the variability along a more extensive section of the flow channel instead of selected locations, it was found that differences between two scenarios are not constant but vary along the trajectory as well (Figure 16). The variability in maximum flow height noticeably increases in high flow height areas, while it generally decreases in sections where flow heights are lower. For instance, differences between the two scenarios are smaller at the trough after ca. 250 m compared to the local peaks at 170 or 470 m downstream of the release zone.

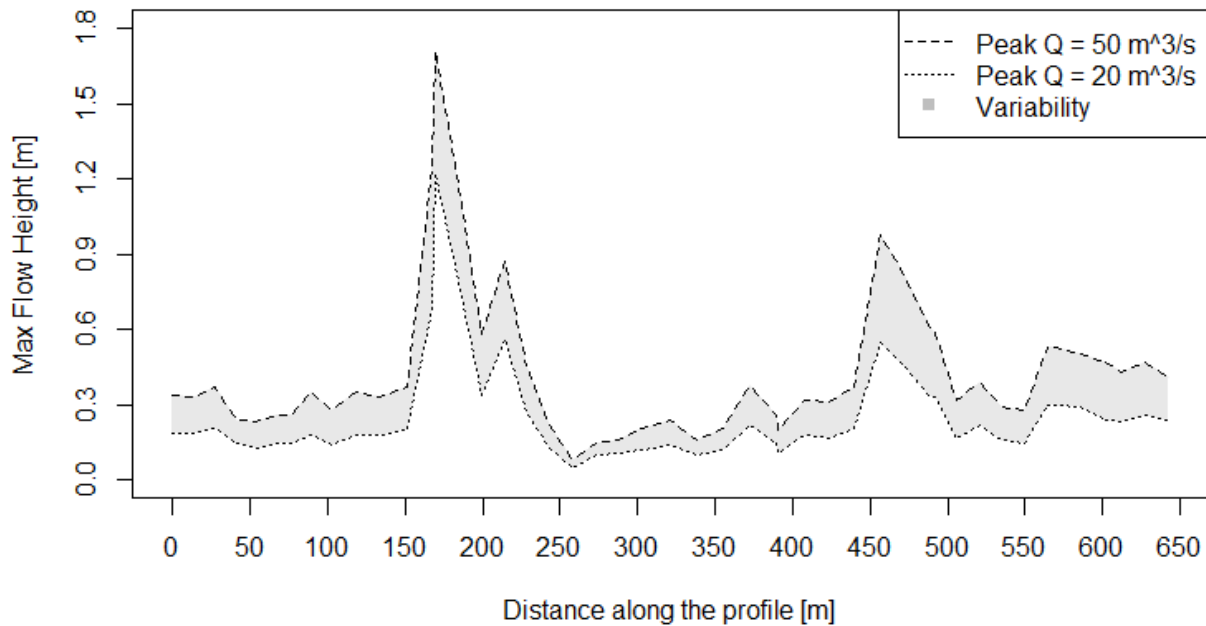


Figure 16: Maximum flow heights are shown in the first 650 m of the Aksay channel for a scenario with an initial peak discharge of $50 \text{ m}^3 \text{ s}^{-1}$ (dashed) and an event with an initial peak discharge of $20 \text{ m}^3 \text{ s}^{-1}$ (dotted). The grey area between the scenarios represents the variability in maximum flow height at each location within the first 650 m downstream of the release area.

5.1.3 Release Volumes

Together with the total inflow duration, the peak discharge set for the hydrograph is coupled directly with the amount of water released which allows for analysing the impact of different lake volumes on flow dynamics. By varying the release volume and discharge scenarios (Table 5, Appx.), the impact on the resulting flow heights was analysed (Figure 17a). It was found that the variability among different discharge simulations starting with the same lake volume is higher for large release volumes than for lower ones. While in simulations with a volume of $300'000 \text{ m}^3$, variations in maximum flow heights range from 0.1 to 0.3 m in the channel section before the debris cone, the smaller release volume of $35'000 \text{ m}^3$ results in differences of approximately 0.05 to almost 0.2 m in the same channel segment.

Additionally, maximum flow heights for lake volumes of $35'000$ and $300'000 \text{ m}^3$ can vary substantially in response to different peak discharges set at the initiation of the mass movement. Maximum flow heights tend to show less variability in low flow height zones, while in areas with increased flow heights, variability between different simulations increases again.

Further analyses reveal that initial peak discharge has a positive effect on peak discharge measured shortly before the debris cone (Figure 17b). The resulting discharge at the debris cone increases with higher initial peak discharges. Furthermore, higher release volumes additionally lead to increased discharge values, which can be derived from discharge measurements showing greater increases for the large release volume compared to the medium and small events. While for an initial peak discharge of $50 \text{ m}^3 \text{ s}^{-1}$, the three different-sized events result in similar discharges at the debris cone, these differences are larger for an initial peak discharge of $100 \text{ m}^3 \text{ s}^{-1}$. An initial peak discharge of $70 \text{ m}^3 \text{ s}^{-1}$ coupled with large release volumes results in higher

discharges than scenarios with an initial peak discharge of $100 \text{ m}^3 \text{ s}^{-1}$ originating at a medium-sized lake.

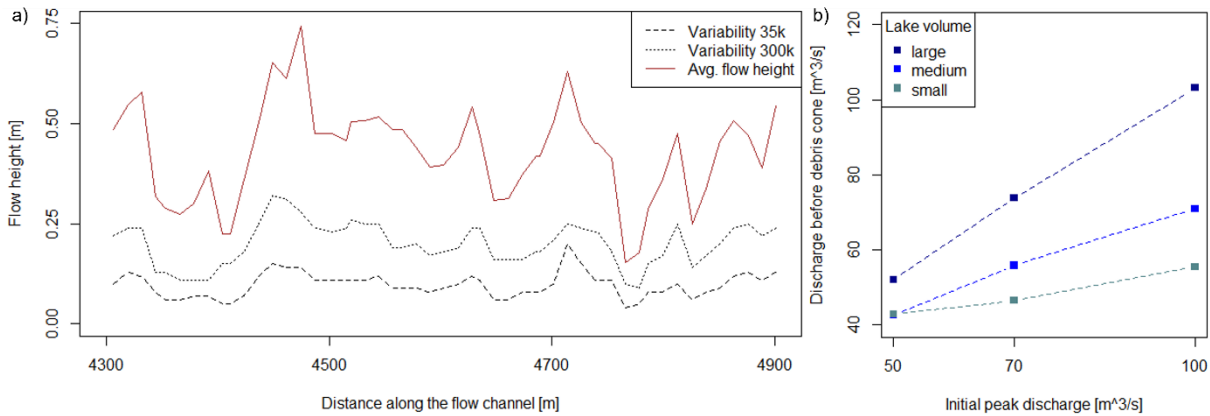


Figure 17: a) Flow heights observed in response to different initial peak discharges and lake volumes. Initial peak discharges were set to 50, 70, and $100 \text{ m}^3 \text{ s}^{-1}$ and lake volumes to $35'000$ and $300'000 \text{ m}^3$. The dotted line represents the difference between the highest and lowest maximum flow heights observed using the three simulations with a lake volume of $35'000 \text{ m}^3$. The dashed line shows the variability for a lake volume of $300'000 \text{ m}^3$ with the same discharge scenarios applied. The brown solid line shows the average maximum flow height recorded in all six scenarios. The data is shown in a channel segment shortly before the debris cone, between 4300 and 4900 m downstream of the release area. b) Discharge measured before the cone against the peak discharge set for the initial hydrograph. In addition to three peak discharge scenarios, discharge values are plotted for three lake volumes (small = $35'000 \text{ m}^3$; medium = $50'000 \text{ m}^3$; large = $300'000 \text{ m}^3$).

5.1.4 Time of Arrival

Not only does the variability in release volumes and especially in peak discharges have an influence on flow heights and velocity, but the duration until mass movements can reach a critical location is affected as well and can vary accordingly (Figure 18).

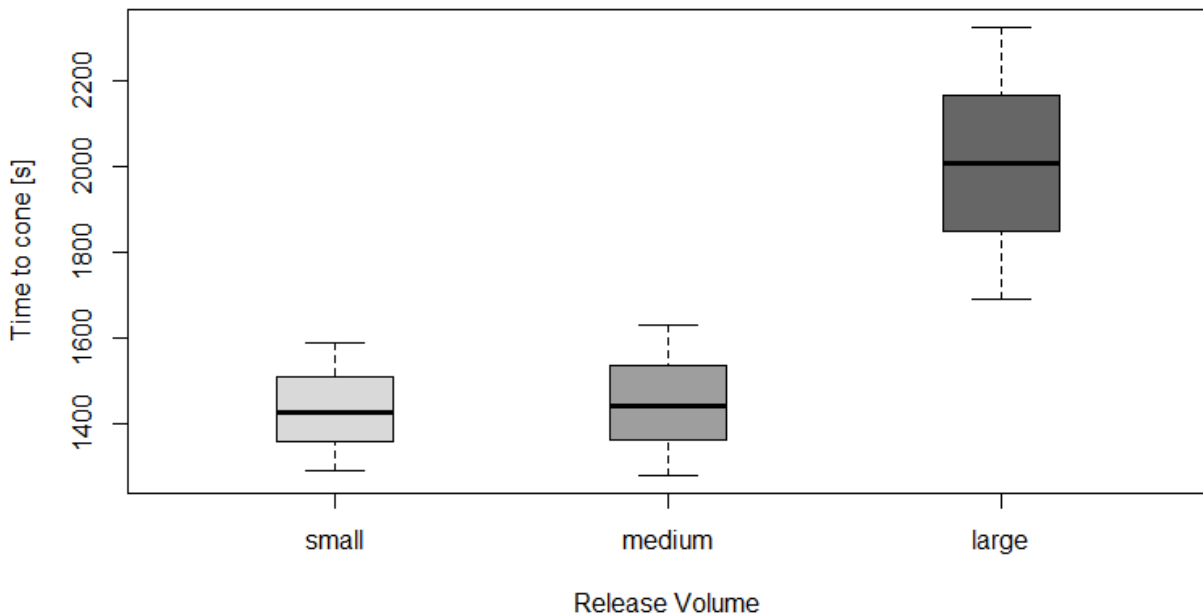


Figure 18: Initial peak discharge values (50 , 70 & $100 \text{ m}^3 \text{ s}^{-1}$) and three lake volumes ($35'000$, $50'000$ & $300'000 \text{ m}^3$) are compared using the time it takes the mass movement to reach measurement point 4 located shortly before the debris cone ($74.495282^\circ \text{ N}$, $42.554430^\circ \text{ E}$). For the small release volume, the time to peak amounts to 280, 200, and 140 s for discharges of 50 , 70 , and $100 \text{ m}^3 \text{ s}^{-1}$ respectively. For the medium release volume, the time to peak was set to 400, 285, and 200 s while for the large scenario, peak discharge was reached after 2400, 1714, and 1200 s respectively. The parameter settings are visible in Table 5, Appx.

It was found that the small and the medium release volume show similar variability in the duration until the debris cone is reached, although the hydrograph shape is slightly altered due to the equations used (section 4.4.1). What is noticeable is that travel times are characterised by a much higher variability for the large release volume, which is reflected by the elongated box compared to the two smaller scenarios. While for the small and medium scenarios, all simulated mass flows reach the location after about 1300 to 1600 s, it can take the large event between 1700 and 2300 s to reach the debris cone, which is a timespan twice as long as the two smaller events. The large difference in absolute values results from the equations that relate the release volume to the time it takes until peak discharge is reached.

5.2 Erosion Dynamics

The findings presented in section 5.1 neglect erosive forces and the resulting dynamics are controlled mainly by the initial conditions. Since available sediment in the channel bed is prone to be eroded by a passing mass flow, analyses were performed to evaluate the impacts of individual parameters on erosive behaviour and how the amount and timing of erosion are controlled by different variables.

5.2.1 Erosion Depths

To account for natural variability in the amount of erodible sediment available in a flow channel, erosion depths were varied in RAMMS so that different scenarios could be simulated (Figure 19). By keeping the hydrograph constant with a peak discharge of $20 \text{ m}^3 \text{ s}^{-1}$, the impact of changing erosion depths on flow dynamics could be analysed. To avoid multiple factors controlling the outcome, the remaining erosion parameters in RAMMS were kept constant (Table 7, Appx.).

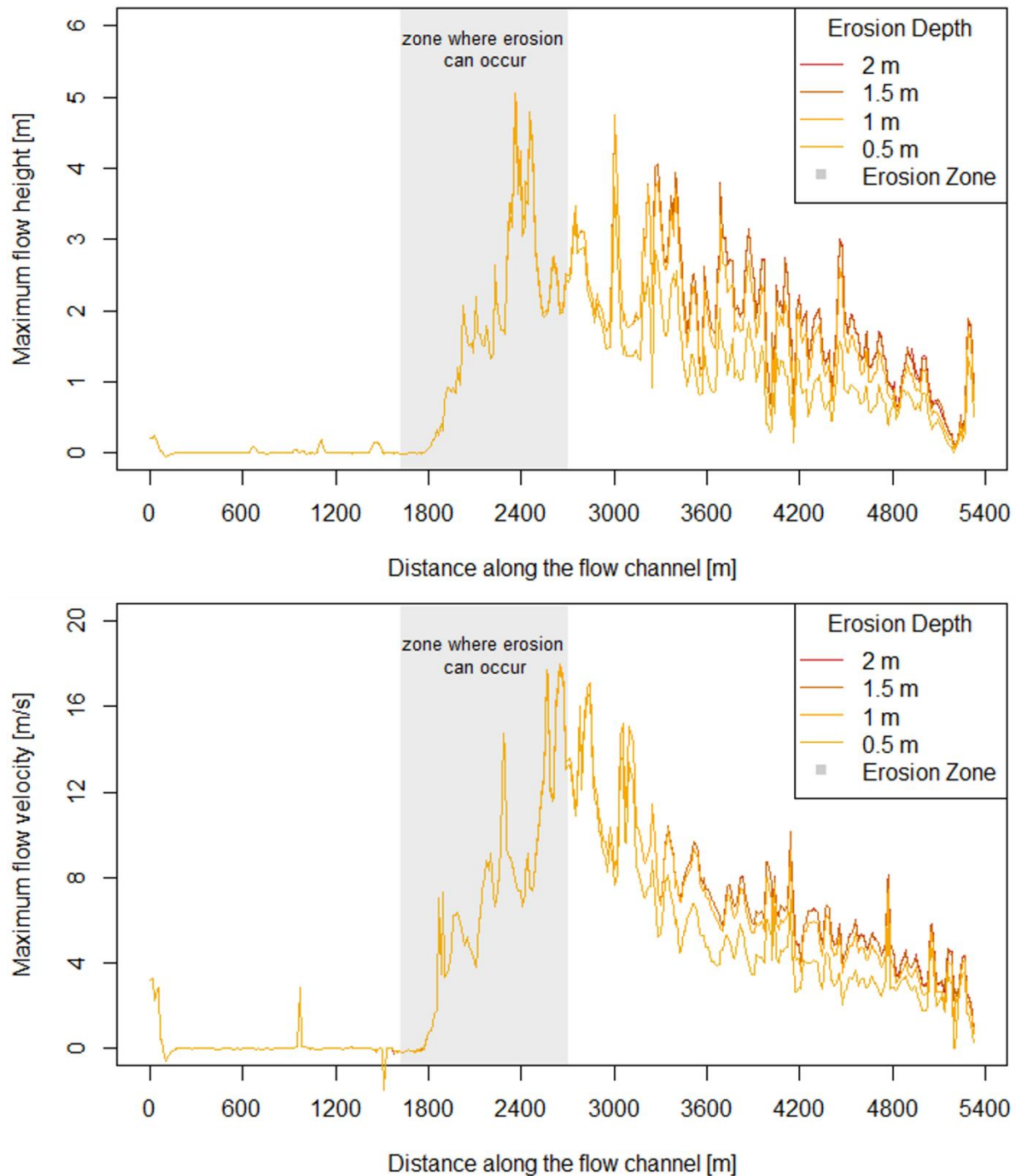


Figure 19: Changes in maximum flow heights (a) and flow velocities (b) in response to four erosion depths are plotted along the entire flow channel. In the canyon between 1625 and 2700 m downstream of the release area, erosion was enabled, and erosion depths were set to 0.5, 1, 1.5, and 2 m in four simulations (Table 7, Appx.). Shaded in grey is the segment where erosion could occur (erosion zone 2). The results are shown relative to a non-erosion scenario.

Maximum flow heights and velocities were found to increase drastically after the mass flow enters the erosion zone at a distance of about 1625 m (Figure 19). While flow heights increased by up to 5 m compared to the non-erosion scenario, flow velocities increased by more than 16 m s^{-1} . Thereby, no apparent differences in both flow heights and velocities in response to varying erosion depths are visible. Only downstream of the erosion zone, different behaviour is observable and scenarios with higher erosion depths tend to result in higher flow heights and

velocities. Although flow heights and velocities decrease again downstream of the erosion zone, it is noticeable that differences between the scenarios with erosion depths of 0.5 and 1 m are larger compared to the simulations using 1.5 and 2 m. Derived data covering the lowest channel segment shows that the gain in flow height and velocity is reduced with increasing erosion depth (Figure 30-33, Appx.).

Apart from the amount of sediment available, the occurrence of entrainment is controlled by the channel segment where erosion can occur. The entrainment occurring in the Aksay canyon has implications on flow dynamics after the mass flow has left the canyon since flow heights and velocities show different behaviour (Figure 19). Nevertheless, the region where the solid material is entrained controls the flow behaviour to a great extent (Figure 20Figure 21).

To evaluate how the spatial dimension of erosion affects flow heights towards the debris cone, erosion was applied in two different segments along the channel (Figure 20b&c). They were compared with the basis simulation which models a pure flood with an initial peak discharge of $20 \text{ m}^3 \text{ s}^{-1}$ and without entrainment. For both scenarios, erosion parameters were fixed at the same values. It becomes visible that resulting from entrainment occurring in zone 2 (Figure 20b), flow heights increase by more than 5 m in some locations compared to the basis simulation, where flow heights never exceeded 1.5 m (Figure 20a). In the case where erosion is allowed only in zone 3, the onset of entrainment increases the flow height substantially along the channel, reaching heights of more than 9 m (Figure 20c). It is noticeable that maximum flow heights also rise in regions downstream of the indicated erosion zones and the effect of erosion is not limited to the demarcated zones (Figure 20b&c).

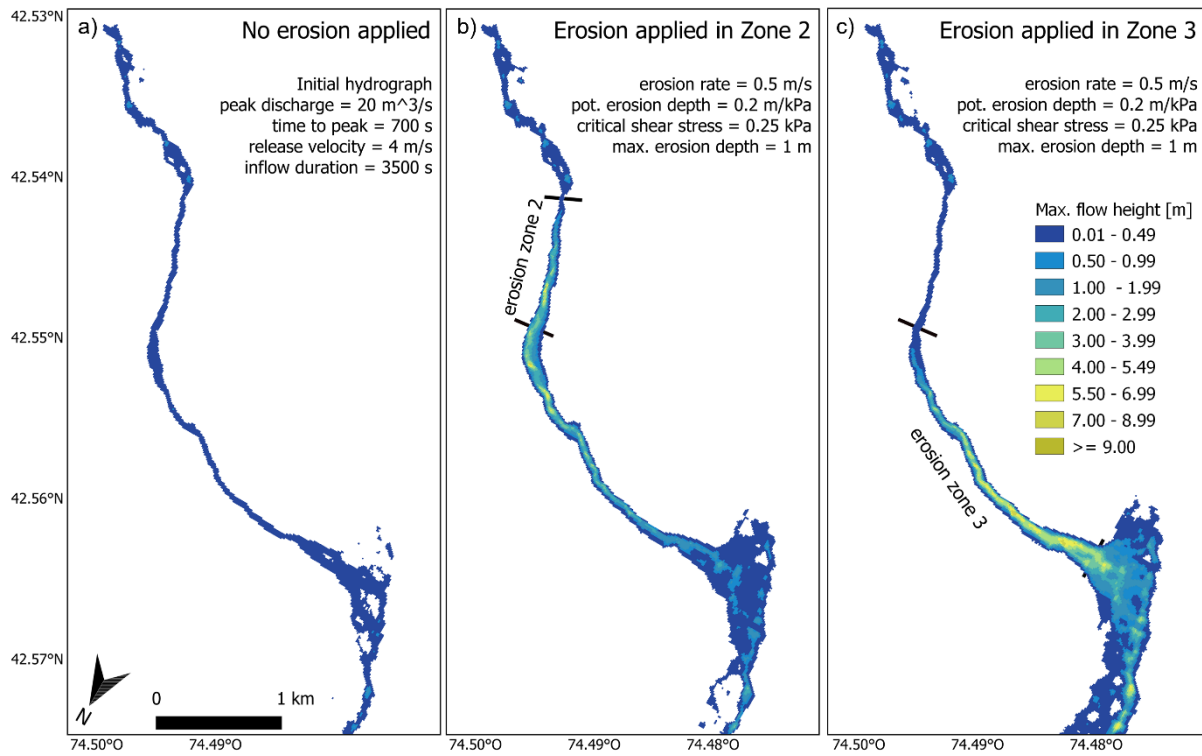


Figure 20: Changes in maximum flow heights resulting from the basis simulation without erosion (a), with erosion in zone 2 (b), and with erosion in zone 3 (c) are shown along the Aksay channel. Erosion settings were set as listed at the top of the map and were applied within the solid black lines. Each scenario is controlled by the hydrograph settings used in the basis simulation (Table 2).

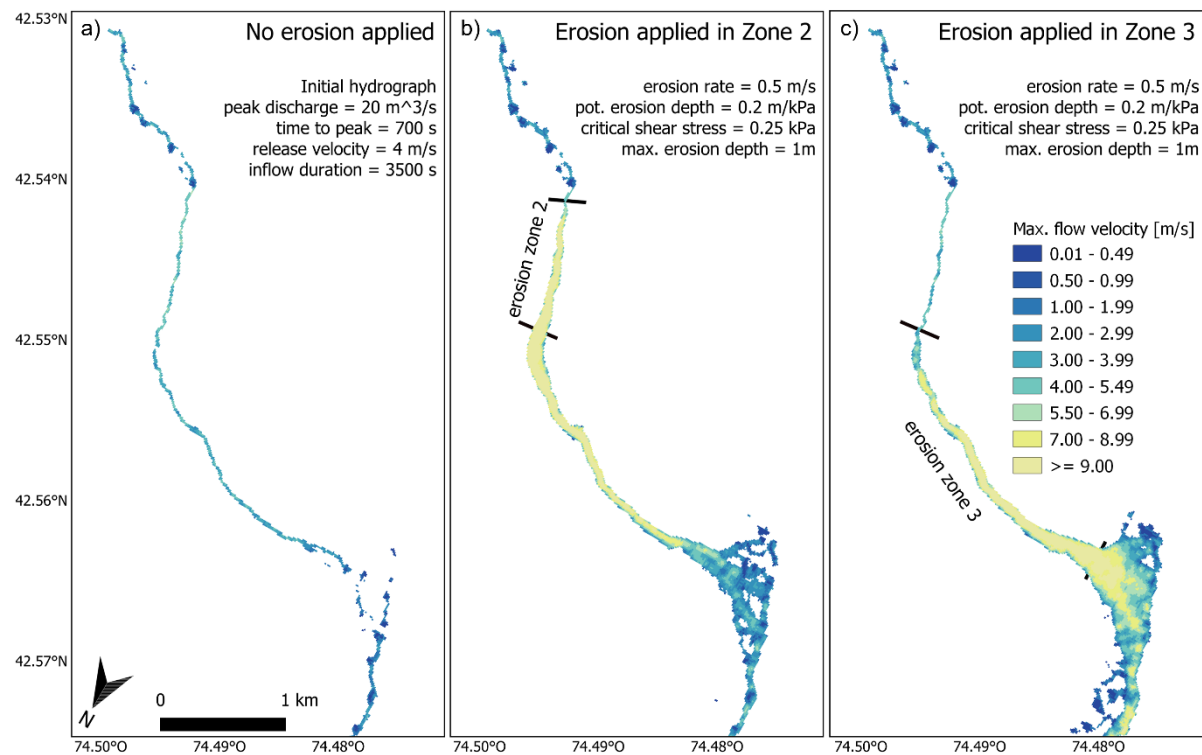


Figure 21: Changes in maximum flow velocities resulting from the basis simulation without erosion (a), with erosion in zone 2 (b), and with erosion in zone 3 (c) are shown along the Aksay channel. Erosion settings were set as listed at the top of the map and were applied within the solid black lines. Each scenario is controlled by the hydrograph settings used in the basis simulation (Table 2).

When it comes to the influence erosion has on flow velocities, it becomes evident that velocities increase if entrainment is considered by the model. While a pure flood simulated in the Aksay channel reaches maximum flow velocities of more than 6 m s^{-1} but in most sections does not exceed 5.5 m s^{-1} (Figure 21a), scenarios where erosion is applied can increase maximum values by a factor of 2 and even 3 in some locations (Figure 21b&c). Once entrainment has set in, maximum flow velocities measured across almost the entire width of the channel increase to more than 9 m s^{-1} and decrease to values lower than 7 m s^{-1} as the mass flow approaches or reaches the debris cone. Even when reaching the southern edge of the map in Figure 21, strong increases in flow velocities compared to the flood scenario are visible.

5.2.2 Limits to Erosion

The increase observed in both flow height and flow velocity owing to the addition of solid material is mainly driven by the sediment volume eroded by the mass flow. As erosion dynamics simulated in RAMMS are controlled by several erosion parameters, the sensitivity of the total eroded volume to individual parameters was analysed. When entrainment occurs in erosion zone 2 or 3, the eroded volume increases if the depth of the sediment layer at the channel bed rises as well (Figure 22a). However, this effect is only visible until a certain threshold, which in this case is reached at an erosion depth of about 1.75 m. If erosion depths are higher than the threshold, any increase in the depth of the erodible sediment layer will not result in a higher volume eroded by the mass. Comparably, if the critical shear stress is lowered meaning that erosion is allowed to start at lower stresses exerted on the channel bed, higher volumes of sediment are entrained (Figure 22b). Nevertheless, the same effect of a stagnating volume increase is observable so that increasing erosion depths above values of 1.75 m do not lead to higher sediment volumes entrained by the flow even if the critical shear stress is reduced (Table 8, Appx.).

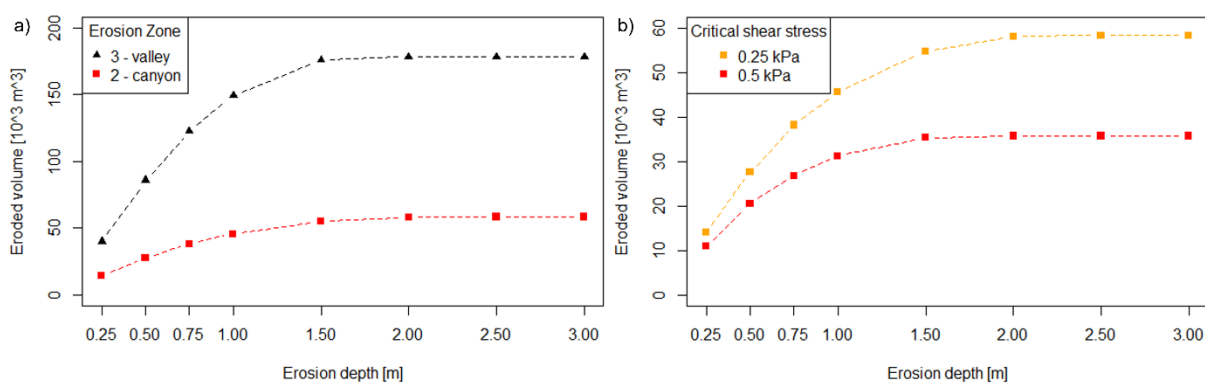


Figure 22: a) The eroded volume recorded in two scenarios is plotted depending on multiple erosion depths given on the x-axis. Erosion was enabled in erosion zone 2 (red) and zone 3 (black). Both scenarios are based on an initial peak discharge of $20 \text{ m}^3 \text{ s}^{-1}$ and a critical shear stress of 0.5 kPa . Erosion depths were fixed at 0.25, 0.5, 0.75, 1, 1.5, 2, 2.5, and 3 m. b) The eroded volumes are plotted against the same erosion depths for scenarios where erosion was applied in erosion zone 2. The red line shows the same data as in Fig. 21a while the data points marked in orange are based on simulations where the critical shear stress was lowered to 0.25 kPa .

Erosion is further controlled by the erosion rate [m s^{-1}] which defines the vertical depth that can be eroded each second. When erosion is applied in the glacier forefield (erosion zone 1) (Figure

23a), the eroded volume is substantially lower compared to the areas further downstream (Figure 23b&c). In addition, the eroded volume remained constant when the erosion depth on the forefield was increased from 0.75 to 1 m. It is also shown that the sediment volume added to the mass flow rises with increasing erosion rates. Results based on erosion occurring in the canyon or the valley demonstrate that the eroded volume not only increases with rising erosion rates but also due to higher erosion depths when erosion rates exceed 0.0125 m s^{-1} (Figure 23b&c). It is noticeable that in erosion zone 2, a 4-fold increase in erosion rate from 0.0125 to 0.05 m s^{-1} does not yield an increase in the eroded volume by the same factor. In contrast, simulations in erosion zone 3 show that a 2-fold increase from 0.0125 to 0.025 m s^{-1} results in volume increases by nearly 200% equalling a factor of three. However, adjusting the erosion rate to 0.05 m s^{-1} does not yield comparable volume increases neither for an erosion depth of 0.75 m nor for a depth of 1 m .

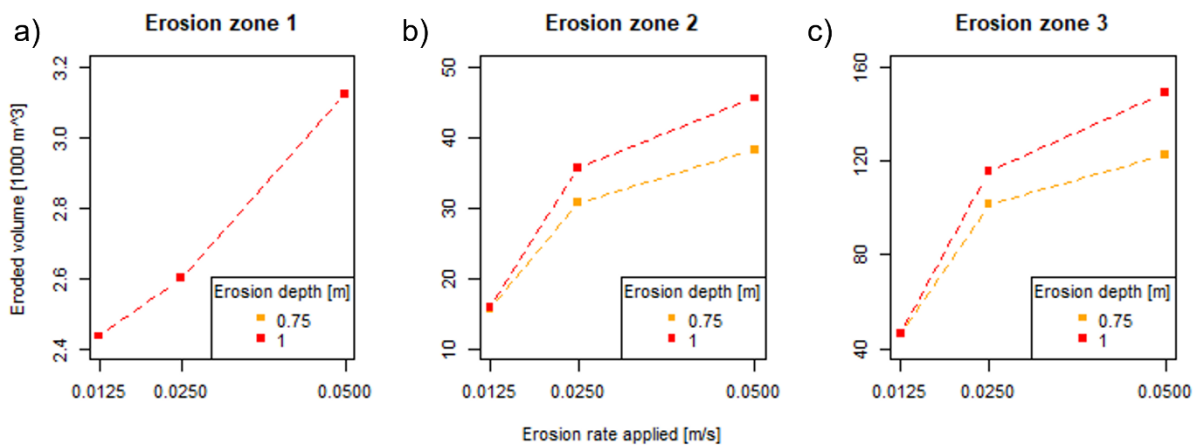


Figure 23: The eroded volume is plotted against varying erosion rates applied in a) the glacier forefield, b) the canyon and c) the valley. Simulations were carried out with an erosion depth of 0.75 m (orange) and 1 m (red) with an initial peak discharge of $20 \text{ m}^3 \text{ s}^{-1}$. For each erosion zone, the erosion rate was set to RAMMS' default values at 0.0125 , 0.025 , and 0.05 m s^{-1} (Table 10, Appx.).

5.2.3 Impact on Temporal Aspects

An aspect that has been lacking in previous analyses is the temporal dimension of entrainment. As a result, the entrainment module of RAMMS was analysed by extracting data on the eroded depth at different time steps. It was found that within 30 s after the mass flow has reached the end of the canyon, more than 90% of the total eroded volume ($35'360 \text{ m}^3$) measured in erosion zone 2 was reached (Figure 24).

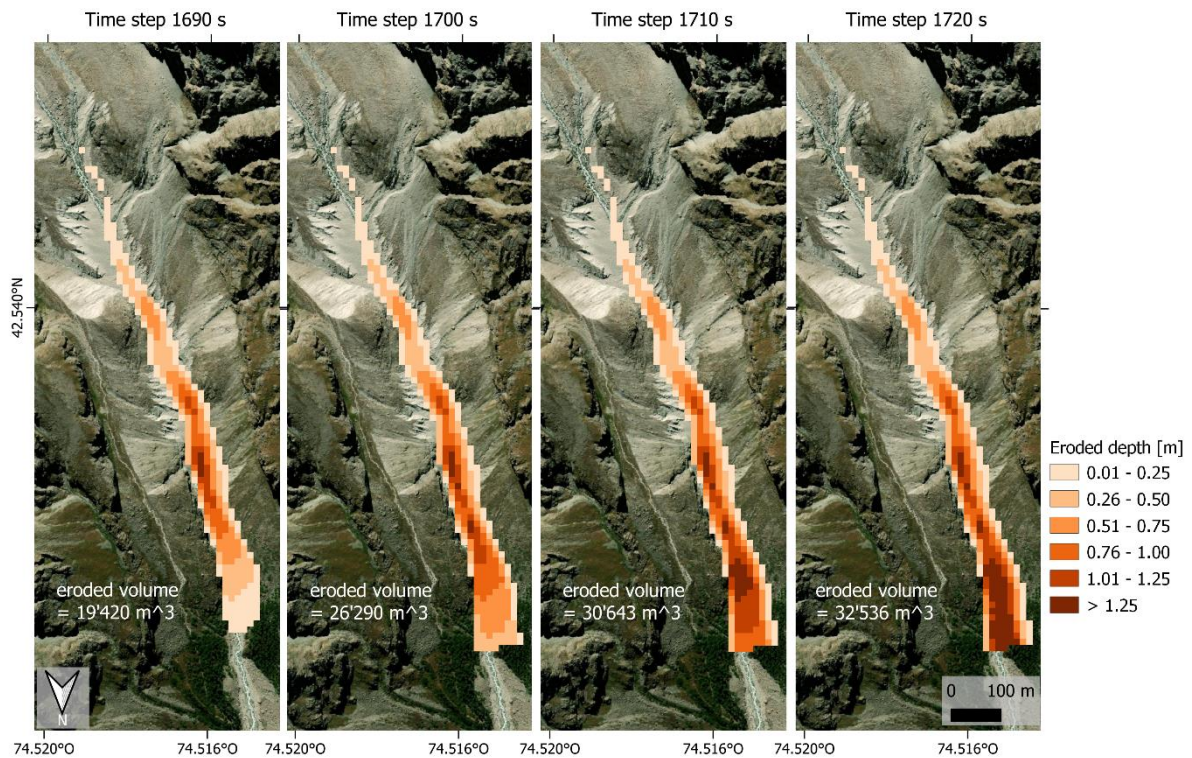


Figure 24: The four maps illustrate the eroded depth per pixel ($12.5 \text{ m} \times 12.5 \text{ m}$) at different time steps. Erosion was enabled in erosion zone 2 whereby a maximum erosion depth of 1.5 m was applied. The erosion rate was set to 0.05 m s^{-1} and critical shear stress was fixed at 0.5 kPa. In white, the eroded volumes at the given time steps are provided. The total eroded volume at the end of the simulation amounted to $35'360 \text{ m}^3$.

Between time step 1690 s and 1720 s, the eroded depth per cell in the lower part of the canyon increases from 0 to more than 1.25 m. Moreover, while there are no drastic changes to erosion depth visible in sections further upstream in the canyon at the given time steps, eroded depths show strong increases close to the flow front. The total eroded volume at the end of the simulation (5640 s) amounts to $35'360 \text{ m}^3$, which is an increase of less than $3'000 \text{ m}^3$ compared to the eroded volume observed until time step 1720 s. Similar results are found for a maximum erosion depth of 0.5 m (Figure 34, Appx.). In that case, the same percentage of the total eroded volume (92%) was reached already 10 s after the mass flow had reached the end of the canyon.

A second temporal aspect often neglected in previous studies relates to the duration until a certain location is reached by a mass movement. It has already been shown that higher peak discharges generally lead to shorter travel times if erosion is neglected (Figure 18). For scenarios where entrainment is considered, the change in flow velocity is expected to affect travel times which reduces the time of arrival. Therefore, the analyses on peak discharges were extended by a series of simulations that consider erosion in the canyon (Figure 25).

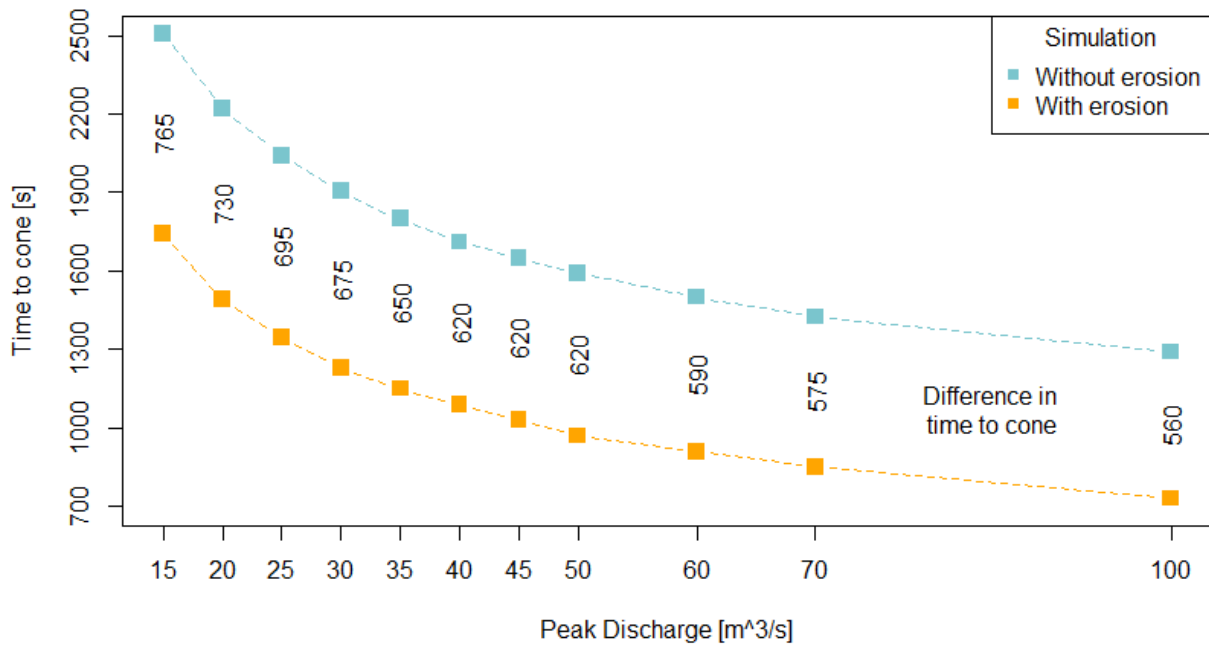


Figure 25: The time required for the simulated mass movements to reach the debris cone is plotted against the initial peak discharge set at the release zone. Simulations with and without erosion were carried out for 11 different hydrograph settings. The data points represent the time at which each scenario crossed a specified cross-section at the upper edge of the debris cone (measurement point 4). The data series in blue shows the scenarios where erosion is neglected. In orange, the resulting times are shown when entrainment with an erosion depth of 0.75 m was enabled along the entire flow channel. The erosion rate was set to 0.05 m s^{-1} and critical shear stress was fixed at 0.5 kPa (Table 11, Appx.). The numbers in black show the time difference between the respective scenarios.

It is visible that the incorporation of entrainment reduces the time a mass flow needs to reach the debris cone by 560 to 765 s for the given hydrograph settings (Figure 25). Furthermore, the time difference decreases with an increasing initial peak discharge. While for relatively low discharge values, erosion reduces travel times by more than 10 minutes, the time differences tend to be smaller when higher discharges are applied. Simulations with initial peak discharges of $60 \text{ m}^3 \text{ s}^{-1}$ or higher show a reduction in the time required to reach the cone of less than 10 minutes compared to the flood scenarios where erosion is neglected.

5.3 Variability in Travel Times

Travel times are highly variable and can be affected by several input parameters. The variability has therefore been evaluated and compared based on several analyses (Figure 26). All four selected variables were found to have an impact on the duration needed to the specified critical point. Thereby, peak discharge, which shapes the release hydrograph, as well as critical shear stress have the highest impact on the time required by the mass flow to reach the debris cone. Varying the initial peak discharge between 5 and $100 \text{ m}^3 \text{ s}^{-1}$ led to an observed range between 1290 and 2505 s until the critical point (measurement point 1) was reached, which amounts to a time difference of 1215 s. For different critical shear stress values, the times observed vary between 1830 to 2700 s, which covers a range of 870 s.

In contrast, the velocity set at the release area and different depths of erodible sediment do not have a strong impact on the duration until the cone is reached. Although the duration is affected

by both variables, the deviations in the times do not exceed 150 s neither with varying initial velocities nor with changed erosion depths.

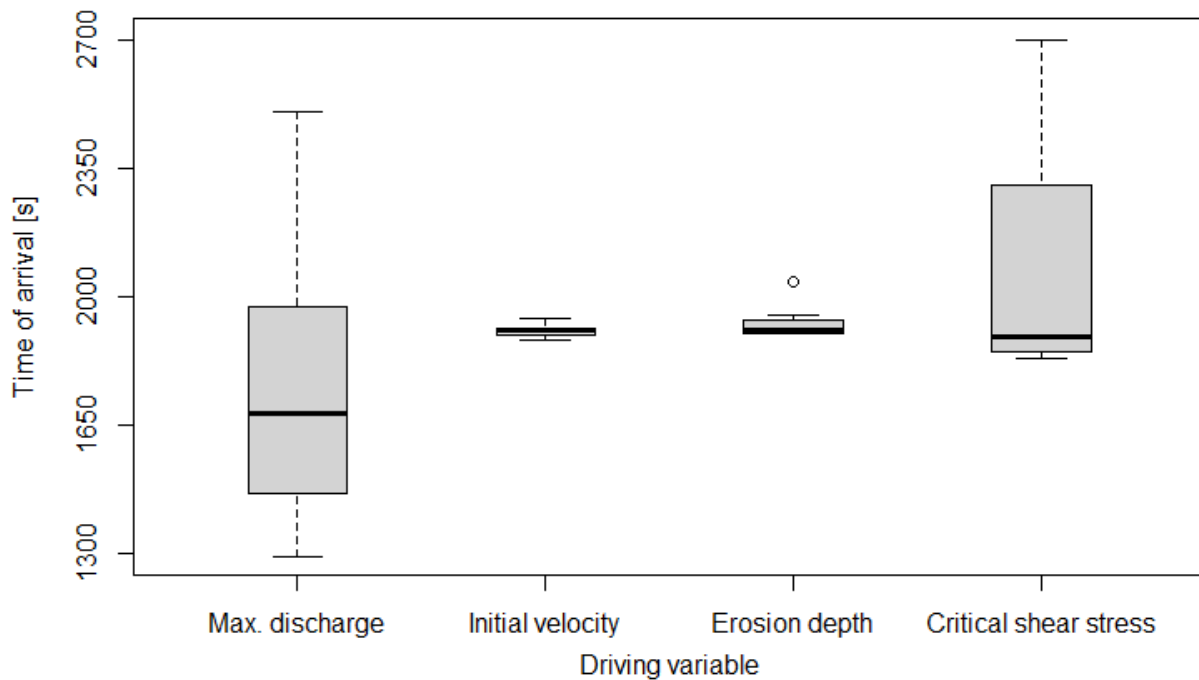


Figure 26: Time of arrival at the debris cone is shown in dependence on four driving variables. Max. discharge considers simulations with initial peak discharges 15, 20, 25, 30, 35, 40, 45, 50, 60, 70, and $100 \text{ m}^3 \text{ s}^{-1}$ and is illustrated separately in Figure 25. Initial velocity considers scenarios where velocities at the release are set to 2, 5, 8, 11, 14, 17, and 20 m s^{-1} . The range of times resulting from different erosion depths takes into account simulations where the erosion depth in erosion zone 2 was varied between 0.25, 0.5, 0.75, 1, 1.5, 2, and 3 m. The fourth boxplot results from varying critical shear stress values applied in erosion zone 2 between 0.025, 0.375, 0.5, and 0.75 kPa. The remaining parameters were adopted from the basis simulation (Table 2).

5.4 Scenario-based Modelling

Although the RAMMS debris flow module is designed specifically to model debris flow dynamics, simulations were performed that approximate the behaviour of different types of mass movements originating at the same release zone (Figure 27). While initial conditions were altered to reflect different scenarios, erosion settings were kept constant to ensure that deviations in the results can be attributed to the changed release conditions (Table 3).

It was found that flow heights tend to increase the more granular the mass flow becomes. While in the flood scenario (Figure 27a), flow heights hardly ever exceed 0.8 m, there is an extensive section before the debris cone where maximum flow heights are higher than 2 m during a granular debris flow (Figure 27c). The scenario between the two extremes shows that flow heights are similar to the flood event, however, the mass does not reach the same distance as the flood scenario (Figure 27b). The granular debris flow stops comparably early and does not travel further downstream along the Ala Archa river as most of the mass is deposited in proximity to the debris cone. Further, it is depicted that discharge values for the granular debris flow within the Aksay catchment are much higher than for the other two scenarios although initial peak discharge was fixed at $20 \text{ m}^3 \text{ s}^{-1}$ for all three scenarios. The granular debris flow

reaches discharge values of more than $200 \text{ m}^3 \text{ s}^{-1}$ at the measurement point closest to the debris cone, while the two low-magnitude events remain below $30 \text{ m}^3 \text{ s}^{-1}$ at the same cross-section.

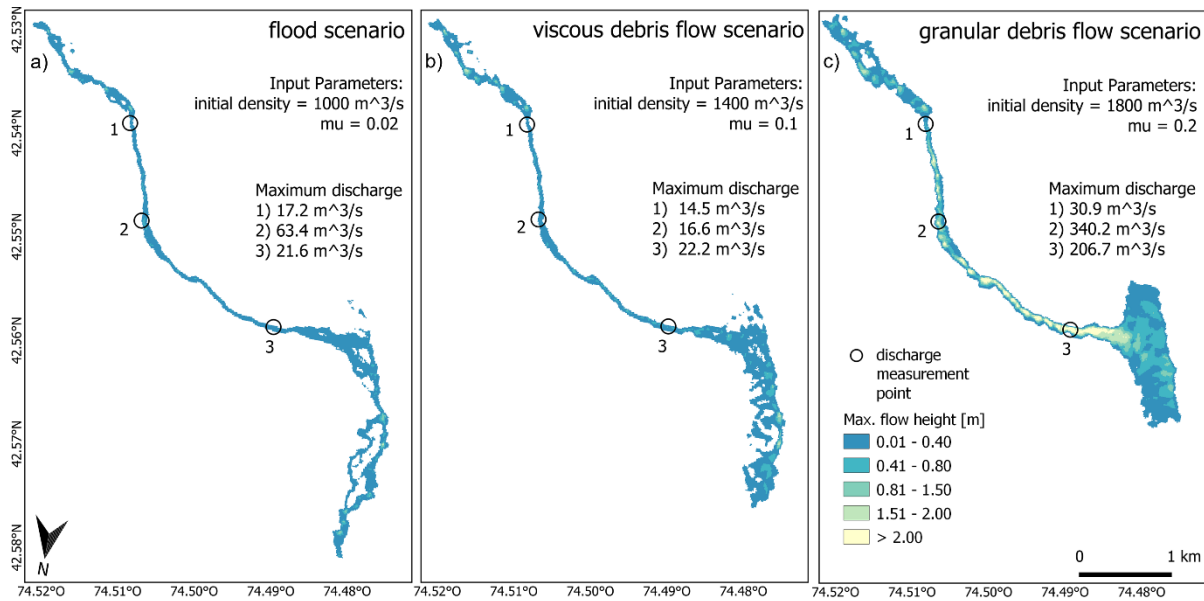


Figure 27: Maximum flow heights of three different scenarios are shown upstream and downstream of the Aksay debris cone. The hydrograph settings in the three scenarios were kept constant with an initial peak discharge of $20 \text{ m}^3 \text{ s}^{-1}$. Erosion was applied along the flow channel until measurement point 4, whereby erosion density was set to 1800 kg m^{-3} . Erosion depth was set to 0.5 m above measurement point 1 and to 1 m below. Initial densities were fixed at 1000, 1400, and 1800 kg m^{-3} for the flood (a), viscous debris flow (b), and granular debris flow (c) scenario respectively. Frictional behaviour was controlled by setting μ to 0.02, 0.1, and 0.2 to account for the different scenarios (Table 3), as suggested by Stricker, (2010). Maximum discharge measured in RAMMS is given at three locations (measurement points 2, 3 & 4) along the flow channel.

When it comes to erosive processes, the scenario approximating the dynamics of a granular debris flow can erode vast amounts of material upstream of the canyon in the glacier forefield whereas there is no erosive activity by the flood scenario in the same area (Figure 28). The eroded volumes at the visualized time steps amount to 402 and $30'035 \text{ m}^3$ for the flood and the granular debris flow simulation respectively. The maximum eroded depth per 12.5-m-grid cell did not exceed 0.05 m in the flood scenario, whereas during the granular debris flow, eroded depths of up to 0.93 m per grid cell were observed. While entrainment during the flood scenario only occurred at specific sections in the canyon where conditions were favourable, the material was entrained during the debris flow along an uninterrupted and wider flow path.

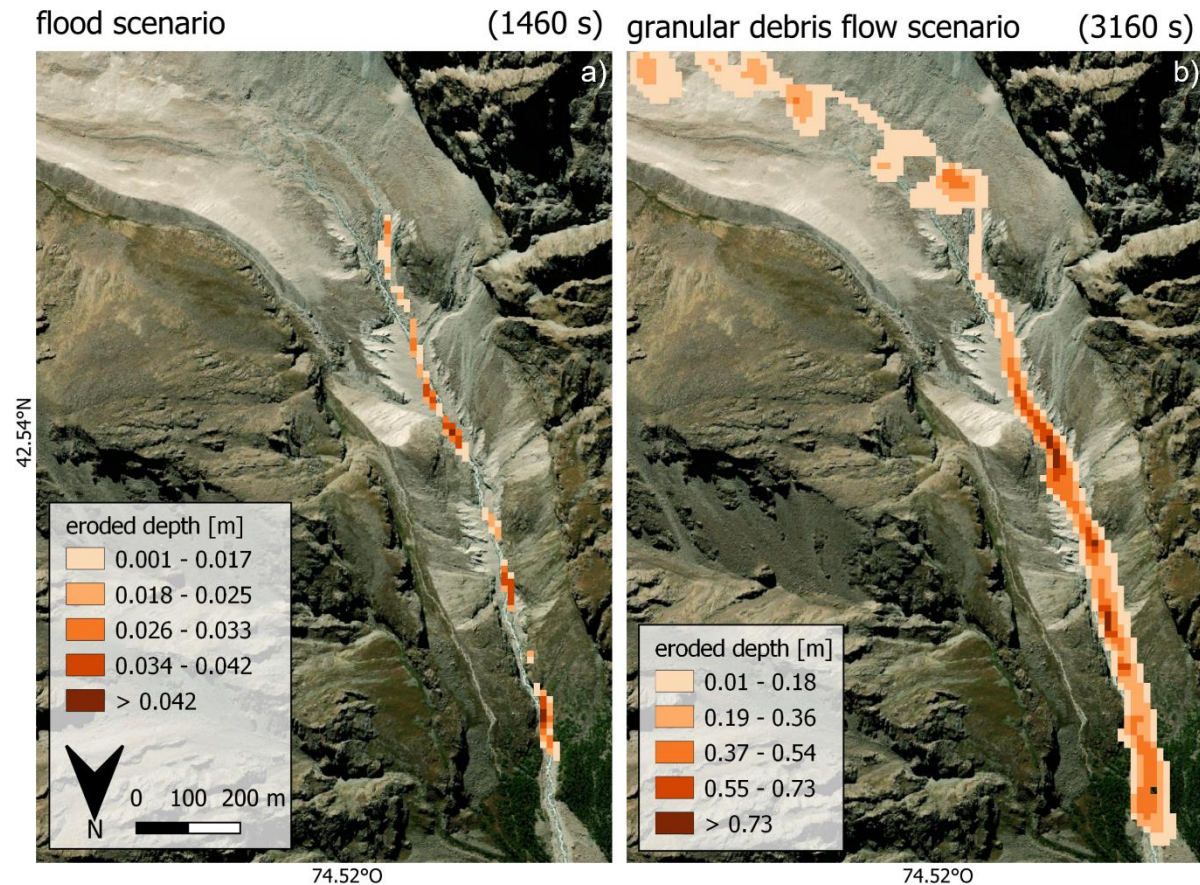


Figure 28: The eroded depth at the time the mass flow reaches the end of the canyon (1460 and 3160 s) is shown for a flood (a) and a granular debris flow (b) scenario. Initial density was set to 1000 and 1800 kg m⁻³ for the flood and debris flow scenario respectively. Friction parameter μ was fixed at 0.02 and 0.2 for the two scenarios. Erosion depth was set to 0.5 m in erosion zone 1 and to 1 m in downstream regions. The critical shear stress was fixed at 0.5 kPa. Hydrograph settings were adopted from the basis simulation (Table 2).

Apart from simulating different flow types by altering the release conditions, flow transformations were approximated by adjusting frictional resistance during the flow (Table 3). It becomes evident that in the case where friction is reduced at the debris cone, the flow reaches further downstream (Figure 29). While both the viscous and granular debris flow come to a halt at the debris cone or a bit further downstream when constant friction is applied (Figure 29a&c), this effect is not observed when friction is reduced (Figure 29b&d). Both scenarios with reduced friction from the beginning of the debris cone travel further along the Ala Archa river and would reach beyond the calculation domain that was fixed for this simulation. These findings demonstrate that multi-phase flow dynamics can roughly be approximated with single-phase models since they coincide with results presented in Meyrat et al. (2021) who show the stopping behaviour of solid and liquid phases. As an additional consequence of the change in flow behaviour, flow heights on the debris cone decrease significantly when friction is lowered downstream of measurement point 4. Compared to the granular debris flow scenario with constant friction (Figure 29c) where flow heights reached values of up to 1.8 m at the debris cone, decreasing frictional resistance resulted in flow heights reaching only 0.7 m in some areas, while a large part of the cone experienced flow heights even lower than 0.3 m. Furthermore, the inundated area is more continuous in the case where friction is treated as constant whereas

simulations where friction is changed during the flow exhibit flow paths that are more dispersed and narrower.

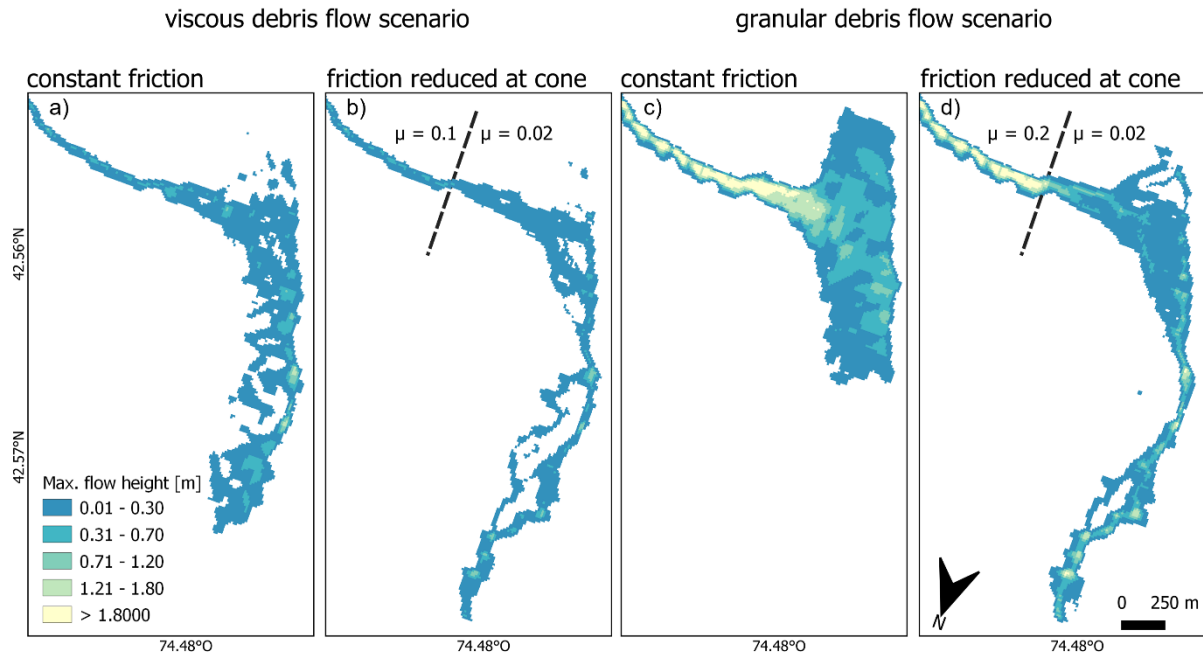


Figure 29: a) Viscous debris flow with constant friction. b) Viscous debris flow with variable friction. c) Granular debris flow with constant friction. d) Granular debris flow with variable friction. Maximum flow heights are shown for two debris flow scenarios whereby each scenario is simulated once with constant friction and once with reduced friction from where the debris cone begins (dashed black line). Initial density was fixed at 1400 and 1800 kg m⁻³ for the viscous debris flow and granular debris flow scenarios respectively. Frictional behaviour was controlled by setting mu to 0.1 for the viscous and 0.2 for the granular debris flow. Downstream of the dashed black line, friction mu was reduced to 0.02 (Table 3).

6 Discussion

Although severe GLOF events in Central Asia have been scarce in the past decades, they are considered one of the largest glacial hazards. The number of glacial lakes in Central Asia rises comparably fast which emphasises the need for adaptive measures and disaster management in vulnerable regions. Zheng et al. (2021) have reported that the increase in lake number mainly concerns moraine-dammed lakes which are considered prone to failure compared to other glacial lake types. Despite smaller lake areas compared to lakes in the Hindukush-Karakoram-Himalaya region, the projected lake area expansion in Central Asia further enhances pressure on local inhabitants and requires adaptive capacities. Above all, and besides the flow magnitude and damage potential, understanding the variability in travel times until critical points along the flow trajectory are reached can be essential regarding evacuation times and real-time disaster response.

The glacial lake in the Aksay catchment drains via subsurface channels which, in the current circumstances, is not expected to result in high flow magnitudes (Zaginaev et al., 2016). While moraine-dammed lakes normally burst upon an obvious trigger, drainage from ice-dammed lakes can additionally be shaped by seasonal variations as subsurface drainage is prone to change rapidly when melting season starts and channels start to open up after they have been temporarily blocked due to ice deformation (Narama et al., 2018). The uncertainty and variability arising from trigger mechanisms and outburst processes are essential when it comes to estimating the impact on regions downstream of the lake. While many studies in current literature focus on uncertainties in dam breach modelling to understand how dam properties and breach magnitudes shape the resulting mass flow, this thesis aimed at understanding the uncertainty in defining boundary conditions and erosive processes within the flow channel.

6.1 Boundary Conditions

Regarding boundary conditions, defining a release hydrograph is a first source of uncertainty as release velocities and volumes heavily depend on trigger and drainage mechanisms. The lack of data on lake bathymetry, drainage characteristics, and past events increases the difficulty in determining a realistic hydrograph shape. What adds to the complexity is that flow dynamics downstream of the lake are governed by additional factors as well, so the impacts of the hydrograph on flow dynamics and inundated areas are blurred.

The analyses presented using variable peak discharges for the release hydrograph have provided multiple insights. On the one hand, flow heights and flow velocities were observed to change along the channel in response to increased peak discharges. While maximum flow heights recorded in the channel increased almost 3-fold for discharges between 5 and 100 m³ s⁻¹, maximum flow velocities varied between 6 and 9 m s⁻¹ when entrainment was neglected. Although flow heights and velocities observed at the measurement points shown in Figure 15 may not be representative of the entire flow channel, it is demonstrated that there were substantial variations already if only initial discharge values changed. On the other hand,

variability was not only found in absolute flow values, but the variability noticeably changed between high-flow and low-flow areas. While distinct hydrograph scenarios might have led to similar behaviour in sections where low flow heights dominate, the variability was enhanced in channel segments where increased flow heights were observed (Figure 16). For scenarios with increased release volumes, this effect was further enhanced, leading to higher variability among the results compared to small release volumes.

Increased variability in flow heights and velocities did also lead to strong variations in discharge values. While for small release volumes, the mass was not able to sustain the peak discharge for a long time, measurements upstream of the debris cone have shown that in the case of large release volumes, discharge values were very similar to the ones specified at the release zone, which shows that high discharge can be sustained if sufficient water is released.

In contrast, simulations of mass flows differing only in initial flow velocities have shown that their behaviour converged rapidly, resulting in very similar flow dynamics, although sediment entrainment was neglected. Whether the mass flow left the drainage channels with 4 m s^{-1} or 20 m s^{-1} did not have an impact on the velocity measured approximately 1200 m downstream. The experiments performed have shown that flow velocities converged and reached similar values within the first 40 m downstream of the release area, showing that topography and geomorphic features could play an essential role in controlling the flow velocities of mass flows.

When it comes to the impact of boundary conditions on travel times, analyses showed that for small release volumes and high initial discharges, the mass flow could reach the debris cone after 20 minutes, assuming that no sediment entrainment occurs. Although the same discharge values applied for large release volumes resulted in longer travel times, the absolute values resulting from variations in release volumes cannot be compared, since the equations used assume that peak discharge is reached after one-fifth of the entire inflow duration. Owing to the enlarged release volume, the inflow duration and therefore also the time until peak discharge was reached increased. Nevertheless, although peak discharge was reached significantly later in the case of large release volumes, the travel time until the debris cone was reached was comparably short. Additionally, the variations observed between a peak discharge of 50 and $100 \text{ m}^3 \text{ s}^{-1}$ were larger for a release volume of $300'000 \text{ m}^3$ (range of 635 s) compared to the medium (350 s) and small (300 s) sized scenarios, which to some degree could also be explained by the lag caused by the equations used. Even though initial discharges of $50 \text{ m}^3 \text{ s}^{-1}$ or higher are very unlikely in the current setting at Uchitel lake, those findings provide indications of how variable the travel times can be in response to changed boundary conditions.

The findings on discharge variations are in line with results presented in Sattar et al. (2020) who, although focused on moraine-dammed lakes, state that discharge variations have a significant impact on flow dynamics further downstream. On the contrary, many studies have revealed that release conditions do not necessarily shape the flow behaviour for a long time, as channel characteristics, geomorphic features, and other flow properties have an impact on flow

mobility (Sattar et al., 2020; Westoby et al., 2014). Nevertheless, the results presented in this thesis coincide with the statements of Westoby et al. (2014) who have argued that the slope and entrainment of solids have a great impact on flow velocities which explains why initial flow velocities are prone to change rapidly after the release zone.

As there has not been much research on how boundary conditions shape the travel times of GLOFs and debris flows, the results presented in this thesis give a first indication of the variability in travel times. However, since the hydrographs were based on empirical equations and the time until peak discharge is reached has not been changed in relative terms, the variability might be underestimated. In the event of an earthquake or other sudden disasters destroying a dam and causing a high-severity event, the time until peak discharge is reached at the release zone might be much shorter than one-fifth of the entire inflow duration (Marchi et al., 2021) which would presumably result in shorter travel times.

The findings suggest that local authorities must consider a high variability in travel times. As tourists visit the national park and tourist facilities were constructed at the centre of the debris cone, the duration until a mass flow could arrive at the debris cone provides indications about possible evacuation times. Although there is high variability proposed by the approach presented in this thesis, related literature suggests that travel times could even be overestimated since further changes in the release hydrograph could be caused by high-severity events, which increases the uncertainty that local decision-makers have to deal with. For robust hazard assessments and analyses on travel times in specific catchments, it is therefore suggested to realistically simulate worst-case scenarios to ensure inhabitants have sufficient time for evacuation.

Furthermore, the general consent about the fact that channel topography and geomorphic features can have a significant impact on flow dynamics has been confirmed. However, the analyses discussed in this thesis imply that variations in flow heights, velocities, and discharge caused by varying outburst mechanisms and release discharges could be underestimated in high-flow areas. While scenarios initiated by distinct boundary conditions resulted in rather similar flow behaviour in low-flow areas where slopes were flatter compared to other channel sections, it was found that high-flow areas are characterised by higher uncertainty and variability, a fact that needs to be considered in hazard management. Predictions of flow heights and velocities during events with higher release volumes or outflow discharges therefore should be treated with care, especially when settlements and infrastructure are in proximity to critical channel segments.

6.2 Erosive Processes

Besides topography and momentum, the entrainment of sediments is known to affect flow behaviour to a large extent. As such, the onset of erosion in the Aksay canyon led to flow heights rising by 5 m and velocities by more than 16 m s^{-1} compared to a non-erosion scenario. Thereby, the depth of the sediment layer had no influence at first, as scenarios with layers of 0.5 and 2 m

produced the same outcome. Further downstream though, flow heights and velocities diverged increasingly, which might be attributable to differences in eroded volumes. It is noticeable that the gain in flow height or velocity decreases with increasing erosion depths, which suggests that there must be factors that limit erosion. The analyses have shown that increasing erosion depths did not necessarily result in higher amounts of eroded material. At some point, additional erodible material at the channel bed was not entrained by the mass movement. To some extent, the amount of erosion is governed by the critical shear stress since simulations with a reduced threshold have led to more eroded material. For mass flows that did not exert sufficient stresses on the channel bed, no material was eroded independent of the sediment depth. Nevertheless, the analyses have additionally shown that the same stagnating effect is observable when lower critical shear stress values were applied. However, the effect set in at a later point in time which allowed the flowing mass to erode additional sediments before the eroded volumes began to stagnate.

Furthermore, it shall be mentioned that the impact on flow dynamics was also noticeable far below the zone where sediment could be entrained. This might seem obvious since entrained material continues to form part of the mass flow also beyond a defined erosion zone. Nevertheless, it is noteworthy that flow heights and velocities showed increased values even if the material was entrained further upstream in the catchment and had been transported over a long distance.

Regarding the timing of erosion, the analyses revealed that most of the sediment was eroded while the flow front was passing at the specific point in the channel. It was shown that more than 90% of the total eroded volume was entrained already 10 to 30 s after the mass flow had reached the measurement point, which presumably owes to the highest shear stresses being exerted on the channel surface. Although there would have been additional erodible material in the channel as defined in the model setup, the lack of erosion occurring after the flow front has passed might be explained by reduced flow heights and therefore also decreased shear stresses in later parts of the mass movement.

Increased flow mobility and velocities due to erosion naturally have implications on travel times. Compared to simulations of pure floods with no added solid material, scenarios where erosion was considered resulted in travel times being reduced by more than 10 minutes in some cases. Interestingly, the strongest effect of erosion on travel times was found with low initial discharges, while for high release discharges, the reduction in time was not as significant. Nevertheless, erosion coupled with high initial discharges almost reduced the travel time to the debris cone by 50%. Despite the uncertainty related to the availability of sediments and the volume eroded by mass flows, it was found that once the critical shear stress was exceeded, the onset of erosion strongly affected the time needed to reach a specified critical location along the trajectory. Thereby, applying different critical shear stresses for varying release volumes led to an increasing range of possible travel times. While low thresholds allowed the mass to erode more sediment and hence to gain speed and momentum, higher threshold values resulted

in longer travel times. On the contrary, the time of arrival at a critical point along the channel did not change significantly with varying erosion depths. Although the availability of sediment is a strong driver of flow velocity, flow mobility did not necessarily depend on the depth of the sediment layer as a relatively thin layer of sediment could already reduce travel times by 50%. Nevertheless, conclusions must be handled with care since erosion is governed by multiple parameters, and interactions between input variables were not specifically considered in the modelling approach which could additionally increase variability and uncertainty.

Although studies exist with the focus on estimating the time available to evacuate affected houses in different scenarios (Melo et al., 2020; Rosli et al., 2021), there is a lack of literature when it comes to relating the evacuation time to variations in erosive behaviour which is why the findings in this thesis cannot be compared with results from literature. However, it becomes evident that differences in flow velocity, potentially caused by erosive processes, significantly shape the temporal characteristics of mass flows and resulting travel times, an aspect that must be taken into account in evacuation management.

Another knowledge gap related to the incorporation of solid material exists regarding the volume increase as the amount of eroded material by the flow is highly uncertain and can suppress the effects of boundary conditions on flow dynamics (Frank et al., 2017). On the one hand, the transport of material by mass flows requires a certain slope angle, below which deposition occurs (Huggel et al., 2002a). Beforehand, the sediment must be eroded by the movement which is mainly controlled by the shear stress acting on the channel bed. Certainly, erosion can only occur if the critical shear stress is exceeded. For mass flows that do not exert sufficient stresses on the channel bed, no material will be eroded independent of the sediment depth. In addition to being limited by the critical shear stress, the potential erosion depth, which is related to channel-bed shear stress (Frank et al., 2015), does additionally control the amount of erosion since the entrainment model in RAMMS is designed in such a way that entrainment is enabled only when the critical shear stress is exceeded again after erosion was initiated and if the potential erosion depth e_m computed by the model does not impede further erosion (Bartelt et al., 2017). This model setup might additionally explain the stagnating effect found in the results presented in this thesis, which is why further literature on the interplay of different erosion parameters is required.

On the other hand, the majority of recent relevant literature agrees that flow height and resulting basal shear stress are strong indicators of the amount of erosion occurring during a GLOF or debris flow, which is also why the flow fronts are considered to be responsible for most of the erosion (Berger et al., 2011; Schürch et al., 2011), a statement that has been confirmed by the conducted analyses on the timing of erosion. Furthermore, since larger particles are found in the front, additional stresses act on the channel bed (Stock and Dietrich, 2006). Resultingly, the volume increase is generally expected to further lead to higher flow depths and velocities, which is also reflected in the results presented in this thesis.

An aspect that is being discussed in current literature relates to whether the solid material should be entrained during the flow or whether it should be included in the boundary conditions. On the one hand, allowing erosion during the flow requires knowledge about sediment availability as well as other properties that determine the erosion parameters in RAMMS. Since detailed field data usually is a limiting factor, assumptions are taken which increases the uncertainty in model results (Frank et al., 2015; Somos-Valenzuela et al., 2016). On the other hand, in models that are incapable of simulating erosive processes during the flow, the solid material might need to be included at the beginning of the flow. However, it is impossible to know the solid volume beforehand, which adds uncertainty already for the boundary conditions. Furthermore, it is discussed in Frank et al. (2015) that the flow behaviour likely deviates from expected dynamics owing to overestimated discharge in the beginning. Additionally, geomorphic features and channel characteristics presumably affect the flow behaviour differently if the flow magnitude and the solid fraction are increased from the beginning, since momentum, flow velocity, and flow height would then be rather overestimated. Moreover, runout distances might be underestimated since loss of momentum and deposition of solids might occur earlier along the flow channel (Frank et al., 2015). Therefore, it is discussed in Frank et al. (2015) that adding mass during flood propagation is considered to reflect flow behaviour better.

The results presented have shown, on the one hand, that there is substantial uncertainty and variability related to the eroded volume which can be partly explained by several variables controlling the erosive behaviour of mass flows. The speed at which erosion can occur is limited by the erosion rate while the volume is dependent on the sediment layer depth as well as on how long the critical shear stress can be sustained. Although contemporary literature has already revealed how flow parameters respond to changes in certain variables, it was found that erosion is limited strongly by the model setup and reflects, to some extent, how erosion can only occur if sufficient shear stress is exerted on the channel bed and that the depth of the available sediment layer does not necessarily drive the amount of eroded volume. On the other hand, the findings support the opinion shared by many scholars that the flow front is responsible for most of the erosion (Schürch et al., 2011) and that the more liquid tail of a debris flow does not exert enough shear stress on the channel bed to erode vast quantities of sediment. Dependent on the velocity of the mass movement, the time in which the flow front can provide the required shear stress varies and determines the amount of erosion. Shallow sediment layers thereby are entirely swept away by the flow whereas deeper sediment covers are only partly eroded before decreasing shear stress will impede further entrainment. Although the stagnating effect found in multiple analyses throughout this thesis is partly due to model assumptions and equations mainly related to critical shear stress, potential erosion depth, and maximum erosion depth, it is reflected in the simulation results that the amount of sediment eroded is highly uncertain and varies when input parameters change slightly.

Therefore, and to prevent model results from being constrained by uncertainties, hazard assessments need to incorporate erosion and should be based on worst-case scenarios since flow magnitudes significantly change in response to sediment entrainment. The knowledge of

channel capacities and simulations on possible flow magnitudes and flow depths might help design necessary protection measures even if precise information on available sediment layers is missing.

Most importantly though, and independent of the area of interest, it is essential to consider that the incorporation of solid material can substantially change the time available for evacuation in addition to the increasing damage potential induced by a greater solid fraction (Liu et al., 2020b). As pointed out in previous literature, flow velocities to a great extent determine travel times of mass movements. However, the analyses in this thesis have shown that entrainment significantly alters the temporal characteristics of mass flows and can, at least in the Aksay catchment, reduce the time of arrival by 50%, meaning that the time available for the evacuation of tourists located around the debris cone decreases significantly.

6.3 Transitional Behaviour

The behaviour of different mass movements was approximated by initiating the mass flow with different bulk densities. As the bulk mass density is proportionally coupled with the shear stress exerted on the channel bed (eq. 8), the erosive behaviour of different mass flow types could roughly be simulated. Additionally, friction in the model was adjusted according to typical values discussed in Stricker (2010) to account for different frictional resistance acting on the mass flow. It was found that scenarios representing debris flow events managed to erode much larger sediment volumes compared to flood-like mass movements whereby flow volumes increased by factors of 3. Discharge measurements upstream of the cone showed that the entrainment of solids caused flow magnitudes to increase drastically compared to the conditions set at the beginning of the mass movement. While the flood scenario was not able to erode the material on the glacial forefield, presumably because the critical shear stress was not exceeded, there was substantial erosion by the simulated debris flow in the same region since the higher density and indirectly also the increased frictional resistance led to rising shear stresses exerted on the channel bed. Also due to increased friction, the debris flow scenarios came to a halt earlier than the flood-like event since flow velocities are forced to decrease once the terrain at the debris cone becomes flatter.

Besides different flow type scenarios, analyses on transitions to other mass movements have shown that changed frictional resistance during the event, which aimed at roughly simulating deposition at the cone while the liquid part of the mass would travel onwards, has resulted in the flow reaching further compared to the simulations with constant friction. This approach was adopted from Frey et al. (2018) whereby the friction parameters were changed at a chosen location to represent the transformation to hyperconcentrated flows. Since the mass flow's density cannot decrease in RAMMS, controlling the flow behaviour using frictional resistance approximately simulates the deposition of solids, whereas the liquid fraction of the mass movement continues its way downstream. Additionally, the scenarios with reduced friction resulted in a decrease in both flow heights and flow velocities at the debris cone as expected.

Changing initial densities to simulate different flow types coincides with aspects discussed in Breien et al. (2008) as higher solid fractions normally promote further erosion, which is also reflected in my simulation results, where debris flow scenarios were able to erode higher volumes of solid material. The results presented also are in line with findings discussed in Huggel et al. (2003) who claim that mass movements' flow volumes can increase 3-fold due to sediment entrainment. Westoby et al. (2014) have argued that the entrainment of solids during the event can lead to observed discharge deviating strongly from initial discharge peaks, a behaviour which was also found in this thesis, mainly in simulations approximating the flow dynamics of granular debris flows. Besides erosion, the typical flow behaviour of debris flow-like movements is known to alternate between regions where erosion dominates and areas where deposition is occurring (Carrivick et al., 2010). Modelling of such flow dynamics is not possible with the used model setup in RAMMS. Nevertheless, simulations of mass movements where friction was reduced from the debris cone have shown how deposition can be approximated with a one-phase model since scenarios with lowered friction reached further downstream than events with constant friction, which possibly could be an alternative way how to model the behaviour of deposition in a specific channel section. Deposits of previous events in the Aksay catchment confirm that vast amounts of solids could no longer be transported beyond the debris cone, a process which, at least to some degree, could be simulated successfully.

Although the RAMMS debris flow module was not specifically designed for simulations of different flow types, the parameters available allowed for modelling certain scenarios in a very simplified manner. For more accurate simulations of flow transformations, I suggest making use of multi-phase models as they consider interactions between solid and liquid particles and account for varying solid-liquid ratios within the same mass flow (Bartelt et al., 2017; Pierson, 1986). The analyses carried out for this thesis confirm that adjusting friction to simulate transformations from debris flows to rather hyperconcentrated flows is possible since floods and hyperconcentrated flows are characterised by a higher liquid ratio than debris flows and can be sustained at lower slope angles (Coussot and Meunier, 1996; Huggel et al., 2002a). The stopping behaviour discussed in Meyrat et al. (2021) can therefore be approximated to some degree, although such multi-phase models would additionally provide benefits compared to simplified single-phase models. Hazard assessments in complex environments where flow type transformations are very likely therefore should make use of available multi-phase models since modelling of complex flow behaviour is improved. Nevertheless, first indications and insights can be obtained from single-phase models under some assumptions.

6.4 Further Limitations

It is pointed out in many studies that GLOF modelling is limited since there is no model available that takes into account all relevant processes and considers the transitional character between pure floods and debris flows (Mergili et al., 2011). Although GLOFs per definition are released with a high liquid fraction, the entrainment of solids during the release and along the

trajectory makes models that can simulate multi-phase dynamics more appropriate (Worni et al., 2014; Mergili et al., 2018b). Nevertheless, the lack of knowledge and information on the study site often complicates the application of physically based two-phase models and emphasises the uncertainties in model results. It is also pointed out by Mitchell et al. (2022) that multi-phase models would theoretically produce more accurate results, but data requirements impede their application and make single-phase models more common in engineering practices. Consequently, the model used for the analyses presented in this study simulates GLOFs in a simplified manner, whereby it is assumed that the relative velocity of solid and liquid particles is identical, and the entire mass behaves as a bulk flow. Additionally, owing to the Voellmy-Salm model, the density of the mass stays constant during the flood, which is hardly true in reality as the flow's front and tail usually have very different solid-liquid ratios. Hence, compressibility and phase interactions are neglected (Christen et al., 2010).

Further, all simulations performed for the scope of this thesis do neglect the impacts on flow dynamics caused by the dam that was constructed at the debris cone (Zaginaev et al., 2019). Although the results obtained for the flow channel upstream of the debris cone are not affected by the dam, the flow trajectory and resulting flow heights and velocities are expected to change at the debris cone and further downstream.

When it comes to the boundary conditions, all simulations assumed that the entire lake volume would drain. Furthermore, the equations used to derive the time at which peak discharge is reached might not be representative of every outburst mechanism, an aspect that needs to be considered when interpreting the results, especially when it comes to time-dependent outcomes.

As for erosive processes, the material swept away from the channel bed is not subtracted from the DEM during the simulation, meaning that channels caused by the passing flow front do not affect the rest of the flowing mass. Furthermore, the model does not account for lateral erosion, which can be an additional source of large amounts of sediment entrained during an event (Liu et al., 2020b).

In general, the sensitivity analyses performed for this study aimed at analysing impacts caused by the change in a single variable. Although the resulting simulations show how flow dynamics are affected by one variable, parameter interactions cannot be noticed, which might have significant effects on the outcomes. For instance, it has been demonstrated that increased erosion rates can lead to higher volumes of sediment being entrained in the flow. However, as long as the critical shear stress is not exceeded, an increase in erosion rate will not result in rising sediment volumes.

7 Conclusion & Future Work

The goal of this thesis was to evaluate different sources of uncertainty related to GLOF modelling and how flow dynamics change in response to natural variability in boundary conditions and erosive processes. Coming back to my first research question, the behaviour resulting from different outburst mechanisms was approached with various simulations. While the release velocity was found to have a minor impact on downstream regions since flow dynamics are rather governed by topography and other channel characteristics, drainage channel capacity and outflow magnitudes during the outburst strongly affect the resulting flow behaviour and maximum flow heights and velocities. While the variations in flow dynamics in response to changed boundary conditions were addressed in previous studies, this thesis highlights that the variability increases with rising peak discharge and lake volume, which concomitantly leads to higher uncertainties for disaster management in downstream areas. What is more, channel sections characterised by high flow were found to show higher variability in flow dynamics which needs to be considered for the installation of protection measures and other activities in downstream regions.

Regarding the second research question, it has been shown that the Aksay catchment is characterised by a substantial amount of variability as travel times can vary between 1330 and 2500 s when only boundary conditions are considered, and erosion is neglected. The incorporation of solid material further exacerbates uncertainties and variability in outcomes as flow heights, velocities, and discharge can rapidly increase and affect travel times even if only thin sediment layers are found at the channel bed. It was found that erosion can reduce the time of arrival by up to 50%. The findings demonstrate that there is substantial variability in model results when high peak discharges are coupled with erosion. Since similar literature on travel times is scarce, the results presented herein emphasise that, on the one hand, the time of arrival at critical points is heavily dependent on the outburst mechanism and magnitude, and, on the other hand, the availability of erodible sediment can further shorten travel times. At the same time, the lack of literature and the findings discussed in this thesis highlight the need for further research on travel times since they can provide essential insights, especially for evacuation management.

When it comes to the third research question, the analyses presented in this thesis revealed that the amount of erosion during an event is limited by the interaction of multiple variables in RAMMS. It is demonstrated that the depth of erodible material can strongly affect flow characteristics at first, whereas at some point, any increase in the depth of the sediment layer will not affect the flow behaviour anymore mainly owing to the interplay between the critical shear stress and the potential erosion depth. While the performed sensitivity analyses show that large variability results from changed erosion parameters and the uncertainty referred to in research question four is enhanced substantially once erosion is considered, hazard assessments should consider a worst-case scenario by allowing the entrainment of large volumes of

sediments so that possible flow extents and runout distances can be estimated, also because field data on erosion parameters usually is not available.

As for the fifth research question, modelling of different mass movements and flow type transformations has shown that highly accurate and realistic simulations are limited by the underlying equations and assumptions given in the single-phase version of RAMMS. Although it was shown that one can model the erosive strength of the flow front and that the stopping behaviour of solid phases can be approximated by applying reduced friction in flatter areas, numerous assumptions had to be taken which prevent realistic simulations of more complex events. Nevertheless, first approximations can be modelled using the single-phase version of RAMMS which can provide additional knowledge without heavy data requirements.

Based on the analyses and findings discussed in this thesis, several aspects were identified where future studies could significantly contribute to closing knowledge gaps and to understanding the dynamics of GLOFs and related mass movements:

- Since drainage characteristics and outburst processes depend to a large extent on the glacial lake type and trigger mechanisms, the temporal evolution of drainage is highly variable, which is why, in addition to different outflow magnitudes, the temporal dimension of release hydrographs such as the timing of peak discharge must be understood better. For the implementation of early warning systems and other adaptation measures, knowledge of travel times is essential. Although this thesis has shown that high flow magnitudes and sediment entrainment can significantly reduce travel times, further research is required to optimally estimate the time available for evacuation in different settings.
- Regarding hazard management in the Aksay catchment and its downstream regions, simulations need to take into account the dam that was constructed in 2016 so that potential runout extents and flow parameters are adjusted correctly.
- As for erosion dynamics, the interaction between shear strength and parameters such as critical shear stress and the potential erosion depth requires further analyses as this determines to a great extent how much sediments eventually travel downstream.
- In general, the understanding of parameter interactions needs to be improved. Like other studies, this thesis focused mainly on the impact single variables can have on simulation results. However, since flow dynamics rarely respond to one individual parameter only, the interaction between several input parameters needs to be studied in detail.
- Although frictional resistance and the density of the flowing mass can be manually adjusted in the single-phase version of RAMMS, flow type transformations can only be simulated based on a substantial number of assumptions. While specific aspects of the flow behaviour of simple GLOF and debris flow events can be approximated, multi-phase models can more accurately simulate the spatial evolution of density and the dilatancy of mass flows consisting of solid and liquid phases.

8 References

- Anaconda, P. I., Mackintosh, A., and Norton, K.: Reconstruction of a glacial lake outburst flood (GLOF) in the Engaño valley, Chilean Patagonia: Lessons for GLOF risk management, *Sci. Total Environ.*, 527–528, 1–11, <https://doi.org/10.1016/j.scitotenv.2015.04.096>, 2015.
- Anaconda, P. I., Norton, K., Mackintosh, A., Escobar, F., Allen, S., Mazzorana, B., and Schaefer, M.: Dynamics of an outburst flood originating from a small and high-altitude glacier in the Arid Andes of Chile, *Nat. Hazards*, 94, 93–119, <https://doi.org/10.1007/s11069-018-3376-y>, 2018.
- ASF DAAC, ALOS PALSAR_Radiometric_Terrain_Corrected_High_res; Includes Material © JAXA/METI 2007. Accessed through ASF DAAC 31.05.2022. DOI: <https://doi.org/10.5067/Z97HFCNKR6VA>
- Baggio, T., Mergili, M., and D’Agostino, V.: Advances in the simulation of debris flow erosion: The case study of the Rio Gere (Italy) event of the 4th August 2017, *Geomorphology*, 381, 107664, <https://doi.org/10.1016/j.geomorph.2021.107664>, 2021.
- Bao, Y., Chen, J., Sun, X., Han, X., Li, Y., Zhang, Y., Gu, F., and Wang, J.: Debris flow prediction and prevention in reservoir area based on finite volume type shallow-water model: a case study of pumped-storage hydroelectric power station site in Yi County, Hebei, China, *Environ. Earth Sci.*, 78, 1–16, <https://doi.org/10.1007/s12665-019-8586-4>, 2019.
- Barandun, M., Pohl, E., Naegeli, K., McNabb, R., Huss, M., Berthier, E., Saks, T., and Hoelzle, M.: Hot Spots of Glacier Mass Balance Variability in Central Asia, *Geophysical Res. Lett.*, <https://doi.org/10.1029/2020GL092084>, 2021.
- Bartelt, P., Bieler, C., Bühler, Y., Christen, M., Deubelbeiss, Y., Graf, C., McArdeLL, B., Salz, M., and Schneider, M.: RAMMS: DEBRISFLOW User Manual v1.7.0, 2017.
- Berger, C., McArdeLL, B., and Schlunegger, F.: Direct measurement of channel erosion by debris flows, Illgraben, Switzerland, *J. Geophys. Res. Earth Surf.*, 116, 1–18, <https://doi.org/10.1029/2010JF001722>, 2011.
- Beven, K., Lamb, R., Leedal, D., and Hunter, N.: Communicating uncertainty in flood inundation mapping: A case study, *Int. J. River Basin Manag.*, 13, 285–295, <https://doi.org/10.1080/15715124.2014.917318>, 2015.
- Bolch, T., Peters, J., Yegorov, A., Pradhan, B., Buchroithner, M., and Blagoveshchensky, V.: Identification of Potentially Dangerous Glacial Lakes in the Northern Tian Shan, in: *Terrigenous Mass Movements*, SPRINGER, Berlin, 369–394, 2012.
- Breien, H., De Blasio, F. V., Elverhøi, A., and Høeg, K.: Erosion and morphology of a debris flow caused by a glacial lake outburst flood, Western Norway, *Landslides*, 5, 271–280, <https://doi.org/10.1007/s10346-008-0118-3>, 2008.
- Carrivick, J. L., Manville, V., Graettinger, A., and Cronin, S. J.: Coupled fluid dynamics-sediment transport modelling of a Crater Lake break-out lahar: Mt. Ruapehu, New Zealand, *J. Hydrol.*, 388, 399–413, <https://doi.org/10.1016/j.jhydrol.2010.05.023>, 2010.
- Cenderelli, D. A. and Wohl, E. E.: Flow hydraulics and geomorphic effects of glacial-lake outburst floods in the Mount Everest region, Nepal, *Earth Surf. Process. Landforms*, 28, 385–407, <https://doi.org/10.1002/esp.448>, 2003.
- Cesca, M. and D’Agostino, V.: Comparison between FLO-2D and RAMMS in debris-flow modelling: A case study in the Dolomites, *WIT Trans. Eng. Sci.*, 60, 197–206,

<https://doi.org/10.2495/DEB080201>, 2008.

Christen, M., Kowalski, J., and Bartelt, P.: RAMMS : Numerical simulation of dense snow avalanches in three-dimensional terrain, *Cold Reg. Sci. Technol.*, 63, 1–14, <https://doi.org/10.1016/j.coldregions.2010.04.005>, 2010.

Cossart, E., Braucher, R., Fort, M., Bourlès, D. L., and Carcaillet, J.: Slope instability in relation to glacial debuitressing in alpine areas (Upper Durance catchment, southeastern France): Evidence from field data and 10 Be cosmic ray exposure ages, *Geomorphology*, 95, 3–26, <https://doi.org/10.1016/j.geomorph.2006.12.022>, 2008.

Coussot, P. and Meunier, M.: Recognition, classification and mechanical description of debris flows, *Earth-Science Rev.*, 40, 209–227, [https://doi.org/10.1016/0012-8252\(95\)00065-8](https://doi.org/10.1016/0012-8252(95)00065-8), 1996.

Cui, P., Dang, C., Cheng, Z., and Scott, K.: Debris flows resulting from glacial-lake outburst floods in Tibet, China, *Phys. Geogr.*, 31, 508–527, <https://doi.org/10.2747/0272-3646.31.6.508>, 2010.

Cuomo, S., Pastor, M., Capobianco, V., and Cascini, L.: Modelling the space–time evolution of bed entrainment for flow-like landslides, *Eng. Geol.*, 212, 10–20, <https://doi.org/10.1016/j.enggeo.2016.07.011>, 2016.

Erokhin, S. A., Zaginaev, V. V., Meleshko, A. A., Ruiz-Villanueva, V., Petrakov, D. A., Chernomorets, S. S., Viskhadzhieva, K. S., Tutubalina, O. V., and Stoffel, M.: Debris flows triggered from non-stationary glacier lake outbursts : the case of the Teztor Lake complex, *Landslides*, 15, 83–98, <https://doi.org/10.1007/s10346-017-0862-3>, 2018.

ESA, Sentinel-2 B MSI. Accessed through Copernicus Open Access Hub 11.08.2021. Access via [https://scihub.copernicus.eu/dhus/odata/v1/Products\('f3d273c7-6b7f-48c8-b92b-4845cbe69239'\)/\\$value](https://scihub.copernicus.eu/dhus/odata/v1/Products('f3d273c7-6b7f-48c8-b92b-4845cbe69239')/$value)

Farinotti, D., Longuevergne, L., Moholdt, G., Duethmann, D., Mölg, T., Bolch, T., Vorogushyn, S., and Güntner, A.: Substantial glacier mass loss in the Tien Shan over the past 50 years, *Nat. Geosci.*, 8, 716–722, <https://doi.org/10.1038/ngeo2513>, 2015.

Frank, F., McArdell, B., Huggel, C., and Vieli, A.: The importance of entrainment and bulking on debris flow runout modeling : examples from the Swiss Alps, *Nat. Hazards Earth Syst. Sci.*, 15, 2569–2583, <https://doi.org/10.5194/nhess-15-2569-2015>, 2015.

Frank, F., McArdell, B., Oggier, N., Baer, P., Christen, M., and Vieli, A.: Debris-flow modeling at Meretschibach and Bondasca catchments , Switzerland: sensitivity testing of field-data-based entrainment model, *Nat. Hazards Earth Syst. Sci.*, 17, 801–815, <https://doi.org/https://doi.org/10.5194/nhess-17-801-2017>, 2017.

Frey, H., Huggel, C., Bühler, Y., Buis, D., Burga, M. D., Choquevilca, W., Fernandez, F., Hernández, J. G., Giráldez, C., Loarte, E., Masias, P., Portocarrero, C., Vicuña, L., and Walser, M.: A robust debris-flow and GLOF risk management strategy for a data-scarce catchment in Santa Teresa , *Landslides*, 13, 1493–1507, <https://doi.org/10.1007/s10346-015-0669-z>, 2016.

Frey, H., Huggel, C., Chisolm, R., Baer, P., McArdell, B., Cochachin, A., and Portocarrero, C.: Multi-Source Glacial Lake Outburst Flood Hazard Assessment and Mapping for Huaraz, Cordillera Blanca, Peru, *Front. Earth Sci.*, 6, 1–16, <https://doi.org/10.3389/feart.2018.00210>, 2018.

Gan, F., He, B., and Wang, T.: Water and soil loss from landslide deposits as a function of gravel content in the Wenchuan earthquake area, China, revealed by artificial rainfall

- simulations, *PLoS One*, 13, 1–19, <https://doi.org/10.1371/journal.pone.0196657>, 2018.
- Gibson, S., Floyd, I., Sánchez, A., and Heath, R.: Comparing single-phase, non-Newtonian approaches with experimental results: Validating flume-scale mud and debris flow in HEC-RAS, *Earth Surf. Process. Landforms*, 46, 540–553, <https://doi.org/10.1002/esp.5044>, 2021.
- GLOFCA: <https://www.glofca.org/>, last access: 15 January 2023.
- Haerberli, W., Schaub, Y., and Huggel, C.: Increasing risks related to landslides from degrading permafrost into new lakes in de-glaciating mountain ranges, *Geomorphology*, 293, 405–417, <https://doi.org/10.1016/j.geomorph.2016.02.009>, 2017.
- Harrison, S., Kargel, J. S., Huggel, C., Reynolds, J., Shugar, D. H., Betts, R. A., Emmer, A., Glasser, N., Haritashya, U. K., Klimeš, J., Reinhardt, L., Schaub, Y., Wiltshire, A., Regmi, D., and Vilímek, V.: Climate change and the global pattern of moraine-dammed glacial lake outburst floods, *Cryosph.*, 12, 1195–1209, 2018.
- Heller, V., Hager, W. H., and Minor, H. E.: Landslide generated impulse waves in reservoirs: Basics and computation, *Mitteilungen der Versuchsanstalt für Wasserbau, Hydrol. und Glaziologie an der Eidgenöss. Tech. Hochschule Zurich*, 1–172, 2009.
- Hooke, R. L.: Englacial and subglacial hydrology: a qualitative review, *Arct. Alp. Res.*, 21, 221–233, <https://doi.org/10.2307/1551561>, 1989.
- Huggel, C., Haerberli, W., Kääh, a, Hoelzle, M., Ayros, E., and Portocarrero, C.: Assessment of Glacier Hazards and Glacier Runoff for Different Climate Scenarios Based on Remote Sensing Data : a Case Study for a Hydropower Plant in the Peruvian Andes, *EARSeL eProceedings*, 23, 22–33, 2002a.
- Huggel, C., Kääh, A., Haerberli, W., Teyssere, P., and Paul, F.: Remote sensing based assessment of hazards from glacier lake outbursts: A case study in the Swiss Alps, *Can. Geotech. J.*, 39, 316–330, <https://doi.org/10.1139/t01-099>, 2002b.
- Huggel, C., Kääh, A., and Haerberli, W.: Regional-scale models of debris flows triggered by lake outbursts : the 25 June 2001 debris flow at Täsch (Switzerland) as a test study, in: *Debris-Flow Hazards Mitigation: Mechanics, Prediction, and Assessment*, edited by: Rickenmann, D. and Chen, C., Millpress, Rotterdam, 1151–1162, 2003.
- Huggel, C., Haerberli, W., Kääh, A., Bieri, D., and Richardson, S.: An assessment procedure for glacial hazards in the Swiss Alps, *Can. Geotech. J.*, 41, 1068–1083, <https://doi.org/10.1139/T04-053>, 2004.
- Huggel, C., Carey, M., Emmer, A., Frey, H., Walker-Crawford, N., and Wallimann-Helmer, I.: Anthropogenic climate change and glacier lake outburst flood risk : local and global drivers and responsibilities for the case of lake Palcacocha , Peru, *Nat. Hazards Earth Syst. Sci.*, 20, 2175–2193, <https://doi.org/https://doi.org/10.5194/nhess-20-2175-2020>, 2020.
- Isaev, E., Ermanova, M., Sidle, R. C., Zaginaev, V., Kulikov, M., and Chontoev, D.: Reconstruction of Hydrometeorological Data Using Dendrochronology and Machine Learning Approaches to Bias-Correct Climate Models in Northern Tien Shan, Kyrgyzstan, *Water (Switzerland)*, 14, <https://doi.org/10.3390/w14152297>, 2022.
- Iverson, R. M., Reid, M. E., Logan, M., LaHusen, R. G., Godt, J. W., and Griswold, J. P.: Positive feedback and momentum growth during debris-flow entrainment of wet bed sediment, *Nat. Geosci.*, 4, 116–121, <https://doi.org/10.1038/ngeo1040>, 2011.
- Janský, B., Šobr, M., and Engel, Z.: Outburst flood hazard: Case studies from the Tien-Shan

- Mountains, Kyrgyzstan, *Limnologica*, 40, 358–364, <https://doi.org/10.1016/j.limno.2009.11.013>, 2010.
- Kapitsa, V., Shahgedanova, M., Machguth, H., Severskiy, I., and Medeu, A.: Assessment of evolution and risks of glacier lake outbursts in the Djungarskiy Alatau, Central Asia, using Landsat imagery and glacier bed topography modelling, *Nat. Hazards Earth Syst. Sci.*, 17, 1837–1856, <https://doi.org/https://doi.org/10.5194/nhess-17-1837-2017>, 2017.
- Kattel, D. B., Mohanty, A., Daiyrov, M., Wang, W., Mishra, M., and Kulenbekov, Z.: Evaluation of Glacial Lakes and Catastrophic Floods on the Northern Slopes of the Kyrgyz Range, *Mt. Res. Dev.*, 40, R37–R47, 2020.
- Klimeš, J., Benešová, M., Vilímek, V., Bouška, P., and Cochachin Rapre, A.: The reconstruction of a glacial lake outburst flood using HEC-RAS and its significance for future hazard assessments: An example from Lake 513 in the Cordillera Blanca, Peru, *Nat. Hazards*, 71, 1617–1638, <https://doi.org/10.1007/s11069-013-0968-4>, 2014.
- Lala, J. M., Rounce, D. R., and McKinney, D. C.: Modeling the glacial lake outburst flood process chain in the Nepal Himalaya: reassessing Imja Tsho's hazard, *Hydrol. Earth Syst. Sci.*, 22, 3721–3737, <https://doi.org/https://doi.org/10.5194/hess-22-3721-2018>, 2018.
- Liu, M., Zhang, Y., Tian, S., Chen, N., Mahfuzr, R., and Javed, I.: Effects of loose deposits on debris flow processes in the Aizi Valley, southwest China, *J. Mt. Sci.*, 17, 156–172, <https://doi.org/10.1007/s11629-019-5388-9>, 2020a.
- Liu, M., Chen, N., Zhang, Y., and Deng, M.: Glacial Lake Inventory and Lake Outburst Flood / Debris Flow Hazard Assessment after the Gorkha Earthquake in the Bhote Koshi Basin, *Water*, 12, 1–20, <https://doi.org/10.3390/w12020464>, 2020b.
- Luna, B. Q., Remaître, A., van Asch, T. W. J., Malet, J. P., and van Westen, C. J.: Analysis of debris flow behavior with a one dimensional run-out model incorporating entrainment, *Eng. Geol.*, 128, 63–75, <https://doi.org/10.1016/j.enggeo.2011.04.007>, 2012.
- Marchi, L., Cazorzi, F., Arattano, M., Cucchiaro, S., Cavalli, M., and Crema, S.: Debris flows recorded in the Moscardo catchment (Italian Alps) between 1990 and 2019, *Nat. Hazards Earth Syst. Sci.*, 21, 87–97, <https://doi.org/10.5194/nhess-21-87-2021>, 2021.
- McArdell, B., Bartelt, P., and Kowalski, J.: Field observations of basal forces and fluid pore pressure in a debris flow, *Geophys. Res. Lett.*, 34, 2–5, <https://doi.org/10.1029/2006GL029183>, 2007.
- Melo, R., Zêzere, J. L., Oliveira, S. C., Garcia, R. A. C., Oliveira, S., Pereira, S., Piedade, A., Santos, P. P., and van Asch, T. W. J.: Defining evacuation travel times and safety areas in a debris flow hazard scenario, *Sci. Total Environ.*, 712, <https://doi.org/10.1016/j.scitotenv.2019.136452>, 2020.
- Mergili, M., Schneider, D., Worni, R., and Schneider, J. F.: Glacial lake outburst floods in the Pamir of Tajikistan: Challenges in prediction and modelling, in: 5th International Conference on Debris-Flow Hazards Mitigation: Mechanics, Prediction and Assessment, 973–982, <https://doi.org/10.4408/IJEGE.2011-03.B-106>, 2011.
- Mergili, M., Fischer, J. T., Krenn, J., and Pudasaini, S. P.: R.avaflow v1, an advanced open-source computational framework for the propagation and interaction of two-phase mass flows, *Geosci. Model Dev.*, 10, 553–569, <https://doi.org/10.5194/gmd-10-553-2017>, 2017.
- Mergili, M., Emmer, A., Ju, A., Cochachin, A., Fischer, J.-T., Huggel, C., and Pudasaini, S. P.:

- How well can we simulate complex hydro- geomorphic process chains? The 2012 multi-lake outburst flood in the Santa Cruz Valley (Cordillera Blanca, Perú), *Earth Surf. Process. Landforms*, 43, 1373–1389, <https://doi.org/10.1002/esp.4318>, 2018a.
- Mergili, M., Emmer, A., Juřicová, A., Cochachin, A., Fischer, J. T., Huggel, C., and Pudasaini, S. P.: How well can we simulate complex hydro-geomorphic process chains? The 2012 multi-lake outburst flood in the Santa Cruz Valley (Cordillera Blanca, Perú), *Earth Surf. Process. Landforms*, 43, 1373–1389, <https://doi.org/10.1002/esp.4318>, 2018b.
- Meyrat, G., McArdell, B., Ivanova, K., Müller, C., and Bartelt, P.: A dilatant, two-layer debris flow model validated by flow density measurements at the Swiss illgraben test site, *Landslides*, 19, 265–276, <https://doi.org/10.1007/s10346-021-01733-2>, 2021.
- Mitchell, A., Zubrycky, S., McDougall, S., Aaron, J., Hübl, J., Kaitna, R., and Graf, C.: Variable hydrograph inputs for a numerical debris-flow runout model, *Nat. Hazards Earth Syst. Sci.*, 22, 1627–1654, <https://doi.org/https://doi.org/10.5194/nhess-22-1627-2022>, 2022.
- Muccione, V. and Fiddes, J.: State of the knowledge on water resources and natural hazards under climate change in Central Asia and South Caucasus, Bern, 7–19 pp., 2019.
- Narama, C., Kicengge, Kubota, J., and Shatravin, V.I. Duishonakunov, M. Moholdt, G., Abdrakhmatov, K.: The lake-level changes in Central Asia during the last 1000 years based on historical map, 11–27, 2010.
- Narama, C., Daiyrov, M., Duishonakunov, M., Tadono, T., Sato, H., Käab, A., Ukita, J., and Abdrakhmatov, K.: Large drainages from short-lived glacial lakes in the Teskey Range, Tien Shan Mountains, Central Asia, *Nat. Hazards Earth Syst. Sci.*, 18, 983–995, <https://doi.org/https://doi.org/10.5194/nhess-18-983-2018>, 2018.
- Nienow, P. W., Sharp, M., and Willis, I. C.: Velocity-discharge relationships derived from dye tracer experiments in glacial meltwaters: Implications for subglacial flow conditions, *Hydrol. Process.*, 10, 1411–1426, [https://doi.org/10.1002/\(sici\)1099-1085\(199610\)10:10<1411::aid-hyp470>3.0.co;2-s](https://doi.org/10.1002/(sici)1099-1085(199610)10:10<1411::aid-hyp470>3.0.co;2-s), 1996.
- Paixão, M. A., Kobiyama, M., Fujita, M., and Nakatani, K.: Sensitivity Analysis of Debris Flow Simulations Using Kanako-2D, *Int. J. Eros. Control Eng.*, 14, 1–11, <https://doi.org/10.13101/ijece.14.1>, 2021.
- Petrakov, D. A., Chernomorets, S. S., Viskhadzhieva, K. S., Dokukin, M. D., Savernyuk, E. A., Petrov, M. A., Erokhin, S. A., Tutubalina, O. V., Glazyrin, G. E., Shpuntova, A. M., and Stoffel, M.: Putting the poorly documented 1998 GLOF disaster in Shakhimardan River valley (Alay Range, Kyrgyzstan/Uzbekistan) into perspective, *Sci. Total Environ.*, 724, 138287, <https://doi.org/10.1016/j.scitotenv.2020.138287>, 2020.
- Phillips, C. J. and Davies, T. R. H.: Determining rheological parameters of debris flow material, *Geomorphology*, 4, 101–110, [https://doi.org/10.1016/0169-555X\(91\)90022-3](https://doi.org/10.1016/0169-555X(91)90022-3), 1991.
- Pierson, T. C.: Flow behavior of channelized debris flow, Mount St. Helens, Washington, in: *Hillslope Processes, the Binghamton symp*, edited by: Abrahams, A. D., Routledge, London, 269–296, <https://doi.org/https://doi.org/10.4324/9781003028840>, 1986.
- Pierson, T. C. and Costa, J. E.: A rheologic classification of subaerial sediment-water flows, *GSA Rev. Eng. Geol.*, 7, 1–12, <https://doi.org/10.1130/REG7-p1>, 1987.
- Rakovec, O., Hill, M. C., Clark, M. P., Weerts, A. H., Teuling, A. J., and Uijlenhoet, R.: Distributed evaluation of local sensitivity analysis (DELSA), with application to hydrologic

- models, *Water Resour. Res.*, 50, 409–426, <https://doi.org/10.1002/2013WR014063>, 2014.
- Richardson, S. D. and Reynolds, J. M.: An overview of glacial hazards in the Himalayas, *Quat. Int.*, 65/66, 31–47, 2000.
- Rickenmann, D.: Empirical relationships for Debris Flows, *Nat. hazards*, 19, 47–77, 1999.
- Rosli, M. I., Che Ros, F., Razak, K. A., Ambran, S., Kamaruddin, S. A., Anuar, A. N., Marto, A., Tobita, T., and Ono, Y.: Modelling debris flow runout: A case study on the Mesilau Watershed, Kundasang, Sabah, *Water*, 13, <https://doi.org/10.3390/w13192667>, 2021.
- Salm, B.: Flow, flow transition and runout distances of flowing avalanches, *Ann. Glaciol.*, 18, 221–226, <https://doi.org/10.3189/s0260305500011551>, 1993.
- Salm, B., Burkard, A., and Gubler, H. U.: Berechnung von Fliesslawinen. Eine Anleitung für Praktiker mit Beispielen, Davos, 1990.
- Sassa, K. and Wang, G.: Mechanism of landslide-triggered debris flows: Liquefaction phenomena due to the undrained loading of torrent deposits, in: *Debris-flow Hazards and Related Phenomena*, edited by: Jakob, M. and Hungr, O., Springer, Berlin, New York, 81–104, https://doi.org/10.1007/3-540-27129-5_5, 2005.
- Sattar, A., Goswami, A., Kulkarni, A. V, and Emmer, A.: Lake Evolution , Hydrodynamic Outburst Flood Modeling and Sensitivity Analysis in the Central Himalaya: A Case Study, *Water*, 12, 1–19, 2020.
- Schraml, K., Thomschitz, B., Mcardell, B. W., Graf, C., and Kaitna, R.: Modeling debris-flow runout patterns on two alpine fans with different dynamic simulation models, *Nat. Hazards Earth Syst. Sci.*, 15, 1483–1492, <https://doi.org/10.5194/nhess-15-1483-2015>, 2015.
- Schürch, P., Densmore, A. L., Rosser, N. J., and Mcardell, B. W.: Dynamic controls on erosion and deposition on debris-flow fans, *Geology*, 39, 827–830, <https://doi.org/10.1130/G32103.1>, 2011.
- Shugar, D. H., Burr, A., Haritashya, U. K., Kargel, J. S., Watson, C. S., Kennedy, M. C., Bevington, A. R., Betts, R. A., Harrison, S., and Stratman, K.: Rapid worldwide growth of glacial lakes since 1990, *Nat. Clim. Chang.*, 10, <https://doi.org/10.1038/s41558-020-0855-4>, 2020.
- Solomina, O. N., Savoskul, O. S., and Cherkinsky, A. E.: Glacier variations, mudflow activity and landscape development in the Aksay Valley (Tian Shan) during the late Holocene, *Holocene*, 4, 25–31, <https://doi.org/10.1177/095968369400400104>, 1994.
- Somos-Valenzuela, M. A., Chisolm, R. E., Rivas, D. S., Portocarrero, C., and McKinney, D. C.: Modeling a glacial lake outburst flood process chain: the case of Lake Palcacocha and Huaraz , Peru, *Hydrol. Earth Syst. Sci.*, 20, 2519–2543, <https://doi.org/10.5194/hess-20-2519-2016>, 2016.
- Stock, J. D. and Dietrich, W. E.: Erosion of Steepland Valleys by Debris Flows, *Geol. Soc. Am. Bull.*, 118, 1125–1148, <https://doi.org/10.1130/B25902.1>, 2006.
- Stricker, B.: Murgänge im Torrente Riascio (TI): Ereignisanalyse, Auslösefaktoren und Simulation von Ereignissen mit RAMMS, University of Zurich, 1–110 pp., 2010.
- Stuart, G., Murray, T., Gamble, N., Hayes, K., and Hodson, A.: Characterization of englacial channels by ground-penetrating radar: An example from austre Brøggerbreen, Svalbard, *J. Geophys. Res.*, 108, 1–13, <https://doi.org/10.1029/2003jb002435>, 2003.

- Thurman, M.: Natural Disaster Risks in Central Asia: A Synthesis Table of Contents, Bratislava, 43 pp., 2011.
- Vicari, H., Nordal, S., and Thakur, V.: The Significance of Entrainment on Debris Flow Modelling: The Case of Hunnedalen, Norway, in: Challenges and Innovations in Geomechanics, edited by: Barla, M., Di Donna, A., and Sterpi, D., Springer, 507–514, https://doi.org/10.1007/978-3-030-64518-2_60, 2021.
- Vilímek, V., Emmer, A., Huggel, C., Schaub, Y., and Würmli, S.: Database of glacial lake outburst floods (GLOFs)-IPL project No. 179, Landslides, 11, 161–165, <https://doi.org/10.1007/s10346-013-0448-7>, 2014.
- Walder, J. S. and Costa, J. E.: Outburst floods from glacier-dammed lakes: The effect of mode of lake drainage on flood magnitude, *Earth Surf. Process. Landforms*, 21, 701–723, [https://doi.org/10.1002/\(SICI\)1096-9837\(199608\)21:8<701::AID-ESP615>3.0.CO;2-2](https://doi.org/10.1002/(SICI)1096-9837(199608)21:8<701::AID-ESP615>3.0.CO;2-2), 1996.
- Wang, X., Ding, Y., Liu, S., and Jiang, L.: Changes of glacial lakes and implications in Tian Shan, central Asia, based on remote sensing data from 1990 to 2010, <https://doi.org/10.1088/1748-9326/8/4/044052>, 2013.
- Westoby, M. J., Glasser, N. F., Brasington, J., Hambrey, M. J., Quincey, D. J., and Reynolds, J. M.: Modelling outburst floods from moraine-dammed glacial lakes, *Earth-Science Rev.*, 134, 137–159, <https://doi.org/10.1016/j.earscirev.2014.03.009>, 2014.
- Westoby, M. J., Brasington, J., Glasser, N. F., Hambrey, M. J., Reynolds, J. M., Hassan, M. A. A. M., and Lowe, A.: Numerical modelling of glacial lake outburst floods using physically based dam-breach models, *Earth Surf. Dyn.*, 3, 171–199, <https://doi.org/10.5194/esurf-3-171-2015>, 2015.
- Worni, R., Huggel, C., Clague, J. J., Schaub, Y., and Stoffel, M.: Coupling glacial lake impact, dam breach, and flood processes: A modeling perspective, *Geomorphology*, 224, 161–176, <https://doi.org/10.1016/j.geomorph.2014.06.031>, 2014.
- Zaginaev, V., Ballesteros-cánovas, J. A., Erokhin, S., Matov, E., Petrakov, D., and Stoffel, M.: Reconstruction of glacial lake outburst floods in northern Tien Shan: Implications for hazard assessment, *Geomorphology*, 269, 75–84, <https://doi.org/10.1016/j.geomorph.2016.06.028>, 2016.
- Zaginaev, V., Falatkova, K., Jansky, B., Sobr, M., and Erokhin, S.: Development of a Potentially Hazardous Pro-Glacial Lake in Aksay Valley, Kyrgyz Range, Northern Tien Shan, *Hydrology*, 6, <https://doi.org/10.3390/hydrology6010003>, 2019.
- Zemp, M., Frey, H., Gärtner-Roer, I., Nussbaumer, S. U., Hoelzle, M., Paul, F., Haeberli, W., Denzinger, F., Ahlstrøm, A. P., Anderson, B., Bajracharya, S., Baroni, C., Braun, L. N., Càceres, B. E., Casassa, G., Cobos, G., Dàvila, L. R., Delgado Granados, H., Demuth, M. N., Espizua, L., Fischer, A., Fujita, K., Gadek, B., Ghazanfar, A., Hagen, J. O., Holmlund, P., Karimi, N., Li, Z., Pelto, M., Pitte, P., Popovnin, V. V., Portocarrero, C. A., Prinz, R., Sangewar, C. V., Severskiy, I., Sigurdsson, O., Soruco, A., Usabaliyev, R., and Vincent, C.: Historically unprecedented global glacier decline in the early 21st century, *J. Glaciol.*, 61, 745–762, <https://doi.org/10.3189/2015JoG15J017>, 2015.
- Zheng, G., Allen, S. K., Bao, A., Ballesteros-Cánovas, J. A., Huss, M., Zhang, G., Li, J., Yuan, Y., Jiang, L., Yu, T., Chen, W., and Stoffel, M.: Increasing risk of glacial lake outburst floods from future Third Pole deglaciation, *Nat. Clim. Chang.*, 11, 411–417, <https://doi.org/10.1038/s41558-021-01028-3>, 2021.

9 Appendix

Table 4: Simulation parameters used for analyses on peak discharge. Parameters changed in comparison to the basis simulation (Table 2) are marked in italics.

Stop Parameter [%]	5	5	5	5	5	5	5	5	5	5	5	5	5
End Time [s]	<i>20000</i>	<i>15000</i>	7500	7500	7500	7500	7500	7500	7500	7500	7500	7500	7500
Dump Step [s]	15	15	15	15	15	15	15	15	15	15	15	15	15
Density [kg m⁻³]	1100	1100	1100	1100	1100	1100	1100	1100	1100	1100	1100	1100	1100
Lambda	1	1	1	1	1	1	1	1	1	1	1	1	1
μ	0.04	0.04	0.04	0.04	0.04	0.04	0.04	0.04	0.04	0.04	0.04	0.04	0.04
ξ [m s⁻²]	500	500	500	500	500	500	500	500	500	500	500	500	500
Inflow Direction [°]	155	155	155	155	155	155	155	155	155	155	155	155	155
Time to Peak Discharge [s]	<i>2800</i>	<i>1400</i>	<i>933</i>	700	560	466	400	350	311	280	233	200	140
Peak Discharge [m³ s⁻¹]	<i>5</i>	<i>10</i>	<i>15</i>	20	25	30	35	40	45	50	60	70	100
Release Velocity [m s⁻¹]	4	4	4	4	4	4	4	4	4	4	4	4	4
Inflow Duration [s]	<i>14000</i>	<i>7000</i>	<i>4666</i>	3500	2800	2333	2000	1750	1555	1400	1166	1000	700
Release Volume [m³]	35000	35000	35000	35000	35000	35000	35000	35000	35000	35000	35000	35000	35000

Appendix

Table 5: Simulation parameters used for analyses on lake volumes. Parameters changed in comparison to the basis simulation (Table 2) are marked in italics.

Parameter	Medium Lake Volume			Large Lake Volume		
Stop Parameter [%]	5	5	5	5	5	5
End Time [s]	7500	7500	7500	<i>20000</i>	<i>15000</i>	<i>10000</i>
Dump Step [s]	15	15	15	15	15	15
Density [kg m⁻³]	1100	1100	1100	1100	1100	1100
Lambda	1	1	1	1	1	1
μ	0.04	0.04	0.04	0.04	0.04	0.04
ξ [m s⁻²]	500	500	500	500	500	500
Inflow Direction [°]	155	155	155	155	155	155
Time to Peak Discharge [s]	<i>400</i>	<i>285</i>	<i>200</i>	<i>2400</i>	<i>1714</i>	<i>1200</i>
Peak Discharge [m³ s⁻¹]	<i>50</i>	<i>70</i>	<i>100</i>	<i>50</i>	<i>70</i>	<i>100</i>
Release Velocity [m s⁻¹]	4	4	4	4	4	4
Inflow Duration [s]	<i>2000</i>	<i>1429</i>	<i>1000</i>	<i>12000</i>	<i>8571</i>	<i>6000</i>
Release Volume [m³]	<i>50000</i>	<i>50000</i>	<i>50000</i>	<i>300000</i>	<i>300000</i>	<i>300000</i>

Appendix

Table 6: Simulation parameters used for analyses on initial flow velocities. Parameters changed in comparison to the basis simulation (Table 2) are marked in italics.

Stop Parameter [%]	5	5	5	5	5	5	5
End Time [s]	7500	7500	7500	7500	7500	7500	7500
Dump Step [s]	15	15	15	15	15	15	15
Density [kg m⁻³]	1100	1100	1100	1100	1100	1100	1100
Lambda	1	1	1	1	1	1	1
μ	0.04	0.04	0.04	0.04	0.04	0.04	0.04
ξ [m s⁻²]	500	500	500	500	500	500	500
Inflow Direction [°]	155	155	155	155	155	155	155
Time to Peak Discharge [s]	700	700	700	700	700	700	700
Peak Discharge [m³ s⁻¹]	20	20	20	20	20	20	20
Release Velocity [m s⁻¹]	2	5	7	<i>11</i>	<i>14</i>	<i>17</i>	20
Inflow Duration [s]	3500	3500	3500	3500	3500	3500	3500
Release Volume [m³]	35000	35000	35000	35000	35000	35000	35000

Appendix

Table 7: Simulation parameters used for analyses on erosion depths. Parameters changed in comparison to the basis simulation (Table 2) are marked in italics.

Stop Parameter [%]	5	5	5	5	5	5	5	5
End Time [s]	7500	7500	7500	7500	7500	7500	7500	7500
Dump Step [s]	15	15	15	15	15	15	15	15
Density [kg m⁻³]	1100	1100	1100	1100	1100	1100	1100	1100
Lambda	1	1	1	1	1	1	1	1
μ	<i>0.08</i>							
ξ [m s⁻²]	500	500	500	500	500	500	500	500
Inflow Direction [°]	155	155	155	155	155	155	155	155
Time to Peak Discharge [s]	700	700	700	700	700	700	700	700
Peak Discharge [m³ s⁻¹]	20	20	20	20	20	20	20	20
Release Velocity [m s⁻¹]	4	4	4	4	4	4	4	4
Inflow Duration [s]	3500	3500	3500	3500	3500	3500	3500	3500
Release Volume [m³]	35000	35000	35000	35000	35000	35000	35000	35000
Erosion applied in Zone	<i>1,2,3</i>							
Erosion Density [kg m⁻³]	<i>1800</i>							
Erosion Rate [m s⁻¹]	<i>0.05</i>							
Potential Erosion Depth [m kPa⁻¹]	<i>0.2</i>							
Critical Shear Stress [kPa]	<i>0.5</i>							
Maximum Erosion Depth [m]	<i>0.25</i>	<i>0.5</i>	<i>0.75</i>	<i>1</i>	<i>1.5</i>	<i>2</i>	<i>2.5</i>	<i>3</i>

Appendix

Table 8: Simulation parameters used for analyses on critical shear stress. Parameters changed in comparison to the basis simulation (Table 2) are marked in italics.

Stop Parameter [%]	5	5	5	5	5	5	5	5
End Time [s]	7500	7500	7500	7500	7500	7500	7500	7500
Dump Step [s]	15	15	15	15	15	15	15	15
Density [kg m⁻³]	1100	1100	1100	1100	1100	1100	1100	1100
Lambda	1	1	1	1	1	1	1	1
μ	<i>0.08</i>							
ξ [m s⁻²]	500	500	500	500	500	500	500	500
Inflow Direction [°]	155	155	155	155	155	155	155	155
Time to Peak Discharge [s]	700	700	700	700	700	700	700	700
Peak Discharge [m³ s⁻¹]	20	20	20	20	20	20	20	20
Release Velocity [m s⁻¹]	4	4	4	4	4	4	4	4
Inflow Duration [s]	3500	3500	3500	3500	3500	3500	3500	3500
Release Volume [m³]	35000	35000	35000	35000	35000	35000	35000	35000
Erosion applied in Zone	<i>1,2,3</i>							
Erosion Density [kg m⁻³]	<i>1800</i>							
Erosion Rate [m s⁻¹]	<i>0.05</i>							
Potential Erosion Depth [m kPa⁻¹]	<i>0.2</i>							
Critical Shear Stress [kPa]	<i>0.25</i>							
Maximum Erosion Depth [m]	<i>0.25</i>	<i>0.5</i>	<i>0.75</i>	<i>1</i>	<i>1.5</i>	<i>2</i>	<i>2.5</i>	<i>3</i>

Appendix

Table 9: Simulation parameters used for analyses on critical shear stress for evaluating the time of arrival. Parameters changed in comparison to the basis simulation (Table 2) are marked in italics.

Stop Parameter [%]	5	5	5	5
End Time [s]	7500	7500	7500	7500
Dump Step [s]	15	15	15	15
Density [kg m⁻³]	1100	1100	1100	1100
Lambda	1	1	1	1
μ	<i>0.08</i>	<i>0.08</i>	<i>0.08</i>	<i>0.08</i>
ξ [m s⁻²]	500	500	500	500
Inflow Direction [°]	155	155	155	155
Time to Peak Discharge [s]	700	700	700	700
Peak Discharge [m³ s⁻¹]	20	20	20	20
Release Velocity [m s⁻¹]	4	4	4	4
Inflow Duration [s]	3500	3500	3500	3500
Release Volume [m³]	35000	35000	35000	35000
Erosion applied in Zone	2	2	2	2
Erosion Density [kg m⁻³]	<i>1800</i>	<i>1800</i>	<i>1800</i>	<i>1800</i>
Erosion Rate [m s⁻¹]	<i>0.05</i>	<i>0.05</i>	<i>0.05</i>	<i>0.05</i>
Potential Erosion Depth [m kPa⁻¹]	<i>0.2</i>	<i>0.2</i>	<i>0.2</i>	<i>0.2</i>
Critical Shear Stress [kPa]	<i>0.25</i>	<i>0.375</i>	<i>0.5</i>	<i>0.75</i>
Maximum Erosion Depth [m]	<i>1</i>	<i>1</i>	<i>1</i>	<i>1</i>

Appendix

Table 10: Simulation parameters used for analyses on erosion rates. Parameters changed in comparison to the basis simulation (Table 2) are marked in italics.

Stop Parameter [%]	5	5	5
End Time [s]	7500	7500	7500
Dump Step [s]	15	15	15
Density [kg m⁻³]	1100	1100	1100
Lambda	1	1	1
μ	<i>0.08</i>	<i>0.08</i>	<i>0.08</i>
ξ [m s⁻²]	500	500	500
Inflow Direction [°]	155	155	155
Time to Peak Discharge [s]	700	700	700
Peak Discharge [m³ s⁻¹]	20	20	20
Release Velocity [m s⁻¹]	4	4	4
Inflow Duration [s]	3500	3500	3500
Release Volume [m³]	35000	35000	35000
Erosion applied in Zone	<i>1,2,3</i>	<i>1,2,3</i>	<i>1,2,3</i>
Erosion Density [kg m⁻³]	<i>1800</i>	<i>1800</i>	<i>1800</i>
Erosion Rate [m s⁻¹]	<i>0.0125</i>	<i>0.025</i>	<i>0.05</i>
Potential Erosion Depth [m kPa⁻¹]	<i>0.2</i>	<i>0.2</i>	<i>0.2</i>
Critical Shear Stress [kPa]	<i>0.25</i>	<i>0.25</i>	<i>0.25</i>
Maximum Erosion Depth [m]	<i>0.75,1</i>	<i>0.75,1</i>	<i>0.75,1</i>

Appendix

Table 11: Simulation parameters used for analyses on erosion for evaluating the time of arrival. Parameters changed in comparison (Table 2) to the basis simulation are marked in italics.

Stop Parameter	5	5	5	5	5	5	5	5	5	5	5
End Time [s]	<i>20000</i>	7500	7500	7500	7500	7500	7500	7500	7500	7500	7500
Dump Step [s]	15	15	15	15	15	15	15	15	15	15	15
Density [kg m⁻³]	1100	1100	1100	1100	1100	1100	1100	1100	1100	1100	1100
Lambda	1	1	1	1	1	1	1	1	1	1	1
μ	0.04	0.04	0.04	0.04	0.04	0.04	0.04	0.04	0.04	0.04	0.04
ξ [m s⁻²]	500	500	500	500	500	500	500	500	500	500	500
Inflow Direction	155	155	155	155	155	155	155	155	155	155	155
Time to Peak Discharge	<i>2800</i>	700	560	466	400	350	<i>311</i>	280	233	200	<i>140</i>
Peak Discharge [m³ s⁻¹]	5	20	25	30	35	40	45	50	60	70	100
Release Velocity [m s⁻¹]	4	4	4	4	4	4	4	4	4	4	4
Inflow Duration [s]	<i>14000</i>	3500	2800	2333	2000	1750	<i>1555</i>	1400	1166	1000	700
Release Volume [m³]	35000	35000	35000	35000	35000	35000	35000	35000	35000	35000	35000
Erosion applied in Zone	<i>1+2+3</i>										
Erosion Density [kg m⁻³]	<i>1800</i>										
Erosion Rate [m s⁻¹]	<i>0.05</i>										
Potential Erosion Depth [m kPa⁻¹]	<i>0.2</i>										
Critical Shear Stress [kPa]	<i>0.5</i>										
Maximum Erosion Depth [m]	<i>0.75</i>										

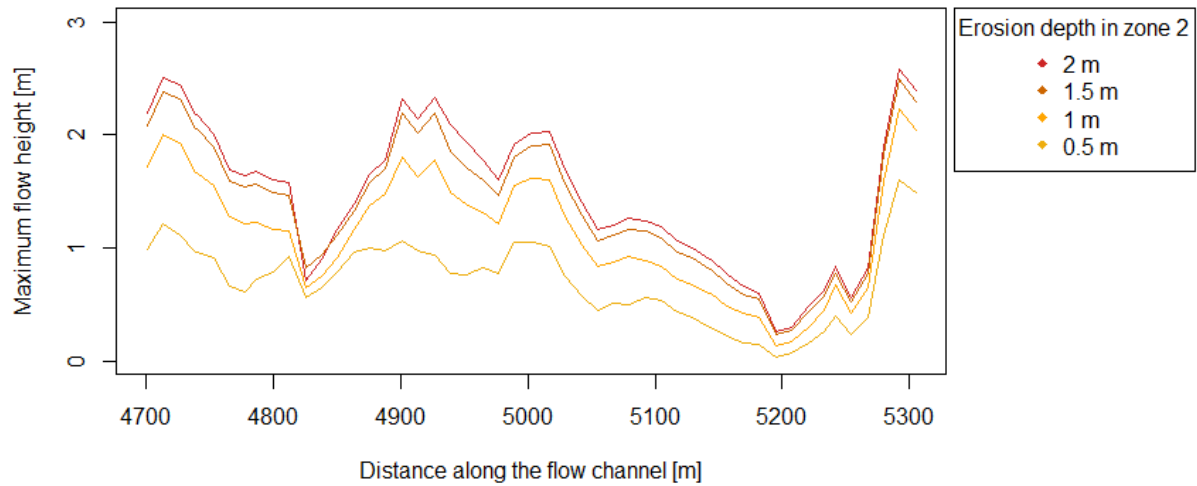


Figure 30: Maximum flow heights of four simulations are shown in a channel segment shortly before the debris cone. The flow heights are shown relative to a non-erosion scenario. Initial peak discharge was set to $20 \text{ m}^3 \text{ s}^{-1}$ and entrainment was considered in erosion zone 2. Erosion depths were set to 0.5, 1, 1.5, and 2 m.

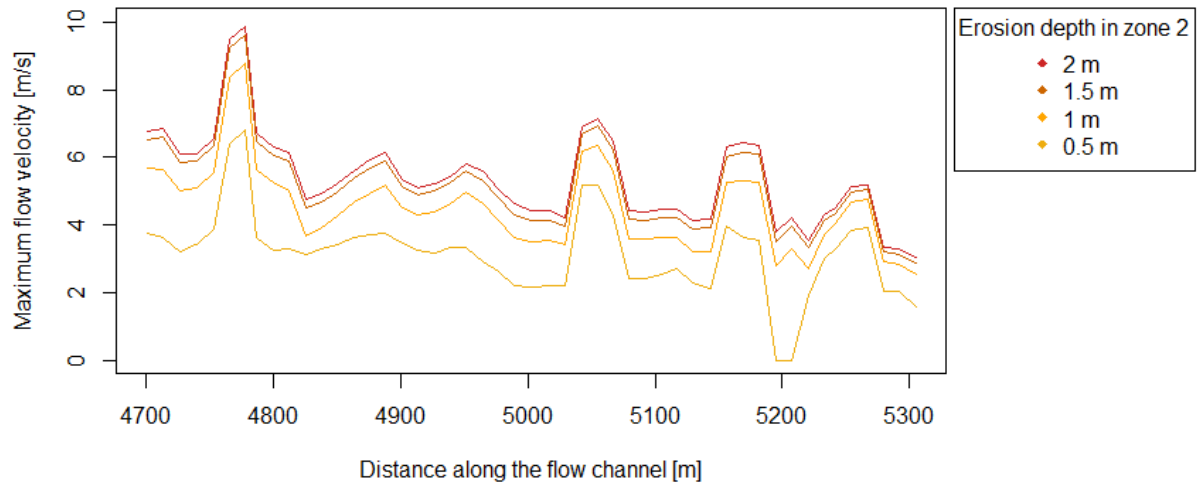


Figure 31: Maximum flow velocities of four simulations are shown in a channel segment shortly before the debris cone. The flow velocities are shown relative to a non-erosion scenario. Initial peak discharge was set to $20 \text{ m}^3 \text{ s}^{-1}$ and entrainment was considered in erosion zone 2. Erosion depths were set to 0.5, 1, 1.5, and 2 m.

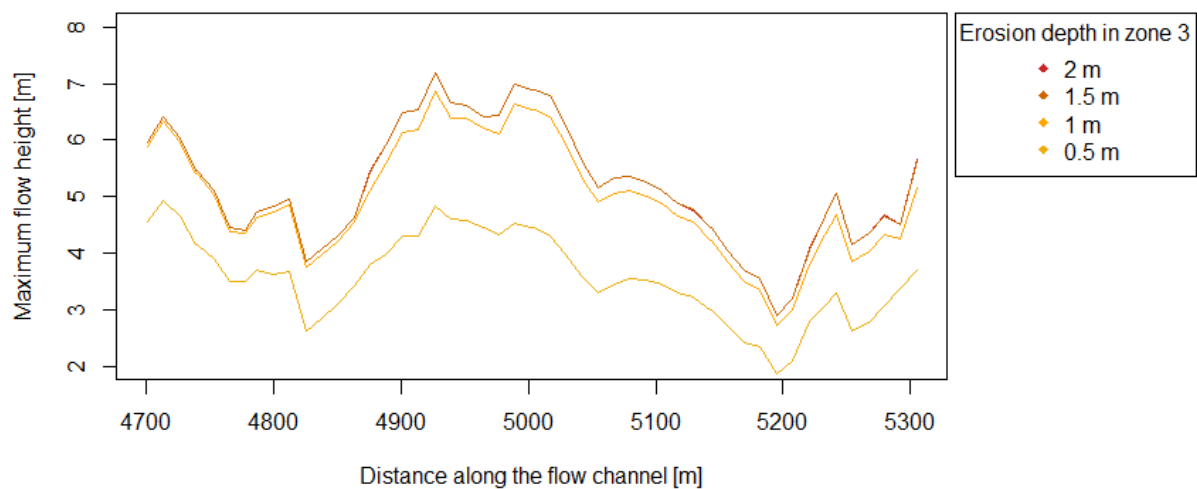


Figure 32: Maximum flow heights of four simulations are shown in a channel segment shortly before the debris cone. The flow heights are shown relative to a non-erosion scenario. Initial peak discharge was set to $20 \text{ m}^3 \text{ s}^{-1}$ and entrainment was considered in erosion zone 3. Erosion depths were set to 0.5, 1, 1.5, and 2 m.

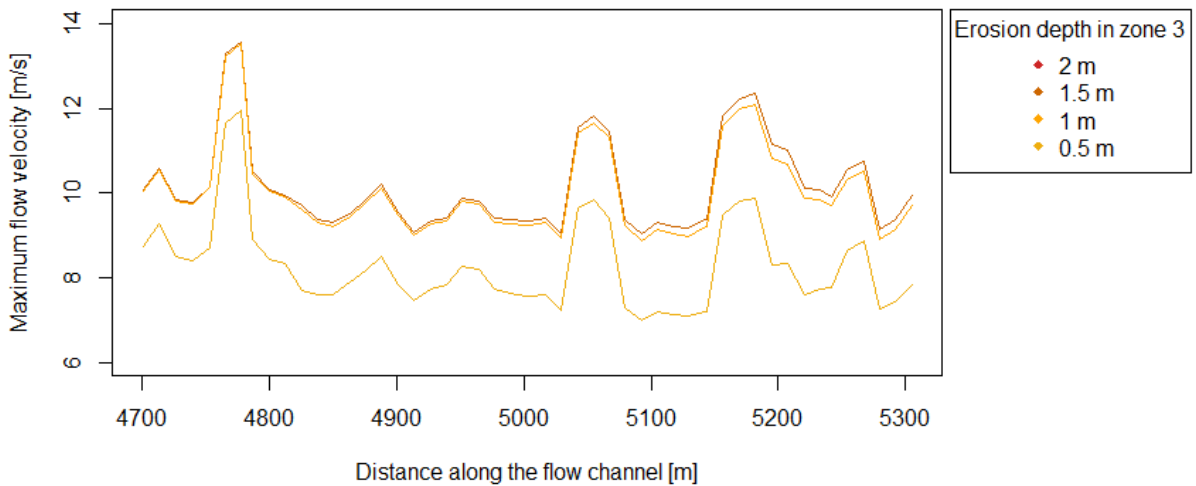


Figure 33: Maximum flow velocities of four simulations are shown in a channel segment shortly before the debris cone. The flow velocities are shown relative to a non-erosion scenario. Initial peak discharge was set to $20 \text{ m}^3 \text{ s}^{-1}$ and entrainment was considered in erosion zone 3. Erosion depths were set to 0.5, 1, 1.5, and 2 m.

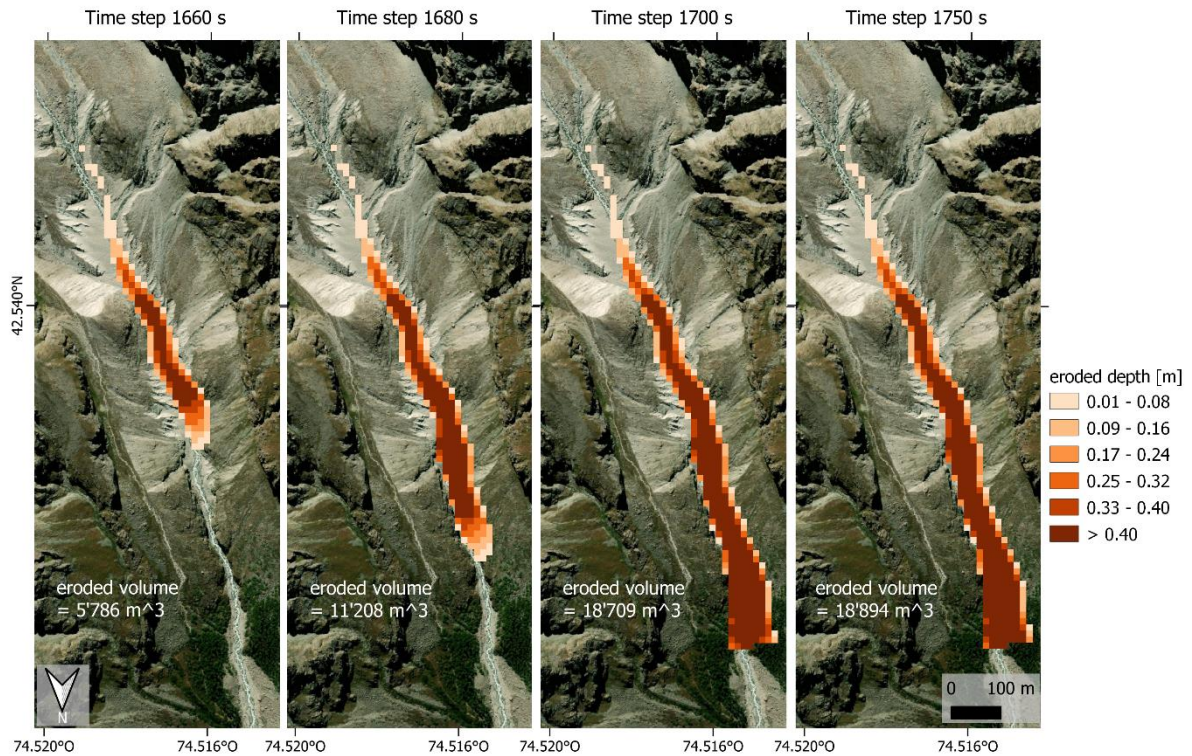


Figure 34: The four maps illustrate the eroded depth per pixel ($12.5 \text{ m} \times 12.5 \text{ m}$) at different time steps. Erosion was enabled in erosion zone 2 whereby a maximum erosion depth of 0.5 m was applied. The erosion rate was set to 0.05 m s^{-1} and critical shear stress was fixed at 0.5 kPa. In white, the eroded volumes at the given time steps are provided. The total eroded volume at the end of the simulation was $20'528 \text{ m}^3$.

Personal Declaration

I hereby declare that the submitted thesis is the result of my own, independent work.

All external sources are explicitly acknowledged in the thesis.

A handwritten signature in black ink, appearing to read 'C. Brüniger', with a long horizontal stroke extending to the right.

Claudius Brüniger

Zürich, 31.01.2023